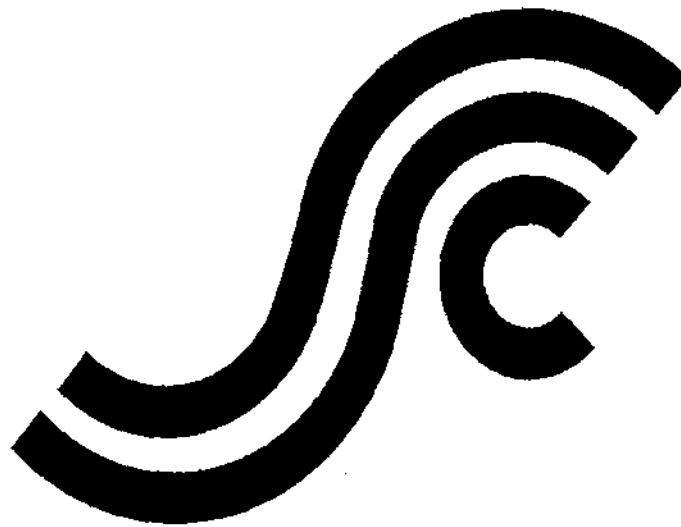


NTIS #PB2000-108443

SSC-411

**EVALUATION OF THE EFFECT OF
CONSTRUCTION TOLERANCES ON
VESSEL STRENGTH**



This document has been approved
For public release and sale; its
Distribution is unlimited

**SHIP STRUCTURE COMMITTEE
2000**

SHIP STRUCTURE COMMITTEE

RADM Robert C. North
U. S. Coast Guard Assistant Commandant,
Marine Safety and Environmental Protection
Chairman, Ship Structure Committee

Mr. Robert McCarthy
Director,
Survivability and Structural Integrity Group
Naval Sea Systems Command

Mr. Joseph Byrne
Director, Office of Ship Construction

Maritime Administration

Mr. Thomas Connors
Director of Engineering

Military Sealift Command

CONTRACTING OFFICER TECHNICAL REP.
Lieutenant David J. Martyn / Ms. Dinah Mulligan
U.S. Coast Guard R & D Center

Dr. Donald Liu
Senior Vice President

American Bureau of Shipping

Mr. Bud Streeter
Director General, Marine Safety,
Safety & Security
Transport Canada

Dr. Neil Pegg
Group Leader - Structural Mechanics

Defence Research Establishment Atlantic

EXECUTIVE DIRECTOR
Lieutenant David J. Martyn
U. S. Coast Guard

SHIP STRUCTURE SUB-COMMITTEE

AMERICAN BUREAU OF SHIPPING

Mr. Glenn Ashe
Mr. Yung Shin
Mr. Phil Rynn
Mr. William Hanzalek

MARITIME ADMINISTRATION

Mr. Chao Lin

NAVAL SEA SYSTEMS COMMAND

Mr. W. Thomas Packard
Mr. Edward E. Kadala
Mr. Allen H. Engle
Mr. Charles L. Null

UNITED STATES COAST GUARD

Captain Mark VanHaverbeke
Mr. Rubin Sheinberg
Mr. Walt Lincoln
Commander Ray Petow

DEFENCE RESEARCH ESTABLISHMENT ATLANTIC

Mr. Layton Gilroy
Mr. John Porter
LCDR Stephen Gibson
Dr David Stredulinsky

MILITARY SEALIFT COMMAND

Mr. Edward Meade
Mr. Rick A. Anderson
Mr. Jeffery E. Beach
Mr. Michael W. Touma

TRANSPORT CANADA

Mr. Nico Pau
Mr. James Reid

CANADIAN COAST GUARD

Mr. Justus Bunckhuysen

Member Agencies:

*American Bureau of Shipping
Defence Research Establishment Atlantic
Maritime Administration
Military Sealift Command
Naval Sea Systems Command
Society of Naval Architects & Marine Engineers
Transport Canada
United States Coast Guard*



**Ship
Structure
Committee**

An Interagency Advisory Committee

Address Correspondence to:

Executive Director
Ship Structure Committee
U.S. Coast Guard (G-MSE/SSC)
2100 Second Street, SW
Washington, D.C. 20593-0001
Ph: (202) 267-0003
Email: dmartyn@comdt.uscg.mil

SR-1382
SSC-411

September 2000

**EVALUATION OF THE EFFECT OF CONSTRUCTION TOLERANCES ON VESSEL
STRENGTH**

The ship construction process introduces geometric imperfections that adversely effect structural integrity. Tolerance limits are imposed on the various fabrication-induced distortions. These maximum allowable deviations are based on construction limitations and failure experiences and do not explicitly account for structural performance.

This report describes a methodology to evaluate the effect of imperfections resulting from the fabrication process on vessel strength. It addresses both strength and fatigue issues relevant to deformed and misaligned structure. Hull girder performance is characterized by the loss of load carrying capacity of the cross section based on predictions made by the computer program ULTSTR. ULTSTR estimates the ductile collapse of the hull girder assuming the collapse results from a sequence of failures of local components. Closed form solutions describing the structural response of these local components have been updated in ULTSTR based on finite element methods to account for fabrication induced imperfections. An approach to determine appropriate maximum misalignment amplitudes based on fatigue considerations is also described. This approach also uses finite element methods to determine stress concentration factors associated with misaligned details.

R. C. NORTH
Rear Admiral, U. S. Coast Guard
Chairman, Ship Structure Committee

1. Report No.	2. Government Accession No.	3. Recipient's Catalog No.	
4. Title and Subtitle Evaluation of the Effect of Construction Tolerances on Vessel Strength		5. Report Date July 2000	
		6. Performing Organization Code	
7. Author(s) Daniel D. Bruchman, David P. Kihl, John C. Adamchak		8. Performing Organization Report No. SR-1382	
9. Performing Organization Name and Address NSWCCD 9500 MacArthur Blvd W. Bethesda, MD 20817-5700		10. Work Unit No. (TRAVIS)	
		11. Contract or Grant No.	
12. Sponsoring Agency Name and Address Ship Structure Committee C/O US Coast Guard (G-MSE/SSC) 2100 Second Street, SW Washington, DC 20593		13. Type of Report and Period Covered Final Report	
		14. Sponsoring Agency Code G-M	
15. Supplementary Notes Sponsored by the Ship Structure Committee. Jointly funded by its member agencies			
<p>16. Abstract</p> <p>The ship construction process introduces geometric imperfections that adversely effect structural performance. In an attempt to ensure structural integrity, tolerance limits are imposed on the various fabrication-induced distortions. These maximum allowable deviations are based on construction limitations and failure experiences and do not explicitly account for structural performance.</p> <p>This report describes a methodology to evaluate the effect of imperfections resulting from the fabrication process on vessel strength. It addresses both strength and fatigue issues relevant to deformed and misaligned structure. Hull girder performance is characterized by the loss of load carrying capacity of the cross section based on predictions made by the computer program ULTSTR. ULTSTR estimates the ductile collapse of the hull girder assuming the collapse results from a sequence of failures of local components. Closed form solutions describing the structural response of these local components have been updated in ULTSTR based on finite element methods to account for fabrication induced imperfections. An approach to determine appropriate maximum misalignment amplitudes based on fatigue considerations is also described. This approach also uses finite element methods to determine stress concentration factors associated with misaligned details.</p>			
17. Key Words Ultimate Strength, Fatigue, Tolerances		18. Distribution Statement Distribution is available to the public through: National Technical Information Service U.S. Department of Commerce Springfield, VA 22151 Ph. (703) 487-4650	
19. Security Classif. (of this report) Unclassified	20. Security Classif. (of this page) Unclassified	21. No. of Pages	22. Price

CONVERSION FACTORS

(Approximate conversions to metric measures)

To convert from	To	Function	Value
LENGTH			
inches	Meters	divide	39.3701
inches	Millimeters	multiply by	25.4000
feet	Meters	divide by	3.2808
VOLUME			
cubic feet	cubic meters	divide by	35.3149
cubic inches	cubic meters	divide by	61,024
SECTION MODULUS			
inches ² feet	centimeters ² meters	multiply by	1.9665
inches ² feet	centimeters ³	multiply by	196.6448
inches ³	centimeters ³	multiply by	16.3871
MOMENT OF INERTIA			
inches ² feet ²	centimeters ² meters ²	divide by	1.6684
inches ² feet ²	centimeters ⁴	multiply by	5993.73
inches ⁴	centimeters ⁴	multiply by	41.623
FORCE OR MASS			
long tons	Tonne	multiply by	1.0160
long tons	Kilograms	multiply by	1016.047
pounds	Tonnes	divide by	2204.62
pounds	Kilograms	divide by	2.2046
pounds	Newtons	multiply by	4.4482
PRESSURE OR STRESS			
pounds/inch ²	Newtons/meter ² (Pascals)	multiply by	6894.757
kilo pounds/inch ²	mega Newtons/meter ² (mega Pascals)	multiply by	6.8947
BENDING OR TORQUE			
foot tons	meter tons	divide by	3.2291
foot pounds	kilogram meters	divide by	7.23285
foot pounds	Newton meters	multiply by	1.35582
ENERGY			
foot pounds	Joules	multiply by	1.355826
STRESS INTENSITY			
kilo pound/inch ² inch ^{1/2} (ksi√in)	mega Newton MNm ^{3/2}	multiply by	1.0998
J-INTEGRAL			
kilo pound/inch	Joules/mm ²	multiply by	0.1753
kilo pound/inch	kilo Joules/m ²	multiply by	175.3
TEMPERATURE			
Degrees Fahrenheit	Degrees Celsius	subtract & divide by	32 1.8

Table of Contents

Abstract	1
1. Introduction and Summary	1
1.1 Hull Girder Performance Defined by Ultimate Capacity	1
1.2 Hull Girder Performance Defined by Operational Life	2
1.3 Structural Reliability Assessment	3
1.4 Overview of Proposed Method	4
1.4.1 Ultimate Capacity	4
1.4.2 Fatigue Strength	6
2. Hull Girder Ultimate Capacity	8
2.1 ULTSTR Approach	8
2.1.1 Plating Effectiveness Relationships	13
2.1.1.1 Effective Breadth	13
2.1.1.2 Effective Width	13
2.1.2 Beam-Column Collapse – Type I	16
2.1.3 Beam-Column Collapse – Type II	19
2.1.4 Stiffener Tripping Collapse	24
2.1.5 Fully Plastic Moment	31
2.1.5.1 Vertical Bending Moment	31
2.1.5.2 Horizontal Bending Moment	36
3. Distortion Effects – Panel Response	37
3.1 Tripping	39
3.2 Buckling	47
3.3 Summary and Conclusions	60
4. Hull Girder Ultimate Strength Methodology Applied to Typical Sections	61
4.1 Distortion Effects on Hull Girder Ultimate Strength	65
4.1.1 Plating Effectiveness Effects	68
4.1.2 Stiffener Tripping Effects	72
4.1.3 Stiffener Buckling Effects	76
5. Fatigue	80
5.1 Operation Profile	80
5.2 Seaway Induced Loads	81
5.3 Fatigue Strength Curves	83
5.4 Linear Cumulative Damage Theory	87
5.5 The Impact of Misalignments on Fatigue Life	88
6. Conclusions and Recommendations for Future Work	92

Acknowledgement	94
References	95

List of Figures

1.4.1 – 1. Ultimate Capacity Flow Chart for Deformed Structure	5
1.4.2 – 1. Fatigue Strength Flow Chart for Misaligned Details	7
2.1 – 1. Incremental Concept for Hull Loading	9
2.1 – 2. Instability Failure Modes	10
2.1 – 3. Typical Gross Panel Load Shortening Curves	12
2.1.4 – 1. Geometrical Tripping Parameters for Tee Stiffeners	25
2.1.5.1 – 1. Geometrical Parameters for Fully Plastic Moment	31
3.1 – 1. Tripping Stress Amplification	40
3.1 – 2. 6x4x7 HS Stiffener on 12.75# Plate	41
3.1 – 3. 6x4x7 HS Stiffener on 25.5# Plate	41
3.1 – 4. 6x4x11 HS Stiffener on 20.4# Plate	42
3.1 – 5. 6x4x11 HS Stiffener on 30.6# Plate	42
3.1 – 6. 8x4x10 HS Stiffener on 15.3# Plate	43
3.1 – 7. 8x4x13 HS Stiffener on 25.5# Plate	43
3.1 – 8. 10x4x11.5 HS Stiffener on 17.85# Plate	44
3.1 – 9. 10x4x15 HS Stiffener on 25.5# Plate	44
3.1 – 10. 10x4x15 HS Stiffener on 30.6# Plate	45
3.1 – 11. 12x4x16.5 HS Stiffener on 15.3# Plate	45
3.1 – 12. 12x4x19 HS Stiffener on 25.5# Plate	46
3.1 – 13. 18x7x12.75#/17.85# HS Stiffener on 25.5# Plate	46
3.2 – 1. Buckling Stress Amplification	49
3.2 – 2. 6x4x7 HS Stiffener on 12.75# Plate	50
3.2 – 3. 6x4x7 HS Stiffener on 25.5# Plate	50
3.2 – 4. 6x4x11 HS Stiffener on 20.4# Plate	51
3.2 – 5. 6x4x11 HS Stiffener on 30.6# Plate	51
3.2 – 6. 8x4x10 HS Stiffener on 15.3# Plate	52
3.2 – 7. 8x4x13 HS Stiffener on 25.5# Plate	52
3.2 – 8. 10x4x11.5 HS Stiffener on 17.85# Plate	53
3.2 – 9. 10x4x15 HS Stiffener on 25.5# Plate	53
3.2 – 10. 10x4x15 HS Stiffener on 30.6# Plate	54
3.2 – 11. 12x4x16.5 HS Stiffener on 15.3# Plate	54
3.2 – 12. 12x4x19 HS Stiffener on 25.5# Plate	55
3.2 – 13. 18x7x12.75#/17.85# HS Stiffener on 25.5# Plate	55
3.2 – 14. 10x3½ MS Angle on 26.5# Plate	56
3.2 – 15. 12x3½ MS Angle on 26.5# Plate	56
3.2 – 16. 13x4 MS Angle on 26.5# Plate	57
3.2 – 17. 15x3¾ MS Angle on 26.5# Plate	57

3.2 – 18.	18x4 MS Angle on 26.5# Plate	58
4 – 1.	Six Point Bending Facility and Test Specimen	62
4 – 2.	Uni-directional Double Hull Test Specimen	63

List of Figures (continued)

4 – 3.	Hog Moment-Curvature Comparison of ULTSTR Versus Test Data for the Uni-Directional Double Hull	64
4 – 4.	Sag Moment-Curvature Comparison of ULTSTR Versus Test Data for the Uni-Directional Double Hull	65
4.1 – 1.	Hull F Midship Section	66
4.1 – 2.	Hull D Midship Section	67
4.1 – 3.	Hull C Midship Section	68
4.1.1 – 1.	Hull F Ultimate Hogging Comparison Evaluating Plating Effectiveness Effects	69
4.1.1 – 2.	Hull F Ultimate Sagging Comparison Evaluating Plating Effectiveness Effects	70
4.1.1 – 3.	Hull D Ultimate Hogging Comparison Evaluating Plating Effectiveness Effects	70
4.1.1 – 4.	Hull D Ultimate Sagging Comparison Evaluating Plating Effectiveness Effects	71
4.1.1 – 5.	Hull C Ultimate Hogging Comparison Evaluating Plating Effectiveness Effects	71
4.1.1 – 6.	Hull C Ultimate Sagging Comparison Evaluating Plating Effectiveness Effects	72
4.1.2 – 1.	Hull F Ultimate Hogging Comparison Evaluating Stiffener Tripping Effects	73
4.1.2 – 2.	Hull F Ultimate Sagging Comparison Evaluating Stiffener Tripping Effects	73
4.1.2 – 3.	Hull D Ultimate Hogging Comparison Evaluating Stiffener Tripping Effects	74
4.1.2 – 4.	Hull D Ultimate Sagging Comparison Evaluating Stiffener Tripping Effects	74
4.1.2 – 5.	Hull C Ultimate Hogging Comparison Evaluating Stiffener Tripping Effects	75
4.1.2 – 6.	Hull C Ultimate Sagging Comparison Evaluating Stiffener Tripping Effects	75
4.1.3 – 1.	Hull F Ultimate Hogging Comparison Evaluating Stiffener Buckling Effects	76
4.1.3 – 2.	Hull F Ultimate Sagging Comparison Evaluating Stiffener Buckling Effects	77
4.1.3 – 3.	Hull D Ultimate Hogging Comparison Evaluating Stiffener Buckling Effects	77

4.1.3 – 4. Hull D Ultimate Sagging Comparison Evaluating Stiffener Buckling Effects	78
4.1.3 – 5. Hull C Ultimate Hogging Comparison Evaluating Stiffener Buckling Effects	78
4.1.3 – 6. Hull C Ultimate Sagging Comparison Evaluating Stiffener Buckling Effects	79

List of Figures (continued)

5.3 – 1. Conventional S/N Fatigue Diagram	84
5.3 – 2. S/N/P Diagram (Constant Scatter in Life at a Given Stress)	85
5.3 – 3. S/N/P Diagram (Increasing Scatter in Life with Decreasing Stress)	85
5.5 – 1. Misaligned Cruciform	89
5.5 – 2. Fatigue of Aligned and Misaligned Detail	90

List of Tables

3 – 1. Typical ASTM Tolerance Ranges	38
3.1 – 1. Distortion Effects on Component Tripping Capacity	47
3.2 – 1. Distortion Effects on Component Buckling Capacity	59

Abstract

This report describes a methodology to evaluate the effect on vessel strength of imperfections resulting from the fabrication process. It addresses both strength and fatigue issues relevant to deformed and misaligned structure. Hull girder performance is characterized by the loss of load carrying capacity of the cross section based on predictions made by the computer program ULTSTR. ULTSTR estimates the ductile collapse of the hull girder assuming the collapse results from a sequence of failures of local components. Closed form solutions describing the structural response of these local components have been updated in ULTSTR based on finite element methods to account for fabrication induced imperfections. An approach to determine appropriate maximum misalignment amplitudes based on fatigue considerations is also described. This approach also uses finite element methods to determine stress concentration factors associated with misaligned details.

1. Introduction and Summary

The ship construction process introduces geometric imperfections that adversely effect structural performance. In an attempt to ensure structural integrity, tolerance limits are imposed on the various fabrication-induced distortions. These maximum allowable deviations are based on construction limitations and failure experiences and do not explicitly account for structural performance. Safety factors are introduced to account for the unknown structural degradation the actual, deformed structure exhibits as compared to the ideal structure.

Structural issues should determine appropriate maximum tolerance magnitudes because these limits exist to ensure a level of structural performance. Although classification societies have introduced a “net ship” approach to account for hull degradation resulting from corrosion after a period of time, little has been done to determine the actual loss of capacity of the built ship resulting from the fabrication process. This task will provide a structural basis for determining appropriate tolerance limits by developing a methodology to evaluate structural responses of as built structures and the effects of fabrication induced structural imperfections on vessel strength. Hull girder ultimate strength and endurance were chosen as the necessary performance issues needed to structurally address appropriate tolerance limits.

1.1 Hull Girder Performance Defined by Ultimate Capacity

The hull girder is designed to withstand the hogging and sagging bending moments encountered during its operating lifetime. In general, the hull girder’s ability to withstand these moments degrades as distortion magnitudes increase. This is because distortions reduce the load carrying capacity of the panels that comprise the hull girder. As the individual panels of the hull girder fail, stress levels in other panels increase as the load is shed to them. In the past, safety factors were introduced to account for this unknown degradation in structural strength resulting from these distortions. Because little is known about deformation effect on component and hull girder strength, this factor of safety likely produced

either a heavier structure than needed to withstand these environmental loads, or an unnecessarily robust design with a high hull girder capacity.

To determine the loss in hull girder capacity resulting from distortions, one must first understand the effect of these distortions on local panel response before combining the panel responses to determine hull girder capacity. There are both advantages and disadvantages associated with the methods used to characterize hull girder ultimate strength and component strength. Any methodology to address local and global strength will ultimately consist of three components: experimental methods, closed-form solutions and numerical techniques such as finite element analysis. Experimental methods can determine structural response with reasonable accuracy if the tests are implemented correctly, the boundary conditions can be reproduced and the test specimen resembles the structure. However tests are very expensive and do not easily lend themselves to parametric analysis. Closed-form solutions have limited applications and often introduce large uncertainties as assumptions are made. Numerical methods offer flexibility not offered by the other two methods, but have modeling uncertainties and costs associated with them as well. An appropriate procedure implementing the available analysis techniques would be somewhat iterative and involve extensive coordination. Numerical models describing the experimental model, the assumptions used, and the boundary conditions in the experiment are needed to demonstrate the ability to duplicate experimental results before building the numerical model of the actual structure. Using this approach, differences in results between the methods and errors in the implementation of the methods can be identified and more easily resolved. As the analyst becomes comfortable with the ability of the numerical model to accurately assess response, parametric studies can be performed. These studies can then be used to develop closed-form solutions describing response and reduce the number of assumptions and uncertainties associated with closed-formed solutions.

1.2 Hull Girder Performance Defined by Fatigue Performance

Structural members subjected to time varying external loadings undergo progressive unrecoverable changes that, after enough load applications, can result in crack initiation, propagation, and ultimately fracture or complete structural failure. Application of load can be of a constant amplitude nature over the service life of the structure or some combination of many different load amplitudes that can occur in a repetitive or a random sequence. It is this second type of load application which is of interest to the naval architect, since the effect of random occurrences of wave-induced loads on a ship's hull girder can eventually lead to the initiation of cracks during the ship's service life.

Providing a method to address the time at which crack initiation occurs can provide the design engineer with an estimate of the ship structure's useful service life to scope and schedule corrective actions. If the ship already exists, such a method would provide a means for identifying "hot spots" requiring monitoring and the amount of time remaining to take appropriate action, prior to structural failure.

This report discusses a way of addressing such issues through the use of linear cumulative damage theory. To implement this theory, two items are required. The first item is the ship's lifetime load history (applied stress levels at a given location on the ship structure and the number of cycles at each stress level). The second item is the ship's material/configuration fatigue behavior characteristics to applied cyclic loads (fatigue resistance to applied stress cycles).

1.3 Structural Reliability Assessment

This report addresses methods of determining structural degradation resulting from imperfections during fabrication. As such, it provides a method to evaluate the structural performance of a given distorted component relative to its undistorted state. Ultimately, system reliability needs to be addressed. The reliability of an engineering system can be defined as its ability to fulfill its design purpose for some time period (Bruchman, Ayyub, et. al. 1997). In a structural system, this ability is a measure of the system's actual capacity or strength as compared to the required capacity needed to withstand expected loadings occurring during a specified time frame. Mathematically, this relationship can be expressed in the general performance function given below:

$$Z = Z(X_1, X_2, \dots, X_n) = \text{Structural strength} - \text{Load effect} \quad (1.3 - 1)$$

Where, Z is the performance function and the X_i 's are the relevant parameters necessary to define system performance. The methods in this report aid in determining appropriate performance functions for distorted components. Probability theory and statistics allow us to modify the classical definition of strength and load effects to account for any number of variations in the strength and load definitions. Therefore, rather than having a failure point where structural capacity equals the demand required by the loads, a reliability analysis defines a "failure surface" where the capacity equals the demand required by the loads. The failure surface (or the limit state) of interest is defined as the condition, $Z=0$. When $Z > 0$, the structure is in a safe state and when $Z < 0$ the structure is in a failure state. Failure can be either a serviceability type of failure or an ultimate failure, depending on the performance function chosen. In estimating this probability, system uncertainties are modeled using random variables with mean values, variances, and probability distribution functions. If the joint probability density function for the basic random variables X_i 's is $f_{x_1, x_2, \dots, x_n}(x_1, x_2, \dots, x_n)$, then the failure probability P_f of a structure can be given by the integral

$$P_f = \int \dots \int_{x_1, x_2, \dots, x_n} f_{x_1, x_2, \dots, x_n}(x_1, x_2, \dots, x_n) dx_1 dx_2 \dots dx_n \quad (1.3 - 2)$$

where the integration is performed over the region in which $Z < 0$. In general, the joint probability density function is unknown, and the integral is a formidable task. For practical purposes, alternate methods of evaluating P_f are necessary. Some of these methods are described in detail in Bruchman and Ayyub (1997).

The reliability of an engineering system described by a given performance function can also be found using direct simulation. Using direct simulation, values for the variables in the performance function are randomly chosen based on the probabilistic characteristics of the variables. If the performance function, Z , yields a negative value with a given set of variables, failure occurs. The probability of failure for the system is then estimated as the number of failures divided by the total number of simulations.

$$\bar{P}_f = \frac{\text{Number of failures}}{\text{Number of Simulation s}} \quad (1.3 - 3)$$

As the number of simulations increases, the accuracy of the estimation increases. Because of the complexity of many performance functions, simulation numbers have to be reduced to maintain a reasonable computational effort. This leads to less accurate results. To reduce the computational effort of direct simulation methods, variance reduction techniques have been used to increase simulation efficiency without jeopardizing accuracy (Ayyub, Ru-Jen Chao, Bruchman, Adamchak, 1995). The use of simulation methods for hull girder, structural reliability assessment has been demonstrated and has proven to be an effective, efficient method for this purpose (Ayyub, Muhanna, and Bruchman, 1997).

1.4 Overview of Proposed Method

Appropriate tolerance limits depend on the ability to estimate deformed and misaligned structural response and fatigue strength. An outline describing a method for determining the structural performance relating to ultimate capacity and fatigue strength is given below.

1.4.1 Ultimate Capacity

Before determining the required ultimate capacity of local structural components or that of a hull girder, design and ultimate loading conditions must be determined. In the case of the hull girder, the vertical bending condition often governs the design and will be the loading condition discussed throughout much of this report.

There are numerous methods for determining a design vertical bending moment, ranging from the static balance on a standard wave to bending moments derived from model tests for specific operating conditions and specific hull shapes. This report will not attempt to suggest which method to use to select a design bending moment, however, this is critical when defining the required capacity and the assumptions, strengths and limitations of the selected method should be recognized and stated.

Following the selection of the design bending moment, the ultimate capacity of the hull girder must be determined. The methods described in this report can be used to determine the capacity of undeformed and deformed local structural components. Hull girder ultimate capacity and the impact of distortions on the hull girder capacity are also addressed. Therefore, these methods will aid in setting tolerance limits on the various deformations as the impact of these deformations adversely impact capacity. If the capacity of the undeformed hull girder does not exceed the required capacity, as defined by the design bending moment and an appropriate factor of safety, then redesign of the hull girder is necessary. Similarly, if the capacity of the undeformed hull girder is acceptable but the deformed hull girder does not exceed the required capacity, as defined by the design bending moment and an appropriate factor of safety, then the deformation is unacceptable. This process is summarized in Figure 1.4.1 – 1.

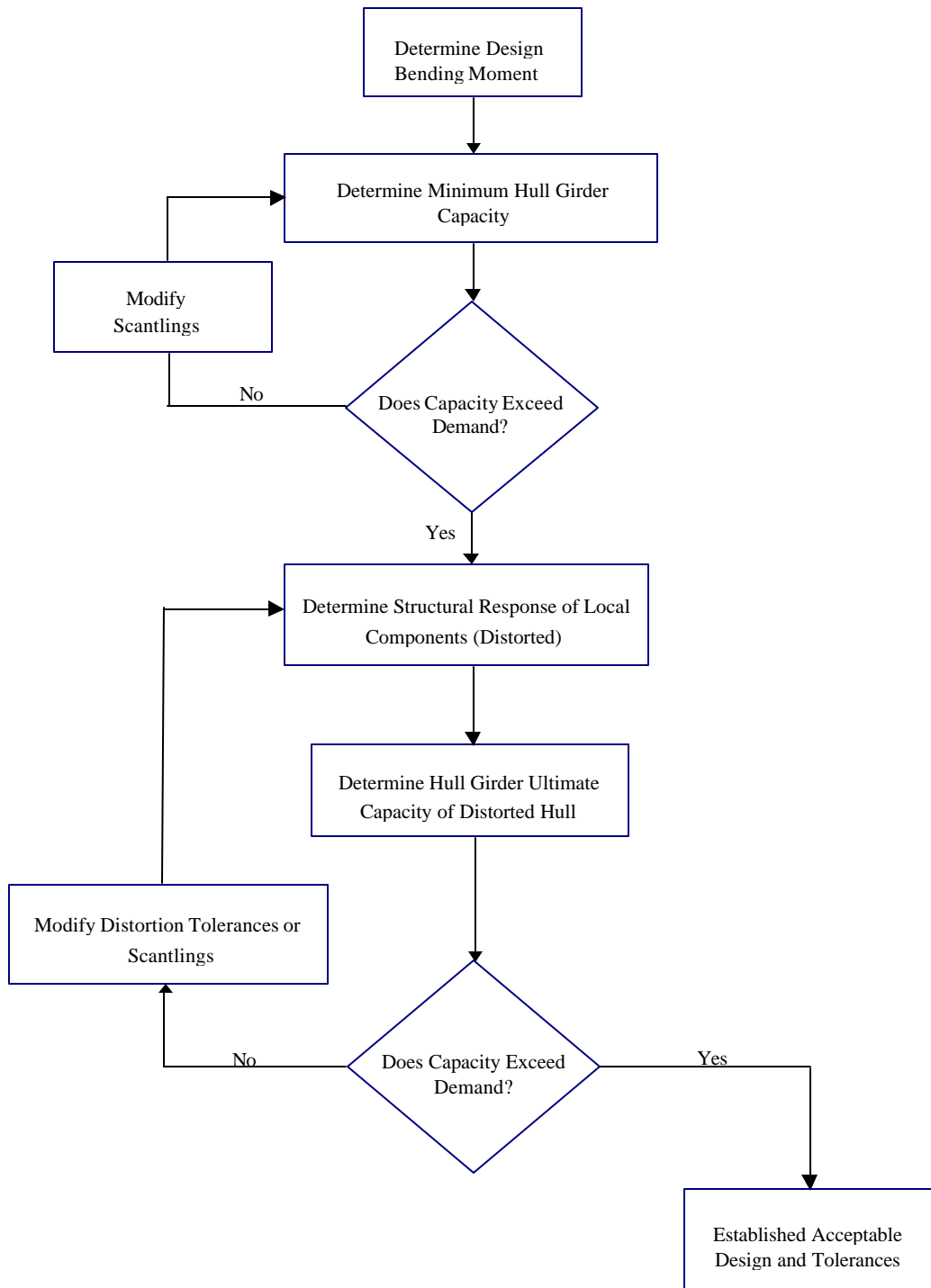


Figure 1.4.1 – 1: Ultimate Capacity Flow Chart for Deformed Structure

1.4.2 Fatigue Strength

The fatigue strength of a structural detail is highly dependant upon the number of applied cycles in a given stress range. In a ship structure, these values depend on the hull form, hull cross-sectional characteristics and the operational profile intended for the ship. A procedure to determine the expected magnitudes and frequencies of hull girder, vertical bending moments is described in section 5 of this report. Based on full-scale trials and model tests, this method is perhaps the most rigorous and straight-forward method for determining vertical bending moment values available. Following the development of a “bending moment exceedance curve” defining the number of expected bending moment occurrences for a given hull form and operational profile, a “stress exceedance curve” for any location in a given cross section can be found. This stress exceedance curve in effect defines the cycles that a structural detail could expect in a given stress range during its operational life. A histogram of applied stress ranges is then generated from the stress exceedance curve.

The fatigue performance of a detail is defined by its S/N curve. This curve defines the number of cycles at given stress ranges the detail could endure before failure, with failure being described as crack initiation. If the stress exceedance curve for a particular detail at a particular location on the hull girder is known and the S/N curve for that detail is known, the fatigue life of that detail can be determined. In this manner, the hull girder can be designed to a particular fatigue life. Given the same stress exceedance curve, a misaligned detail will fail at a reduced number of cycles as compared to the aligned detail because of the increased stress from the misalignment. This stress concentration factor will increase as the misalignment increases, causing a further reduction in fatigue life. Depending on the location of the detail in the hull girder, the misalignment could reduce the fatigue life of the detail to an unacceptable value and corrective action would need to be taken. However, to obtain the same fatigue life, an unacceptable misalignment for a detail in a high stress region may be acceptable for the same detail in a low stress region. This “design for fatigue” process is summarized in Figure 1.4.2 – 1.

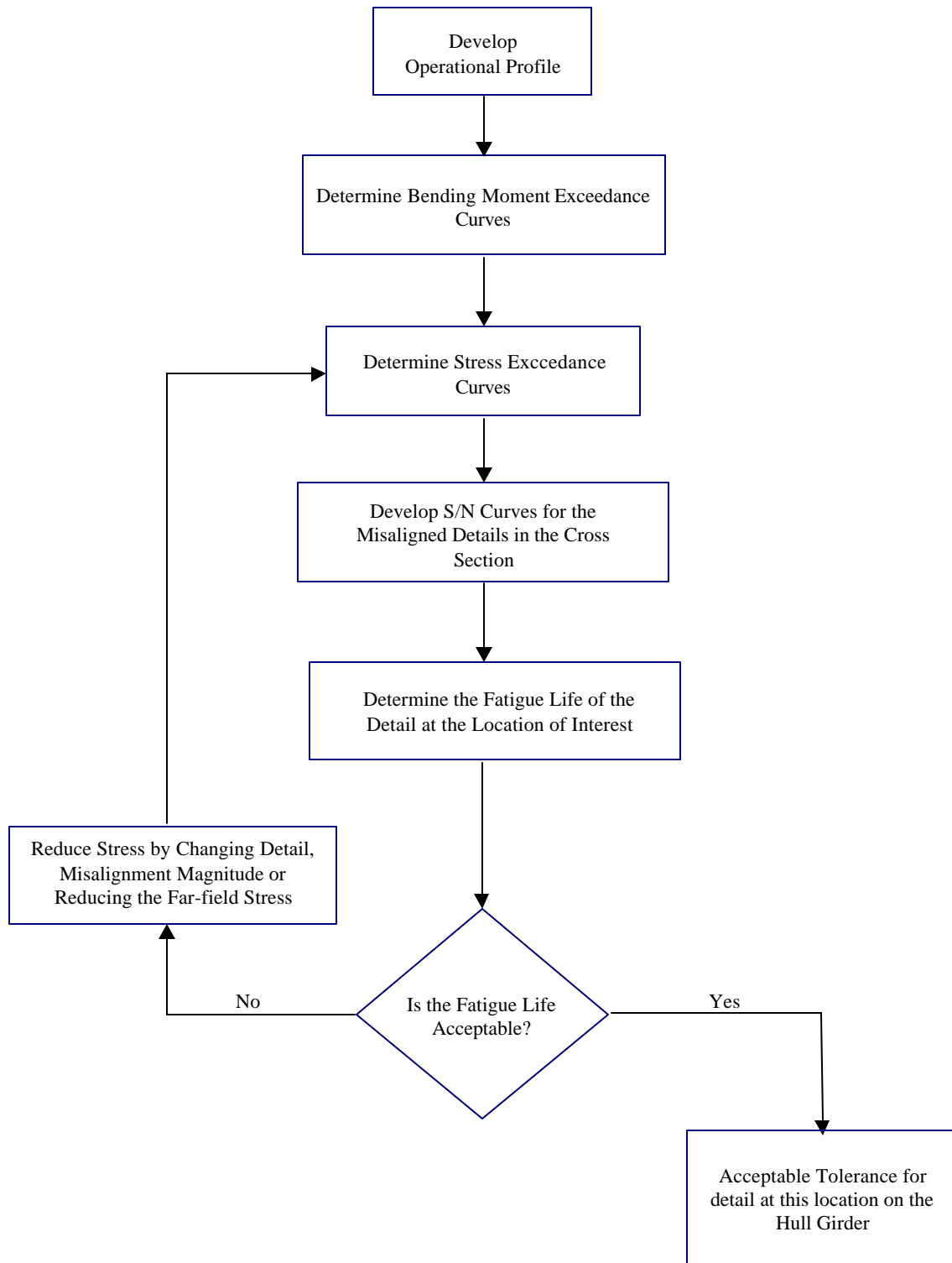


Figure 1.4.2 – 1: Fatigue Strength Flow Chart for Misaligned Details

2. Hull Girder Ultimate Capacity

One obvious but unknown impact of fabrication induced deformations on vessel performance is the resulting ultimate capacity of the local and global structure in resisting applied loads. If one assumes the ductile collapse of the hull girder results from a sequence of failures of local components, one can address the collapse behavior of the hull by concentrating on the collapse behavior of the local components that make up the cross section, whether such components are represented as a single plate-beam combination, an individual gross panel (comprised of several plate-beams), or a complete cross-stiffened grillage. This is certainly convenient, since the collapse behavior of the above-mentioned components is technically tractable, although to varying degrees, and a significant body of literature exists on this subject. This does not imply that the collection of solutions for the collapse of local components is absolutely comprehensive and totally consistent, but rather that their behavior is understood well enough to allow development of a collapse model which provides both speed and accuracy and can be used in a practical fashion to address major structural considerations. In contrast, addressing this problem as an overall simultaneous instability of the complete cross section presents a major practical obstacle. Numerical analysis, and, specifically, the finite element method, is most likely the only approach currently available which could be used to address this problem with any degree of rigor. And in theory, the finite element method could treat this problem. However, the size and complexity of the mathematical model needed to treat the typical hull cross section is still effectively beyond the practical limits of time, cost and capacity of today's computing systems. Fortunately, it is believed in the vast majority of cases that ductile hull collapse is due to a sequence of local failures rather than a simultaneous occurrence. With the possible exception of grillage general instability, the most probable ductile failure modes are primarily local phenomena in which there is relatively little direct influence from the other major components of the cross section. (Of course, the overall cross-section parameters of the hull do influence the stress-strain levels on the individual components.) Without this significant interaction between major components, simultaneous failure is unlikely. Instead, a failure mode something like a chain reaction is more probable. Thus the choice of a solution technique to determine hull girder ultimate capacity was dictated by what most likely occurs rather than by expediency alone. Given these assumptions, the Naval Surface Warfare Center Carderock Division (NSWCCD) has developed a computer code, ULTSTR, to address the ductile collapse of the hull girder under longitudinal bending. This computer code, with modifications to account for the effect of fabrication induced distortions, is ideal for estimating component and hull girder capacities of deformed structure and can therefore be utilized to determine appropriate tolerance limits for various distortions.

2.1 ULTSTR Approach

The actual solution approach involves dividing the hull cross section into a set of "gross panel" elements and "hard corner" elements and then imposing a curvature on the hull in small finite increments. This incremental loading concept is illustrated in Figure 2.1 - 1.

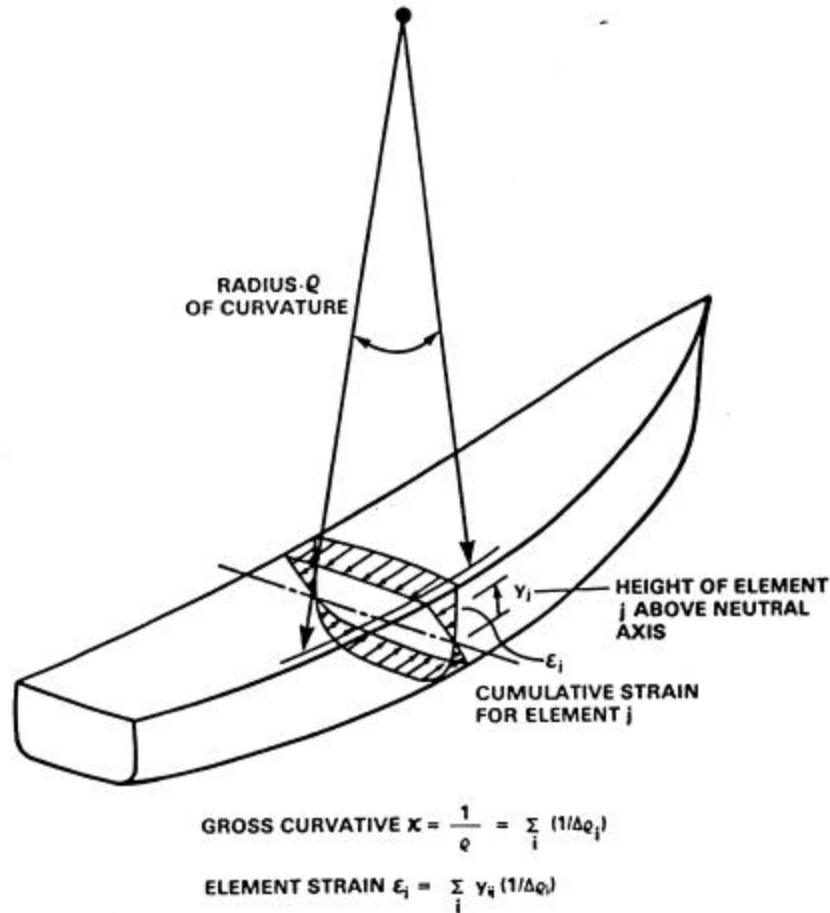


Figure 2.1 - 1: Incremental Concept for Hull Loading

Each increment of curvature is assumed to produce a linear strain distribution through the depth of the cross section. The location of zero strain corresponds to what will be referred to as the "instantaneous" or "incremental" neutral axis. The assumption of linear strain through the cross section is common practice in naval architecture and is certainly "sufficiently" valid for stress levels at or below the so-called design values. When strain levels reach values at which structural components begin to demonstrate significant changes in behavior (buckling, yielding, formation of plastic hinges, etc.) then the validity of this assumption becomes more questionable. It is impossible to be certain at present; thus it has been assumed that the application of linear strain is also "sufficiently" valid up to the point of hull collapse. This is certainly consistent with the degree of engineering accuracy expected and with the approximations that of necessity have been made concerning other aspects of the program. As experience is gained with this program the validity of this assumption may be more clear, and changes may be required. Future versions of the program can be expected to incorporate the necessary modifications.

At each value of curvature, the program evaluates the equilibrium state of each gross panel and hard corner element relative to its state of stress and stability corresponding to its particular value of strain. It then computes the total moment on the cross section by summing the moment contributions (stress x effective area x lever arm) of all of the elements that make up the section. In this manner, a

moment-curvature relationship is defined. Since the stress distribution, unlike that of strain, is not necessarily linear across the depth of the section, the location of the instantaneous neutral axis must be determined in an iterative fashion from the condition that the net axial force on the cross section must be zero. This force is computed in the same fashion as the bending moment, that is, by summing the contributions of all the elements of the cross section. In the iteration process, the position of the instantaneous neutral axis is varied until the value of the net force is less than some predefined acceptable limit. In spite of the "motion" of the instantaneous neutral axis from increment to increment, the cumulative strain distribution that results is still linear through the depth of the cross section, since it represents the superposition of a number of linear increments.

Gross panel elements in the cross section can "fail" either through material yielding (in either tension or compression), material rupture (in tension only) or through some form of structural instability (in compression only). The instability failure modes presently incorporated include: (1) Euler beam-column buckling and (2) stiffener lateral-torsional buckling (tripping). These modes are symbolically illustrated in Figure 2.1 - 2.

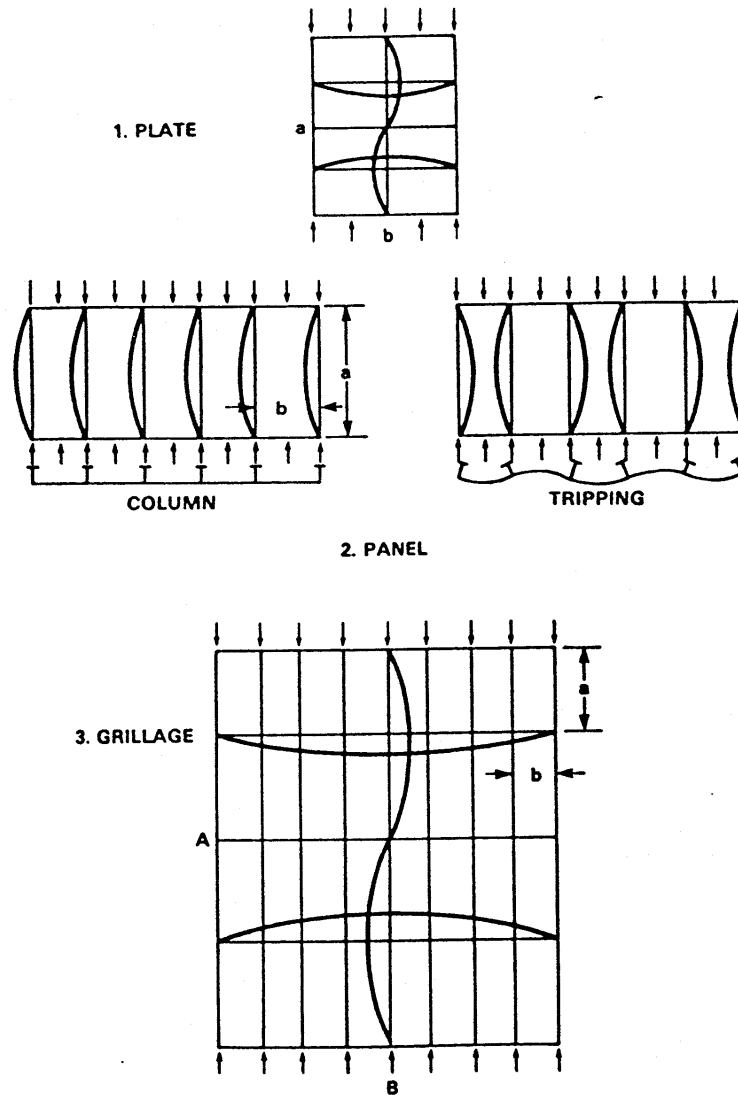


Figure 2.1 - 2: Instability Failure Modes

Plate buckling is not specifically included as a separate failure mode because (for longitudinal framing) it influences collapse more indirectly, that is, through its effect on plating effectiveness relationships. These effects are taken into account in the analysis. Grillage general instability has also been omitted as a failure mode in the current version of the program. The incorporation of general instability will involve some rather significant modifications in programming logic, consequently it was determined that this enhancement would be more appropriate for a future version of the program. For most applications, the lack of a general instability mode need not be regarded as a serious shortcoming of the program at present; the structural proportions found in typical surface ships currently in design or service seldom have general instability as their primary mode of failure. However, there may be instances when general instability may be important, for example, if "light-weight" grillages incorporating thin-gage, high-strength steels are adopted for primary structure, or if the structure is in a damaged state where supporting members (which would normally prohibit general instability) have effectively been destroyed. In any

case, grillage general instability should not be ignored; it should be a prime candidate for one of the future modifications of the program.

Although it is impossible to determine at a glance what failure mode may be most critical for a particular gross-panel element, it has been assumed that once instability is detected in a given mode, the behavior follows through to failure in that same mode. Interaction amongst different modes of failure is an extremely complex problem should receive further attention in future studies.

Regardless of the specific type of failure involved, the general nature of an element's behavior can be described in terms of a "load-shortening" curve, illustrated in Figure 2.1 - 3.

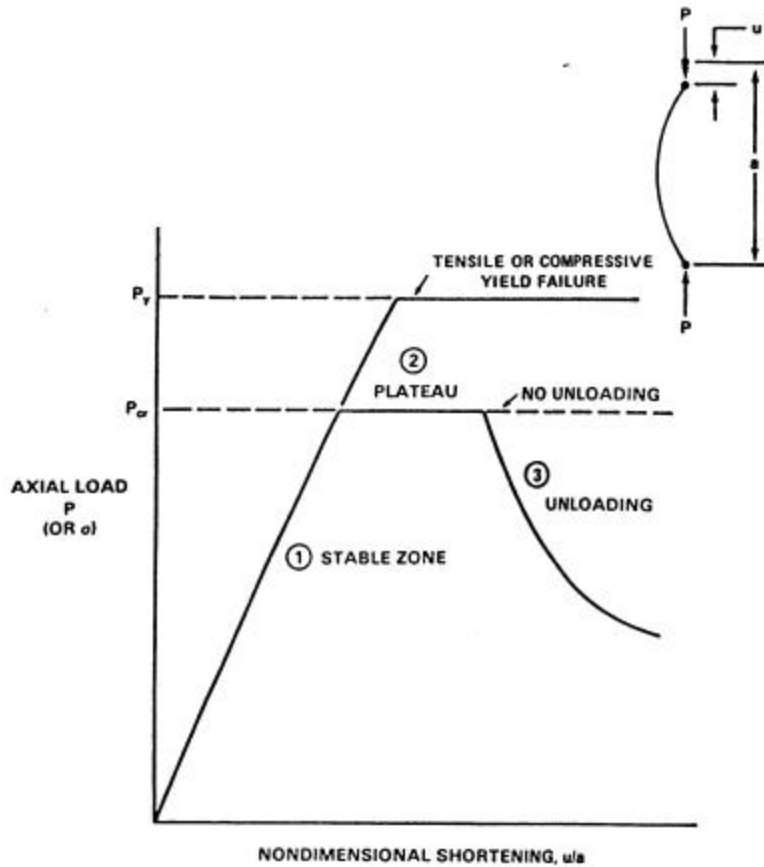


Figure 2.1 - 3: Typical Gross Panel Load Shortening Curves

This curve has three distinct zones of behavior. The first zone represents stable behavior in which the load applied to the element is less than the critical value corresponding to its preferred mode of failure. Since load-dependent effectiveness relationships are used in this program for gross panel elements, the curve in this region will generally have only slight nonlinear deviations. The second zone, or plateau, occurs after an element has reached its critical load. On this plateau, the element will continue to deform without any increase in loading. This critical load may correspond to one of the possible forms of buckling or to the condition of material yielding. As the figure indicates, some elements can remain indefinitely in the second zone after reaching their critical load. Gross panel elements under tension and hard corner elements (under either tension or compression) can be characterized by this type of

behavior. A recent program enhancement allows either gross panel or hard corner elements under tension to suddenly rupture; that is, their load carrying capability at and above the defined rupture level will drop immediately to zero. The third zone of behavior, for compression only, is characterized by a drop-off in the element's load carrying capability as deformation increases. This necessity for reducing load to maintain an element's equilibrium, called "unloading", can significantly affect the behavior of the overall hull cross section. Originally this type of behavior was restricted to gross panel elements, but a modified theory was recently introduced into the program that implements an unloading type of behavior for hard corner elements under compression as well.

2.1.1 Plating Effectiveness Relationships

Plating effectiveness relationships play an important role throughout the collapse mode theories summarized in the following paragraphs. In ULTSTR a distinction is made between "effective breadth" and "effective width" since the phenomena they represent have certain fundamental differences. The effectiveness relationships for these two phenomena which are used in these theories are concisely presented here, with a minimum of theoretical and empirical back-up. Tension is assumed positive and compression negative throughout this report.

2.1.1.1 Effective Breadth

Effective breadth, closely related to the phenomenon of shear lag, is treated first because of the extremely simple form of the assumed relationship. Since it plays a less important role in the collapse theories, a relatively simple relationship is considered to be acceptable. Denoting the effective breadth by b_e , its relationship to the longitudinal frame spacing b is the following:

$$b_e = \frac{1}{2}b \quad (2.1.1.1 - 1)$$

This assumption is based on the work of Clarkson (1965).

2.1.1.2 Effective Width

The theory behind the effective width formulations is somewhat involved and is described in Evans, J.H. (1975) and Faulkner, D., Adamchak, J., et. al. (1973). The results of these developments are summarized here.

The effective width relationships can be represented in a more concise form if the plate slenderness parameter, b , is introduced. This parameter is defined as

$$b = \frac{b}{t} \sqrt{\frac{s_{yp}}{E}} \quad (2.1.1.2 - 1)$$

where t is the plate thickness, s_{yp} is the tensile yield stress of the plate material and E the Young's modulus of the plate material. A modification of this slenderness, b_e , can also be defined,

$$b_e = \frac{b}{t} \sqrt{\frac{-s_e}{E}} \quad (2.1.1.2 - 2)$$

which is the original slenderness b with the yield stress replaced by the actual inplane compressive edge stress s_e in the plating.

Using the above slenderness parameters, the effective width relationship used in the hull collapse program is the following generic expression:

$$\frac{b_e}{b} = \left\{ c_0 + \frac{c_1}{b_e} + \frac{c_2}{b_e^2} \right\} R_r \quad (2.1.1.2 - 3)$$

In this expression b_e now refers to the effective width, R_r , a residual stress reduction factor (to be described later), and the C_i terms are empirical constants derived from experimental data. (Note that the above expression is valid only for $\frac{b_e}{b} \leq 1.0$. For values of b_e which yield values of $\frac{b_e}{b}$ greater than 1.0, the effective width ratio is automatically set equal to 1.0.) Currently in ULTSTR, the user may choose from four sets of these constants which are intended to address plating which has varying degrees of initial distortion. The values of these constants and the conditions that they are intended to represent are the following:

Plating nearly perfectly flat:	$C_0 = 0.0$ $C_1 = 2.55$ $C_2 = -1.50$
Moderate distortions: (Frankland's expression)	$C_0 = 0.0$ $C_1 = 2.25$ $C_2 = -1.25$
Moderate-high distortions: (Faulkner's expression)	$C_0 = 0.0$ $C_1 = 2.0$ $C_2 = -1.0$
Severe distortions:	$C_0 = 0.0$ $C_1 = 1.75$ $C_2 = -0.75$

The expression (2.1.1.2 - 3) as written is load-dependent, that is, the plating effective width depends on the value of the applied edge stress, s_e . An alternative to (2.1.1.2 - 3) is to substitute b for b_e in the second and third terms on the right of (2.1.1.2 - 3), resulting in an expression for b_e which is no longer load dependent but rather a constant since the yield stress has been substituted for the applied edge stress. This is also an option in ULTSTR.

The residual stress reduction factor, R_r , referred to earlier, is a parameter intended to take into account the reduction in plating effectiveness resulting from fabrication-induced residual stress. This factor is defined as follows. Introducing the constant parameter,

$$c_k = \frac{4p^2}{12(1-n_p^2)} \quad (2.1.1.2 - 4)$$

in which n_p refers to the Poisson's ratio of the plate material, the structural tangent modulus ratio, E_t/E can be computed from the relationship

$$\frac{E_t}{E} = \begin{cases} \left(\frac{C_k b^2}{C_k^2 + p_r(1-p_r)b^4} \right)^2 & b^2 < \frac{C_k}{p_r} \\ 1.0 & b^2 \geq \frac{C_k}{p_r} \end{cases} \quad (2.1.1.2 - 5)$$

in which p_r is a structural proportional limit ratio (a value of 0.5 is the default value in ULTSTR). With these initial definitions, the residual stress reduction factor can then be defined as follows,

$$R_r = \begin{cases} 1.0 - \frac{-s_r}{s_{yp}} \frac{E_t}{E} & b \leq b_0 \\ 1.0 - \frac{-s_r}{s_{yp}} \frac{E_t}{E} \left(C_0 + \frac{C_1}{b} + \frac{C_2}{b^2} \right) & b > b_0 \end{cases} \quad (2.1.1.2 - 6)$$

The ratio (s_r/s_{yp}) relates the level of compressive residual stress in the plating s_r , to the plate's yield stress. (Note that, in the above expressions, the parameter b_0 refers to the value of b for which the expression in parentheses involving the constants C_i is equal to 1.0. This variable depends on which set of constants is selected.) It is assumed that this compressive stress must balance the tensile yield zone along the edge of the stiffener induced by welding the stiffener to the plate. The width of this tensile block on each side of the stiffener is denoted by ht and hence equilibrium requires that the level of residual compressive stress be defined by the relationship

$$\frac{-s_r}{s_{yp}} = \frac{2h}{\frac{b}{t} - 2h} \quad (2.1.1.2 - 7)$$

Faulkner D. and Adamchak, J. (1973) recommend that values of h of 4.5 to 6 are typical for ships as welded, but values of 3 to 4.5 are more appropriate for design after allowing for shakedown.

Since the effective width defined by Equation (2.1.1.2 - 3) is based on the total edge stress s_e , it might be called a "cumulative" effective width. Closely related to this cumulative effective width is what has been termed a tangent width, reduced effective width, or even an incremental effective width, so called because it represents the effectiveness of the plating as it is stressed from the level s_e to $s_e + Ds_e$. Denoting this quantity by b_e' , it can readily be shown that if b_e' is defined as $\Delta P = \Delta s_e b_e' t$, then this leads directly to the relationship

$$b_e' = b_e + \frac{db_e}{d(-s_e)}(-s_e) \quad (2.1.1.2 - 8)$$

Thus the formulation of b_e' is not independent of that for b_e , and if the above is applied to Equation (2.1.1.2 - 3), the result becomes

$$\frac{b_e'}{b} = \begin{cases} R_r & \mathbf{b}_e \leq 0.5 \frac{C_1}{1 - C_0} \\ R_r \left(C_0 + 0.5 \frac{C_1}{\mathbf{b}_e} \right) & \mathbf{b}_e > 0.5 \frac{C_1}{1 - C_0} \end{cases} \quad (2.1.1.2 - 9)$$

Note that the above development for the reduced effective width is only appropriate if the effective width formulation selected is load dependent. If a constant effective width model is selected (one based on \mathbf{b} rather than \mathbf{b}_e) then the effective width and reduced effective width are identical, i.e., $b_e = b_e'$.

A similar parameter will also exist with respect to the concept of effective breadth. However, with the assumption of effective breadth as defined by Equation (2.1.1.1 - 1), the effective breadth and the reduced or incremental effective breadth are identical.

2.1.2 Beam-Column Collapse - Type I

Consider a beam-column of length "a" as shown on Figure 2.1 - 2 loaded by a uniform lateral loading q (force per unit length) and an axial inplane force P and characterized by an initially distorted shape which is approximately represented by the function

$$w_0 \sin \frac{px}{a} \quad (2.1.2 - 1)$$

The behavior of this beam-column in terms of its additional lateral deflection w is described by the following differential equation,

$$EI \frac{d^2 w}{dx^2} - Pw = Pw_0 \sin \frac{px}{a} - M_e - \frac{1}{2} q(ax + x^2) \quad (2.1.2 - 2)$$

Since this beam-column is considered one of many repetitive elements (in the longitudinal direction) that are essentially similar in geometry and loading, the boundary conditions at its ends (where transverse web frames or bulkheads provide the support) are assumed clamped. With these assumptions, straightforward strength of materials methods can be used to determine the values of the bending moments (positive when the plate is in compression) at the beam-column's ends and center as well as its total ($w + w_0$) midpoint deflection. These moments and deflections are given by

$$M_e = \frac{I}{\tan I} \left[\frac{1}{4} q(a/I)^2 + \frac{2w_0 P}{p(1-a)} \right] - \frac{1}{4} q(a/I)^2 \quad (2.1.2 - 3)$$

for the ends and

$$M_c = \left[\frac{1}{4} q l (a/l)^2 + \frac{2lw_0P}{p(1-a)} \right] \sin l + \left[\frac{l}{\tan l} \left\{ \frac{1}{4} q (a/l)^2 + \frac{2w_0P}{p(1-a)} \right\} \right] \cos l - \frac{1}{4} q (a/l)^2 - \frac{w_0P}{(1-a)} \quad (2.1.2-4)$$

$$w_c = w_0 + \frac{a^2}{4EI l^2} \left[\left\{ \frac{1}{4} q \left(\frac{a}{l} \right)^2 + \frac{2Pw_0}{p(1-a)} \right\} \left[l \sin l - \frac{l(1-\cos l)}{\tan l} \right] \right] - \frac{1}{32} q \frac{a^4}{EI l^2} + \frac{aw_0}{1-a}$$

for the center. In these expressions the parameters α and λ are defined as

$$a = -\frac{Pa^2}{p^2 EI} \quad (2.1.2-5)$$

$$l = p \sqrt{\frac{a}{4}} \quad (2.1.2-6)$$

in which the moment of inertia I is computed assuming an effective breadth of plating equal to $b/2$. (Note, as previously indicated, the sign convention adopted makes compression negative.) The above expressions are assumed valid provided that neither M_e nor M_c as defined above exceeds the fully plastic moment for the cross section. If either of them does, then modifications of the above expressions must be employed. Since idealized materials with no strain hardening are assumed, neither M_e nor M_c can exceed the fully plastic moment, M_{pl} . In general two possibilities exist. The first is that the end moments have reached $\pm M_{pl}$ (depending on the direction of loading and of w_0), while the center moment remains below this limit. In this case, the moments and deflection are given by the expressions

$$M_e = \pm M_{pl} \quad (2.1.2-7)$$

$$M_c = \left[\pm M_{pl} + \frac{1}{4} q (a/l)^2 \right] (\tan l \sin l + \cos l) - \frac{1}{4} q (a/l)^2 - \frac{Pw_0}{1-a} \quad (2.1.2-8)$$

$$w_c = w_0 + \frac{a^2}{4EI l^2} \left[\pm M_{pl} + \frac{1}{4} q (a/l)^2 \right] \left[\frac{1-\cos l}{\cos l} \right] - \frac{1}{32} q \frac{a^4}{EI l^2} + \frac{aw_0}{1-a} \quad (2.1.2-9)$$

If the center moment reaches the fully plastic moment before the end moments do, the situation is described by the following,

$$M_e = \frac{1}{\cos I} \left[\begin{array}{l} \pm M_{pl} + \frac{1}{4} q(a/I)^2 (1 - \cos I - I \sin I) \\ + \frac{Pw_0}{1-a} \left(1 - \frac{2}{p} I \sin I\right) \end{array} \right] \quad (2.1.2 - 10)$$

$$M_c = \pm M_{pl}$$

$$w_c = w_0 + \frac{a^2}{4EI^2} \left[\begin{array}{l} \left\{ \frac{1}{4} q(a/I)^2 + \frac{2Pw_0}{p(1-a)} \right\} I \sin I \\ + \left\{ M_e + \frac{1}{4} q(a/I)^2 \right\} (\cos I - 1) \end{array} \right] - \frac{1}{32} q \frac{a^4}{EI^2} + \frac{aw_0}{1-a} \quad (2.1.2 - 11)$$

At some point, as the axial end displacement $-u$ continues to increase, the situation will be reached when both end and center moments are at their fully plastic values. When this occurs plastic hinges are assumed to form at the ends and center, and the beam-column is further deformed as rigid body motion of two bars linked together. In this case the total lateral deflection w_T of the midpoint of the beam-column is given approximately by

$$w_T = w_{cpl} \pm \frac{2a}{p} \left[\left(\frac{u}{a} \right)_{pl} - \frac{u}{a} \right]^{\frac{1}{2}} \quad (2.1.2 - 12)$$

where $(u/a)_{pl}$ is the value of axial end "strain" at which both M_e and M_c achieve their fully plastic value, (u/a) is the current value of this "strain," and w_{cpl} is the value of total lateral deflection (midpoint) corresponding to $(u/a)_{pl}$. In this situation, as the beam-column is further compressed, the lateral displacement w_T continues to grow. (Note that expression (2.1.2 - 12) is appropriate for small to moderate levels of lateral displacement. For large values this relationship must be modified.) Since the moment capacity at the three hinge locations is limited by their respective fully plastic values, equilibrium can be maintained only if the absolute value of the axial force P decreases in the correct proportion. This is referred to as "unloading." At one time the values of the fully plastic moment for M_e and M_c were assumed to remain constant, but recently there has been some indication that this assumption is overly conservative, particularly if moment-curvature data in the post collapse range is of interest. The relationship between lateral displacement and axial force for this unloading behavior is given by

$$P = \frac{\left(M_{epl} - M_{cpl} + \frac{1}{8} qa^2 \right)}{w_T} \quad (2.1.2 - 13)$$

in which the terminology indicates that the respective fully plastic values for M_e and M_c (with their appropriate signs) are used. Since the fully plastic moment values are functions of the axial loading, equation (2.1.2 - 13) must be solved in an iterative fashion.

Since the total cross section moment for the hull is computed by integrating the stress over its effective area, the axial load above is converted to edge stress s_e by simply dividing by the effective area A_e (based on the effective width b_e),

$$s_e = \frac{P}{A_e} \quad (2.1.2 - 14)$$

In this expression, it is assumed that the effective area remains constant at the value corresponding to the peak value of P , namely that value occurring when the end shortening is equal to $(u/a)_{pl}$ and both M_e and M_c have just achieved their fully plastic values. This assumption has been made recognizing that a more rigorous investigation is a potential subject for the future. In any case, the stress computed according to Equation (2.1.2 - 14) is the actual edge stress only if stiffener and plate are of the same material; if stiffener and plate materials differ, this stress is, in effect, a mean cross section stress. This is acceptable, since the integration for the computation of the longitudinal moment does not require that the precise state of stress in plate and stiffener be known in this case.

An estimate of the tangent modulus in the unloading region can be made by computing the derivative $d(s_e)/d(u/a)$. This parameter used to be used in the ULTSTR program to estimate the instantaneous neutral axis location; however, this is no longer the case. Consequently, for informational purposes only, a simple finite difference approach is considered adequate

$$E_t = \frac{(s_e)_i - (s_e)_{i-1}}{\Delta e} \quad (2.1.2 - 15)$$

in which the index i refers to the (curvature) increment number and Δe refers to the element's current strain increment.

From the expressions presented, it should be clear that the direction of w_0 (indicated by its sign) can have a significant influence on the behavior of the beam-column. Since there are not enough experimental data from actual naval vessels to clearly define the directional patterns to be expected for w_0 , the program assumes that the distortion occurs in its potentially most damaging direction, that is, in the same direction as the applied lateral load. If no lateral load is present, a positive value of w_0 is arbitrarily adopted, since, in this case, the value of the axial collapse load is independent of the sign of w_0 .

2.1.3 Beam-Column Collapse – Type II

In contrast with the Type I form of beam-column collapse, beam-columns can also collapse in a mode in which the lateral deflections alternate in directions from one bay to the next. In this case, the beam-column behaves more as if it were simply supported at the support points provided by the transverse web frames and bulkheads.

Consider first the situation where a straight column of length a is loaded only by an axial load. The elastic buckling load for the column is calculated according to the relationship

$$\mathbf{s}_{cre} = -\frac{\mathbf{p}^2 EI}{A_e a^2} \quad (2.1.3 - 1)$$

in which the moment of inertia I of the combined plate-stiffener cross section is based on the reduced effective width b_e' , whereas the effective area A_e is based on the effective width b_e .

If both plate and stiffener materials are identical, then the elastic buckling stress is modified using the tangent modulus as follows

$$\mathbf{s}_{cr} = \left(\frac{E_t}{E} \right) \mathbf{s}_{cre} \quad (2.1.3 - 2)$$

In this case, the tangent modulus is approximated using the Ostenfeld-Bleich quadratic parabola, namely

$$\frac{E_t}{E} = \frac{\mathbf{s}(\mathbf{s}_y - \mathbf{s})}{p_r(1 - p_r)\mathbf{s}_y^2} \quad (2.1.3 - 3)$$

Replacing \mathbf{s} by \mathbf{s}_{cr} above leads to the expression for the inelastic column buckling stress

$$\frac{\mathbf{s}_{cr}}{\mathbf{s}_y} = \begin{cases} \frac{\mathbf{s}_{cre}}{\mathbf{s}_y} & -\mathbf{s}_{cre} \leq p_r \mathbf{s}_y \\ -1 - p_r(1 - p_r) \frac{\mathbf{s}_{ym}}{\mathbf{s}_{cre}} & -\mathbf{s}_{cre} > p_r \mathbf{s}_y \end{cases} \quad (2.1.3 - 4)$$

in which p_r is the structural proportional limit ratio, the default for which in ULTSTR is 0.5. Since b_e and b_e' may be stress dependent (if that option was selected), the above equations must be solved in an iterative fashion, the cycles completed only when the stress value assumed in computing b_e and b_e' is "tolerably" close to the computed value of \mathbf{s}_{cr} .

If the plating and stiffener materials have different yield strengths, then the above computation procedure must be modified somewhat. In this case, the inelastic "modification" depends on which material has the higher yield stress. If the plating tensile yield, \mathbf{s}_{yp} , is greater than that of the stiffener, \mathbf{s}_{ys} , the inelastic column buckling stress is based on an area-weighted mean yield stress, \mathbf{s}_{ym} , in the following manner

$$\frac{(\mathbf{s}_{cr})_m}{\mathbf{s}_{ym}} = \begin{cases} \frac{\mathbf{s}_{cre}}{\mathbf{s}_{ym}} & -\mathbf{s}_{cre} \leq p_r \mathbf{s}_{ym} \\ -1 - p_r(1 - p_r) \left[\frac{\mathbf{s}_{ym}}{\mathbf{s}_{cre}} \right] & -\mathbf{s}_{cre} > p_r \mathbf{s}_{ym} \end{cases} \quad (2.1.3 - 5)$$

$$\text{where, } \mathbf{s}_{ym} = \frac{\mathbf{s}_{yp}bt + \mathbf{s}_{ys}A_s}{bt + A_s} \quad (2.1.3 - 6)$$

and A_s is the stiffener cross section area. Equation (2.1.3 - 5) is used only if the absolute value computed from $(\mathbf{s}_{cr})_m$ is less than \mathbf{s}_{ys} ; otherwise, the critical inelastic stress is set equal to $-\mathbf{s}_{ys}$. Since the current procedure allows differences only in yield strengths between plate and stiffener materials (no modulus variations are acceptable), values of $(\mathbf{s}_{cr})_m$ calculated from Equation (2.1.3 - 5) correspond to the stress levels in both plate and stiffener.

If $\mathbf{s}_{ys} > \mathbf{s}_{yp}$, the inelastic modification is made with respect to the higher yield stress material, namely

$$\frac{(\mathbf{s}_{cr})_{stiff}}{\mathbf{s}_{ys}} = \begin{cases} \frac{\mathbf{s}_{cre}}{\mathbf{s}_{ys}} & -\mathbf{s}_{cre} \leq p_r \mathbf{s}_{ys} \\ -1 - p_r(1 - p_r) \left(\frac{\mathbf{s}_{ys}}{\mathbf{s}_{cre}} \right) & -\mathbf{s}_{cre} > p_r \mathbf{s}_{ys} \end{cases} \quad (2.1.3 - 7)$$

Once the inelastic buckling stress is computed for the stiffener material using the above expressions, the inelastic stress level for the plating is computed simply from the condition of strain compatibility of the two components and the knowledge of the two materials' stress-strain curves. Except for these modifications, the iteration procedure for similar versus different materials is identical.

When the end shortening u/a reaches the value of the strain corresponding to the inelastic column buckling stress, the column is assumed to have buckled. As the shortening increases beyond this value, the edge stress on the column (and hence the axial load P) is assumed to remain at the inelastic buckling value while lateral deflections at the midpoint of the column grow according to the relationship

$$w = \frac{2a}{P} \sqrt{\left(\frac{u}{a} \right)_{cr} - \frac{u}{a}} \quad (2.1.3 - 8)$$

where $(u/a)_{cr}$ is the end shortening corresponding to \mathbf{s}_{cr} and (u/a) the current value of the shortening. (The origin of Equation (2.1.3 - 8) is in nonlinear slender column theory.) If P_w remains less than the fully plastic moment at the center of the beam (considering the appropriate signs of the moment), the axial inplane edge stress \mathbf{s}_e and hence the load P remains constant as previously indicated.

At some value of (u/a) the applied moment Pw will reach and then exceed the fully plastic value, M_{pl} , which is the maximum value the column can support. Because of the alternating nature of the buckling pattern, a hinge at the center is all that is required to cause the beam-column to behave like two rigid, linked bars. As the shortening continues to grow beyond this (u/a) value, unloading must occur if the column is to remain in equilibrium. Thus the absolute magnitude of the axial load will drop in accordance with the relationship

$$P = \pm \frac{M_{pl}}{w} \quad (2.1.3 - 9)$$

As with Type I beam-column collapse, the assumption is made that the effective area remains constant (at the value corresponding to $(u/a)_{cr}$ during the unloading process, but that the fully plastic moment M_{pl} will gradually increase as the axial loading drops. Thus, satisfying (2.1.3 - 9) must be done in an iterative fashion. For small to moderate levels of shortening (u/a) , the relationship between w and (u/a) defined by (2.1.3 - 8) is appropriate; but, for larger values, modifications to this expression must be made. Once this process has converged the edge stress (representing a mean value if plate and stiffener materials differ) is simply determined according to

$$s_e = \frac{P}{A_e} \quad (2.1.3 - 10)$$

The presence of lateral pressure is assumed not to influence the critical stress s_{cr} at which buckling in this mode occurs. Because of the alternating pattern of the lateral displacements the presence of small to moderate levels of pressure will alternately reinforce and resist the tendency for the beam-column to fail. What pressure can do, particularly at higher levels, however, is to force the column to fail by the Type I mode of failure (previously discussed). Thus when lateral pressure is present, the program will check both Type I and Type II failure modes and select the one which results in the lower peak collapse strength.

With regard to initial stiffener distortion, even when the user does not specifically define any initial distortion level, the empirical nature of the above solution effectively assumes some unknown, but finite, level of such distortion. If initial stiffener distortion is explicitly defined, however, the only impact on the above approach is to add the initial distortion value to the lateral deflection w as defined by equation (2.1.3 - 8). Thus, in this case, the effect is only seen in the post-buckling range.

It is pretty clear that, if large enough levels of initial stiffener distortion are present, some effect will be seen before the post-buckling range. Therefore, when initial stiffener distortion is explicitly defined, the ULTSTR program also evaluates an alternate failure theory for Type II beam-column failure. In this case the initial distortion is assumed to be represented approximately by the distribution

$$w_0 \sin \frac{px}{a} \quad (2.1.3 - 11)$$

where w_0 is the peak amplitude of lateral distortion. In this approach the beam-column's peak load is assumed to occur when

$$P(w + w_0) = M_{pl} \quad (2.1.3 - 12)$$

where, as before, M_{pl} is the cross-section's fully plastic moment and w is the additional lateral displacement due to the action of the axial load acting on the "slightly curved" beam-column. The midspan moment and total lateral displacement are defined by

$$M_c = P \left[\frac{w_0}{1 - \mathbf{a}} \right] \quad (2.1.3 - 13)$$

$$w + w_0 = \left[\frac{w_0}{1 - \mathbf{a}} \right] \quad (2.1.3 - 14)$$

In these expressions α is a "magnification factor" whose definition is as follows:

$$P_{crit} = \frac{\mathbf{p}^2 EI_{ef}}{a^2} \quad (2.1.3 - 15)$$

$$\mathbf{a} = \frac{P}{P_{crit}} \quad (2.1.3 - 16)$$

In the above expressions the moment of inertia I_{ef} is computed using an effective breadth of $b/2$. (Note also that in defining P_{crit} purely elastic properties are used, no correction is made for inelastic effects.) The edge stress is then computed in the usual manner,

$$\mathbf{s}_e = \frac{P}{A_e} \quad (2.1.3 - 17)$$

in which A_e is the effective cross section area based on an effective width formulation as discussed earlier. If a load-dependent effective width model is selected the computation of \mathbf{s}_e must be done in an iterative manner. If the cross section is made up of differing materials, the actual stresses in plating and stiffener may be different, in this case \mathbf{s}_e as defined above will in effect represent a "mean" edge stress.

As described above, when an initial stiffener distortion is specified explicitly, both beam-column failure models will be evaluated and the one yielding the lower peak collapse load will be used for all further calculations. For small initial distortion values, the original failure model will most likely be the appropriate model, but as distortions increase in magnitude, at some threshold value this will change in favor of the alternative model.

In any case, as with the type 1 failure mode, the tangent modulus in the unloading region can readily be estimated. This is now done as a simple finite difference,

$$E_t = \frac{(\mathbf{s}_e)_i - (\mathbf{s}_e)_{i-1}}{\Delta \mathbf{e}} \quad (2.1.3 - 18)$$

in which the index i refers to the strain increment number and $D\mathbf{e}$ the current strain increment for the element in question. At one time, E_t was used more frequently in the logic of the program but now is only effectively used for presentation purposes.

2.1.4 Stiffener Tripping Collapse

A comprehensive treatment of stiffener tripping (but not including post-buckling behavior) has been published by Adamchak J. (1979). For the development of the theories summarized below readers should consult that reference.

The elastic inplane tripping stress (denoted here by $-s_{cre}$) for a stiffener under inplane axial loading can be written in the form of a quadratic equation as follows,

$$-s_{cre}^2(k_2k_4 - k_6^2) - s_{cre}(k_1k_4 + k_2k_3 - 2k_5k_6) + (k_1k_3 - k_5^2) = 0 \quad (2.1.4 - 1)$$

in which the k_j 's are defined as

$$\begin{aligned} k_1 &= EI_z \left[\frac{m\mathbf{p}}{a} \right]^2 + 3 \frac{D_w}{d_c^3} \left[\frac{a}{m\mathbf{p}} \right]^2 (1 + 3R) \\ k_2 &= -A_s + d_c t_w \left[\frac{18}{35} + \frac{19}{140} R - \frac{3}{140} R^2 \right] \\ k_3 &= GJ + EI \left[\frac{m\mathbf{p}}{a} \right]^2 + 3 \frac{D_w}{d_c} \left[\frac{a}{m\mathbf{p}} \right]^2 \left[1 + \frac{R}{3} \right] \\ k_4 &= -I_{ps} + d_c^3 t_w \left[\frac{11}{35} + \frac{1}{84} R - \frac{1}{420} R^2 \right] \\ k_5 &= -\frac{3D_w}{d_c^2} \left[\frac{a}{m\mathbf{p}} \right]^2 (1 + R) \\ k_6 &= d_c^2 t_w \left[\frac{3}{35} - \frac{17}{420} R + \frac{1}{140} R^2 \right] \end{aligned} \quad (2.1.4 - 2)$$

Many of the parameters appearing in Equation (2.1.4 - 2) are defined on Figure 2.1.4 - 1. The rest are defined in Equation 2.1.4 - 3.

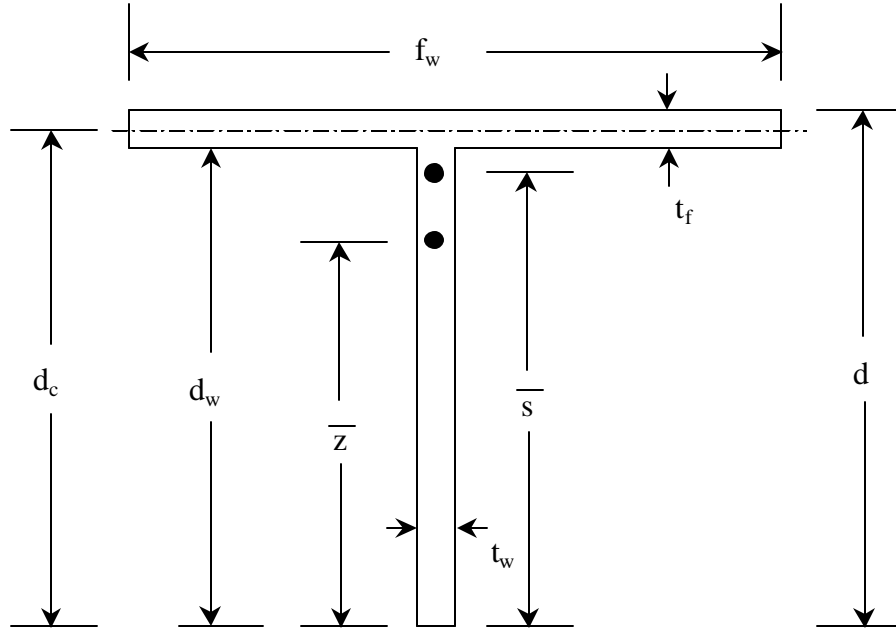


Figure 2.1.4 – 1: Geometrical Tripping Parameters for Tee Stiffeners

$$I_z = \frac{1}{12}(t_f f_w^3 + d_w t_w^3)$$

$$\bar{s} = \frac{1}{2} \left[d_w + \frac{d_w + t_f}{1 + (d_w/t_f)(t_w/f_w)^3} \right] \approx d_c$$

$$\Gamma = \frac{1}{36} \left(t_w^3 d_w^3 + \frac{1}{4} t_f^3 f_w^3 \right) \quad (2.1.4 - 3)$$

$$J = \frac{1}{3} (d_w t_w^3 + f_w t_f^3)$$

$$I_t = \frac{1}{3} t_w d_w^3 + f_w t_f \left(d_c^2 + \frac{1}{12} t_f^2 \right)$$

$$I_p = I_t + I_z$$

$$\bar{z} = \left[\frac{\frac{1}{2} t_w d_w^2 + f_w t_f d_c}{t_w d_w + f_w t_f} \right]$$

$$D_w = \frac{Et_w^2}{12(1-\nu_s^2)}$$

$$A_s = d_w t_w + f_w t_f$$

$$I_{ps} = I_p + A_s d_c^2 - 2A_s d_c \bar{z}$$

$$G = \frac{E}{2(1+\nu_s)}$$

$m =$ Tripping Mode Number

The parameter R is a dimensionless rotational restraint parameter that indicates the amount of rotational restraint that the plating to which the stiffener is attached provides to resist tripping. This parameter is defined as

$$R = \frac{\frac{Cd_c}{4D_w}}{1 + \frac{Cd_c}{4D_w}} \quad (2.1.4 - 4)$$

in which the parameter C is the rotational spring constant (in units of moment/rad/length) of the supporting plating. The formulation for C recommended in Adamchak (1979) is:

$$C = \begin{cases} C_0 \left[1 - \frac{\mathbf{s}_e}{\mathbf{s}_{pb}} \right] & \mathbf{s}_e > \mathbf{s}_{pb} \\ 0 & \mathbf{s}_e \leq \mathbf{s}_{pb} \end{cases} \quad (2.1.4 - 5)$$

in which \mathbf{s}_{pb} is the plate buckling stress

$$\mathbf{s}_{pb} \begin{cases} \mathbf{s}_{pbe} \\ -\mathbf{s}_{yp} \left[1 - \frac{1}{4} \frac{\mathbf{s}_{yp}}{(-\mathbf{s}_{pbe})} \right] \end{cases} \quad \begin{cases} -\mathbf{s}_{pbe} \leq 0.5\mathbf{s}_{yp} \\ -\mathbf{s}_{pbe} > 0.5\mathbf{s}_{yp} \end{cases} \quad (2.1.4 - 6)$$

based on the classical elastic plate buckling stress

$$\mathbf{s}_{pbe} = \frac{4\mathbf{p}^2 D}{tb^2} \quad (2.1.4 - 7)$$

and C_0 is the unloaded rotational spring constant. The recommended relationship for C_0 is

$$C_0 = \frac{1}{2} \frac{\mathbf{p}^2 D}{b} \left[1 + \left(\frac{b}{a} \right)^2 \right]^2 \quad (2.1.4 - 8)$$

in which the parameter D , also appearing in the expression for \mathbf{s}_{pbe} , refers to the flexural rigidity of the plating. Hence

$$D = \frac{Et^3}{12(1-\mathbf{n}_p^2)} \quad (2.1.4 - 9)$$

The elastic tripping stress calculated according to Equation (2.1.4 - 1) is corrected for "inelastic effects" in a fashion similar to that for beam-column buckling, namely

$$\frac{\mathbf{s}_{cr}}{\mathbf{s}_{ys}} = \begin{cases} \frac{\mathbf{s}_{cre}}{\mathbf{s}_{ys}} & -\mathbf{s}_{cre} \leq p_r \mathbf{s}_{ys} \\ -1 + p_r (1 - p_r) \frac{\mathbf{s}_{ys}}{-\mathbf{s}_{cre}} & -\mathbf{s}_{cre} > p_r \mathbf{s}_{ys} \end{cases} \quad (2.1.4 - 10)$$

in which p_r is the structural proportional limit ratio (default value = 0.5).

Since the rotational resistance provided by the plating is load dependent, the solution for \mathbf{s}_{cr} must be carried out in an iterative fashion. Convergence is achieved when the computed value of \mathbf{s}_{cr} from Equation (2.1.4 - 10) is within an accepted tolerance of the value of \mathbf{s}_e assumed in Equation (2.1.4 - 5).

In the theoretical development of the tripping Equation (2.1.4 - 1), the mode number m , strictly speaking, should take on only integer values. However, one may notice that, in the expressions for the coefficients k_j , the mode number always occurs in combination with the panel or stiffener length, a . Thus it is possible to define an effective length for tripping, labeled a_{et} , which is equal to a/m , and which can be used to approximate various degrees of rotational restraint in the plane of the stiffener web provided by the connecting structure at the stiffener's ends. For example, the effective length is sometimes defined with $m = 2$, that is, the effective length assumed for tripping is equal to $a/\sqrt{2}$. This value of "m" approximates a boundary condition that is neither fully fixed nor fully simply supported. For the hull collapse program, it is reasonable (as a rough guide) to assume values for a_{et} in the range a to $a/\sqrt{2}$ when no ILS (Intermediate Lateral Supports) are present, and appropriately smaller values when such supports are present. The specific values depend on the number and location of the supports.

When lateral pressure is present, the axial tripping stress is modified to reflect its influence. The beam is treated as uniformly loaded with clamped end supports. The angle of rotation, \mathbf{b} , about its line of attachment to the plating is assumed in the form

$$\mathbf{b} = \mathbf{b}_0 \left[K \sin \frac{px}{a_{et}} + (K - 1) \sin \frac{3px}{a_{et}} \right] \quad (2.1.4 - 11)$$

in which the (initially) unknown coefficient, K , controls the relative mix of the first and third mode shapes. The effect of the rotational resistance provided by the plating is ignored in dealing with uniform pressure loading because experience with the solution has shown it to be overly optimistic when rotational restraint is included. This is a conservative decision that can be at least partially justified on the grounds that: (1) the amount of rotational restraint present is frequently small or zero because of the value of s_{cr} relative to s_{pb} ; and (2) critical tripping pressures are usually quite high because of the relatively small regions of compressive stress in the stiffener.

The solution for the critical lateral pressure for elastic tripping can be presented in the form

$$q_{cre} = - \frac{12IGJ}{sa^2} \frac{H_n(K)}{F_n(K)} \quad (2.1.4 - 12)$$

where I is the vertical moment of inertia of the plate-beam combination (with an effective breadth of $b/2$), and s is a geometrical parameter defined as

$$s = \frac{1}{4} \left[t_w d_w^4 - 4 \left(h - \frac{1}{2} t \right) I_p + 4 d_c \left(f_w t_f d_c^2 + \frac{1}{12} t_f f_w^3 \right) \right] \quad (2.1.4 - 13)$$

where h is the height of the neutral axis of the plate-beam combination from the midplane of the plating, and $H_n(K)$ and $F_n(K)$ are quadratic functions in the coefficient K . Defining, in essence, a "modified" mode number

$$n = \frac{a}{a_{et}} \quad (2.1.4 - 14)$$

these functions are defined as follows

$$H_n(K) = \left[n^2 K^2 + (n+2)^2 (K-1)^2 + \left(\frac{p}{a} \right)^2 \left\{ n^4 K^2 + (n+2)^4 (K-1)^2 \right\} \left[\frac{E}{GJ} \right] \left(I_z^{-2} + \Gamma \right) \right] \quad (2.1.4 - 15)$$

$$F_n(K) = -\frac{3}{p^2} K^2 + \frac{6}{p^2} n(n+2) \left\{ 1 + \frac{1}{(n+1)^2} \right\} K(1-K) - \frac{3}{p^2} (K-1)^2 - \frac{6d_w}{p^2 s} \left[f_w t_f^2 \left(d_c - h + \frac{1}{2} t \right) + b_e t^2 h \right] \left[K^2 + (K-1)^2 \right] \quad (2.1.4 - 16)$$

Adamchak, J. (1979) describes in complete detail how the appropriate value of K is determined for use in Equations (2.1.4 - 12), (2.1.4 - 15), and (2.1.4 - 16).

With q_{cre} determined, the critical elastic tripping stress \mathbf{s}_{cre} computed from Equation (2.1.4 - 1) is modified as follows

$$(\mathbf{s}_{cre})_{q \neq 0} = (\mathbf{s}_{cre})_{q=0} \left[1 - \frac{q}{q_{cre}} \right] \quad (2.1.4 - 17)$$

This stress, which now includes the effects of pressure, is then used in exactly the same fashion (Equation (2.1.4 - 10)) in determining the inelastic axial tripping stress \mathbf{s}_{cr} (including the iteration process) as previously described.

The approach to handling tripping in the post-buckling regions is very similar to that for beam-column buckling. Once tripping has occurred, the axial force in the stiffener is assumed to remain constant, while the sideways deflection of the stiffener increases with increasing end shortening. Denoting the sideways deflection of the flange by v , its relationship to the end shortening (by analogy with slender column theory) is hypothesized by

$$v = \frac{2a_{et}}{p} \sqrt{\left(\frac{u}{a} \right)_{cr} - \frac{u}{a}} \quad (2.1.4 - 18)$$

where $(u/a)_{cr}$ in this case corresponds to the critical end shortening associated with \mathbf{s}_{cr} for stiffener tripping. As long as $P_s (vz/d_c)$ (the subscript s indicates the load in the stiffener) is less than the fully plastic moment of the stiffener alone about its web plane, the constant load, constant stress behavior will continue. When $P_s (vz/d_c)$ exceeds this value, however, a plastic hinge forms in the stiffener and unloading will occur (due to the alternating nature of the lateral tripping deflections). The load in the stiffener then becomes

$$P_s = \frac{\pm M_{pl}}{v(z/d_c)} \quad (2.1.4 - 19)$$

where in this case M_{pl} refers to the horizontal fully plastic moment. As with the beam-column failure modes, P_s must be determined in an iterative fashion since the fully plastic moment is axial load dependent.

Although the load in the stiffener P_s (and its corresponding stress \mathbf{s}_{es}) peaks at \mathbf{s}_{cr} and then decreases, the edge stress in the plating, designated here by \mathbf{s}_{ep} , will continue to grow until it reaches its yield value, \mathbf{s}_{yp} . (Should the panel fail in a beam-column mode, either Type I or II, before the plate yield value is achieved, this is handled by the appropriate theories previously discussed.) Thus the total load in the cross section is given by

$$P_T = P_p + P_s = \mathbf{s}_{ep} b_e t + \mathbf{s}_{es} A_s \quad (2.1.4 - 20)$$

where the effective width b_e is calculated in accordance with the theories presented in section 2.1.1. Although the effective width b_e decreases as the axial stress \mathbf{s}_{ep} increases (that is, if a load dependent effective width option is being used), generally the net effect will be for the load in the plate to continue to increase until its yield stress value is reached. However, at the same time the load in the stiffener will be decreasing such that at some point the total load P_T will hit its peak value. This may not occur until the plate stress reaches yield or it may occur sooner, but in any case this peak load is the collapse load for the plate-stiffener in tripping, and it is this load which the ULTSTR program uses to determine the preferred or critical buckling mode.

Once the plating has reached its yield stress, its effective width b_e is assumed to continue to decrease as further axial strain is applied. (Were this not the case, the load in the plating would never decrease.) In order to do this, a "pseudo-stress" is defined as follows,

$$(\mathbf{s}_e)_{pseudo} = \mathbf{e} \left(\frac{\mathbf{s}_{yp}}{\mathbf{e}_{ydp}} \right) \quad (2.1.4 - 21)$$

in which \mathbf{e}_{ydp} is the yield strain of the plate material and \mathbf{e} is the cumulative strain in the plate. This pseudo-stress is then used in the appropriate effective width expressions as described in section 2.1.1. Of course, this is only relevant if load dependent effective models have been chosen.

If the effective edge stress \mathbf{s}_e is defined as P_T/A_s , the tangent modulus E_t can be estimated (for informational purposes only) from the finite difference relationship

$$E_t = \frac{(\mathbf{s}_e)_i - (\mathbf{s}_e)_{i-1}}{\Delta \mathbf{e}} \quad (2.1.4 - 22)$$

in which the index i refers to the curvature increment number and $\Delta \mathbf{e}$ the strain increment for the particular element resulting from the applied curvature.

2.1.5 Fully Plastic Moment

2.1.5.1 Vertical Bending Moment

The expressions for the fully plastic moment are presented below. They are valid for plate-beam combinations of the same material, as well as those in which the plating and stiffeners are made of materials having different yield strengths. The calculations are made on the basis of an equivalent section, assumed to be totally of one material. In the case of the stiffener, the thickness of the plating remains unchanged, but the actual width of the material, assumed to be effective, b_{ep1} , is replaced by an equivalent width, b_{eq} . Refer to Figure 2.1.5.1 – 1, below.

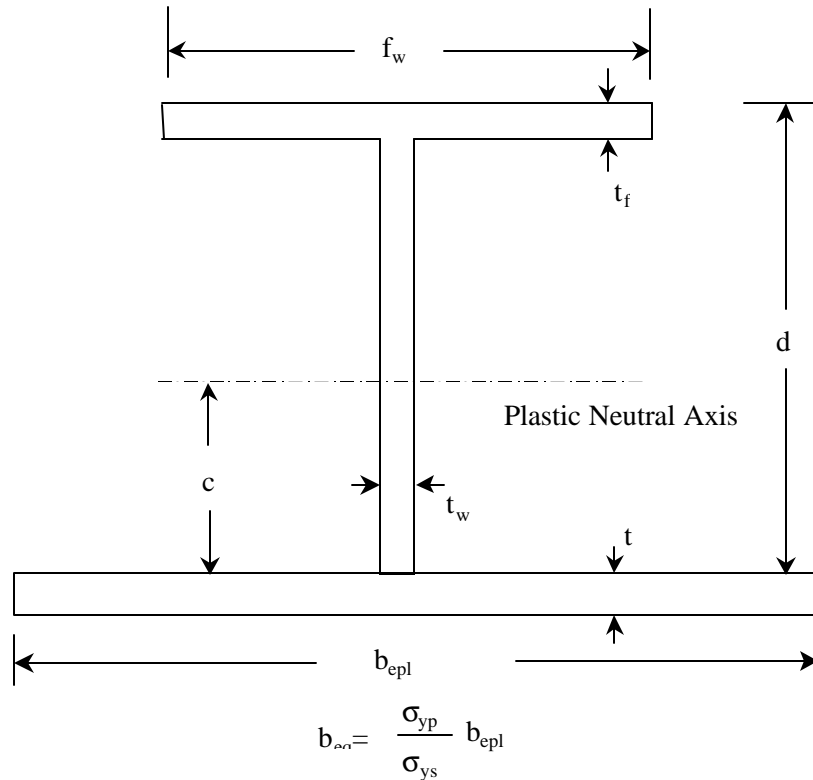


Figure 2.1.5.1 – 1: Geometrical Parameters for Fully Plastic Moment

To facilitate the writing of the expressions which follow, some shorthand notation is introduced. The parameters defined are:

Plate Area: $A_p = b_{eq} t$

Web Area: $A_w = (d - t_f) t_w = d_w t_w$

Flange Area: $A_f = f_w t_f$

Mean Depth: $d_m = \frac{1}{2}(d + t)$

The expressions that follow are based on the assumption that the total axial load, P , is known, and that the fully plastic moment in the presence of this load is what is desired. In this case, the knowledge of P and the geometry of the cross section completely define the location of the plastic neutral axis c above the outer surface of the plate, and thus the value of the fully plastic moment, M_{pl} . However, three possible locations for c must be considered, each of which results in unique expressions for c and M_{pl} .

- Plastic Neutral Axis in the Plate ($0 \leq c \leq t$)

$$c = \frac{[A_p + A_w + A_f - (P / \mathbf{s}_{ys})]}{2b_{eq}}$$

$$M_{pl} = \mathbf{s}_{ys} \left[b_{eq} c \left(d + t - \frac{1}{2} c - \frac{1}{2} b_{eq} \frac{c}{f_w} \right) \right]$$

for $b_{eq} c \leq A_f$

$$M_{pl} = \mathbf{s}_{ys} \left[b_{eq} c \left(d_m - \frac{1}{2} c \right) + s t_w \left(d_w + t - \frac{1}{2} s - d_m \right) + A_f \left(d_w + t + \frac{1}{2} t_f - d_m \right) \right]$$

for $s = \frac{b_{eq} c - A_f}{t_w}$

and $A_f \leq b_{eq} c \leq A_f + A_w$

$$M_{pl} = \mathbf{s}_{ys} \left[b_{eq} c \left(d_m - \frac{1}{2} c \right) + b_{eq} s \left(t - \frac{1}{2} s - d_m \right) + A_w \left(t + \frac{1}{2} d_w - d_m \right) + A_f \left(d_w + t + \frac{1}{2} t_f - d_m \right) \right]$$

for $s = \frac{b_{eq} c - A_f - A_w}{b_{eq}}$

and $A_f + A_w \leq b_{eq} c \leq A_f + A_w + (t - c) b_{eq}$

$$M_{pl} = \mathbf{s}_{ys} \left[b_{eq} s \left(d_m - \frac{1}{2} s \right) + b_{eq} (t - c) \left(\frac{1}{2} t + \frac{1}{2} c - d_m \right) + A_w \left(t + \frac{1}{2} d_w - d_m \right) + A_f \left(d_w + t + \frac{1}{2} t_f - d_m \right) \right]$$

for $s = \frac{A_f + A_w + b_{eq} (t - c)}{b_{eq}}$

and $(t - c) b_{eq} + A_w + A_f \leq b_{eq} c$

• Plastic Neutral Axis in the Web ($t \leq c \leq d_w + t$)

$$c = \frac{A_f + A_w - A_p + 2tt_w - (P/s_{ys})}{2t_w}$$

$$M_{pl} = \mathbf{s}_{ys} \left[A_p \left(d_m - \frac{1}{2}t \right) + t_w(t-c) \left(\frac{1}{2}c + \frac{1}{2}t - d_m \right) + f_w s \left(d + t - \frac{1}{2}s - d_m \right) \right]$$

$$\text{for } s = \frac{A_p + t_w(c-t)}{f_w}$$

$$\text{and } A_p + t_w(c-t) \leq A_f$$

$$M_{pl} = \mathbf{s}_{ys} \left[A_p \left(d_m - \frac{1}{2}t \right) + t_w(t-c) \left(\frac{1}{2}c + \frac{1}{2}t - d_m \right) + st_w \left(d_w + t - \frac{1}{2}s - d_m \right) + A_f \left(d_w + t + \frac{1}{2}t_f - d_m \right) \right]$$

$$\text{for } s = \frac{A_p + t_w(c-t) - A_f}{t_w}$$

$$\text{and } A_f \leq A_p + t_w(c-t) \leq A_f + t_w(d_w - c + t)$$

$$M_{pl} = \mathbf{s}_{ys} \left[A_p \left(d_m - \frac{1}{2}t \right) + t_w s \left(d_m - t - \frac{1}{2}s \right) + t_w(d_w - c + t) \left(\frac{1}{2}(c + d_w + t) - d_m \right) + A_f \left(d_w + t + \frac{1}{2}t_f - d_m \right) \right]$$

$$\text{for } s = \frac{A_f - A_p + t_w(d_w - c + t)}{t_w}$$

$$\text{and } A_f + t_w(d_w - c + t) \leq A_p + t_w(c-t) \leq A_f + d_w t_w$$

$$M_{pl} = \mathbf{s}_{ys} \left[b_{eq} s \left(d_m - \frac{1}{2}s \right) + t_w(d_w - c + t) \left(\frac{1}{2}(d_w + t + c) - d_m \right) + A_f \left(d + t - \frac{1}{2}t_f - d_m \right) \right]$$

$$\text{for } s = \frac{A_f + t_w(d_w - c + t)}{b_{eq}}$$

$$\text{and } A_f + t_w d_w \leq A_p + t_w(c-t)$$

- Plastic Neutral Axis in the Flange ($d_w + t \leq c \leq d_w + t + t_f$)

$$c = \frac{A_f - A_p - A_w + 2f_w(d_w + t) - (P/s_{ys})}{2f_w}$$

$$M_{pl} = \mathbf{s}_{ys} \left[A_p \left(d_m - \frac{1}{2}t \right) + A_w \left(d_m - t - \frac{1}{2}d_w \right) + f_w(d_w + t - c) \left(\frac{1}{2}(c + d_w + t) - d_m \right) + f_w s \left(d + t - \frac{1}{2}s - d_m \right) \right]$$

$$\text{for } s = \frac{A_p + A_w + f_w(c - d_w - t)}{f_w}$$

$$\text{and } A_p + A_w + f_w(c - d_w - t) \leq A_f + f_w(d_w + t - c)$$

$$M_{pl} = \mathbf{s}_{ys} \left[A_p \left(d_m - \frac{1}{2}t \right) + A_w \left(d_m - t - \frac{1}{2}d_w \right) + f_w s \left(d_m - d_w - t - \frac{1}{2}s \right) + f_w(d + t - c) \left(\frac{1}{2}(d + t + c) - d_m \right) \right]$$

$$\text{for } s = \frac{f_w(d + t - c) - A_p - A_w}{f_w}$$

$$\text{and } A_f + f_w(d_w + t - c) \leq A_p + A_w + f_w(c - d_w - t) \leq A_f$$

$$M_{pl} = \mathbf{s}_{ys} \left[A_p \left(d_m - \frac{1}{2}t \right) + t_w s \left(d_m - t - \frac{1}{2}s \right) + f_w(d + t - c) \left(\frac{1}{2}(d + t + c) - d_m \right) \right]$$

$$\text{for } s = \frac{f_w(d + t - c) - A_p}{t_w}$$

$$\text{and } A_f \leq A_p + A_w + f_w(c - d_w - t) \leq A_f + A_w$$

$$M_{pl} = \mathbf{s}_{ys} \left[b_{eq} s \left(d_m - \frac{1}{2}s \right) + f_w(d + t - c) \left(\frac{1}{2}(d + t + c) - d_m \right) \right]$$

$$\text{for } s = (f_w / b_{eq})(d + t - c)$$

$$\text{and } A_w + A_f \leq A_p + A_w + f_w(c - d_w - t)$$

The above expressions employ the sign convention adopted generally, that is, tension is positive and compression negative. If a positive value of \mathbf{s}_{ys} is used in the above (meaning tension in the stiffener flange), the resulting moment, M_{pl} , will be positive and will cause compression in the plating.

2.1.5.2 Horizontal Bending Moment

In the prediction of collapse due to stiffener tripping, the horizontal (or lateral) fully plastic moment for the stiffener alone is required. As in the previous case, it is assumed that the axial load (in this case not the total load but that in the stiffener, P_s) is known and that the fully plastic moment in the presence of this load is desired. This leads to the following:

- Plastic Neutral Axis in the Web ($|c| \leq t_w/2$)

$$c = -\frac{1}{2} \frac{P_s}{\mathbf{s}_{ys} (d_w + t_f)}$$

$$M_{pl} = \mathbf{s}_{ys} \left[d_w \left(\frac{1}{4} t_w^2 - c^2 \right) + t_f \left(\frac{1}{4} f_w^2 - c^2 \right) \right]$$

- Plastic Neutral Axis in the Web ($t_w/2 \leq c \leq f_w/2$)

$$c = \frac{1}{2t_f} \left[-A_w + \left| \frac{P_s}{\mathbf{s}_{ys}} \right| \right]$$

$$M_{pl} = \mathbf{s}_{ys} t_f \left[\frac{1}{4} f_w^2 - c^2 \right]$$

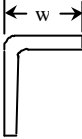
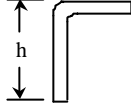
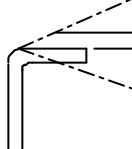
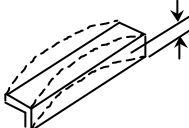
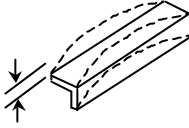
If the sign of c , representing the side of the web on which the plastic neutral axis is located, were significant, there would need to be two distinct expressions for c for the case "outside of the web." Since only the value of the moment is required by the program, the expression above, which effectively gives the absolute value of neutral axis location c , is sufficient.

3. Distortion Effects – Panel Response

The mathematical expressions to define local panel response described earlier must be modified to reflect distortion effects before the global impact on hull girder strength can be addressed. Because of the large matrix of solutions that must be rigorously addressed before recommendations can be made for tolerance limits, cost and flexibility considerations dictate the methodology for determining distorted component response. Eventually empirical expressions can be developed to describe distorted component response based on strength of materials approaches, experimental results and numerical approaches such as the finite element method. However, these expressions don't currently exist and there is not enough information available to develop them. The most effective approach to determine local panel strength dependence on distortion amplitudes hinges on the finite element method, which allows the flexibility for rapid geometric modifications to perform parametric analyses.

Current tolerance limits are determined by various societies and are largely based on construction limitations. Table 3-1 is an example of the tolerance limits for steel hull construction as determined by the American Society of Testing and Materials (ASTM) Designation: F 1053- 87.

Table 3 - 1: Typical ASTM Tolerance Ranges

Flanged Plate Longitudinal	Standard Range	Tolerance Limits	Corrective Action
<p>Breadth of Flange</p> 	±1/8" (3)mm	+1/4" (6)mm -3/16" (5)mm	Trim to correct width, or build up with weld, not to exceed thickness/2.
<p>Height of Longitudinal</p> 	±1/8" (3)mm	+1/4" (6)mm -3/16" (5)mm	
<p>Angle between Flange and Web</p> 	±1/8" (4)mm $\left(\frac{3}{100}\right)$	±3/16" (4)mm $\left(\frac{5}{100}\right)$	
<p>Sweep in 400 (10) of Length</p> 	±3/8" (10)mm	±1" (25)mm	
<p>Camber in 400 (10) of Length</p> 	±3/8" (10)mm	±1" (25)mm	

Eventually, the impact of each type of distortion on the failure modes of the local component must be determined. Using the finite element method, a sensitivity analysis relating the component response to various distortions can be determined as parameters such as stiffener length, web height, flange width, plating thickness, etc. are varied. Although this sensitivity analysis is outside the scope of the current effort, the distortion believed to play the predominant mode in both tripping behavior and buckling behavior was investigated. The effect of other distortions on the various failure modes was not considered at the present time, but should certainly be considered in future investigations.

3.1 Tripping

Non-linear finite element models were used to determine the effect of distortions on tripping behavior. The finite element code, ABAQUS, was selected to perform the analysis. To demonstrate the methodology, stiffeners with large depth to flange width ratios were chosen, as they are considered the most susceptible to tripping failure. The stiffener spacing selected to demonstrate the methodology was 24 inches. The models were loaded in the axial direction along the neutral axis and restrained against vertical motion and rotations about the longitudinal axis at the ends. At the reaction end, the webs were restrained against rotation about the transverse axis and the plate was not allowed to rotate about the vertical axis. The side edges of the plate were restrained from rotational movement about the longitudinal axis. Bar elements with high inertial properties were used and proved quite effective for distributing the load along the loaded end and maintaining a straight, loaded flange.

Out of plane distortion of the stiffener web will have the most severe adverse effect on load carrying capacity of a plate-stiffener combination. It was selected to demonstrate the methodology in the tripping failure mode. A computer program to rapidly generate deformed panel geometries was developed for this purpose. In the deformed geometry, the stiffener web has a sinusoidal shape with the peak amplitude at mid-span of the flange-web intersection. In future studies, it will be necessary to model other distortions to determine their effect on panel capacity relative to the tripping failure mode, but it is unlikely other distortion effects will significantly degrade tripping capacity.

The nonlinear geometry finite element solution technique using linear material properties was used to perform the analysis. Results of the analysis were used to incorporate distortion effects on the load shortening curves in the tripping failure mode. This was accomplished by monitoring stress increases at the flange edge at stiffener midspan as distortion magnitudes increase and developing distortion amplification factors based on the results. The contour plot in Figure 3.1 - 1 clearly presents the regions of interest and the magnitudes of stress increase exhibited in the finite element analysis.

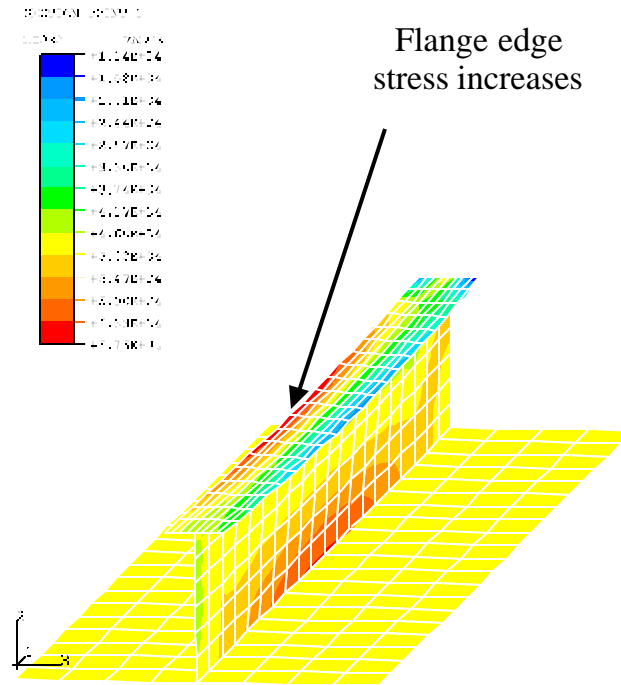


Figure 3.1 - 1: Tripping Stress Amplification

Based on the results of the finite element analysis, the ULTSTR load shortening curves were updated to account for the reduced load carrying capacity of the distorted structure. To illustrate the effect of this type of distortion on component response, several plate-stiffener combinations were analyzed using ULTSTR. To analyze the response of individual stiffeners, ULTSTR allows the user to load the structure axially rather than using the traditional moment-curvature approach. The midspan distortion was varied between 3.0% and 10.0% of the overall stiffener depth as the stiffeners were axially loaded. The various distorted stiffener performances are shown in Figures 3.1 – 2 through 3.1 – 13.

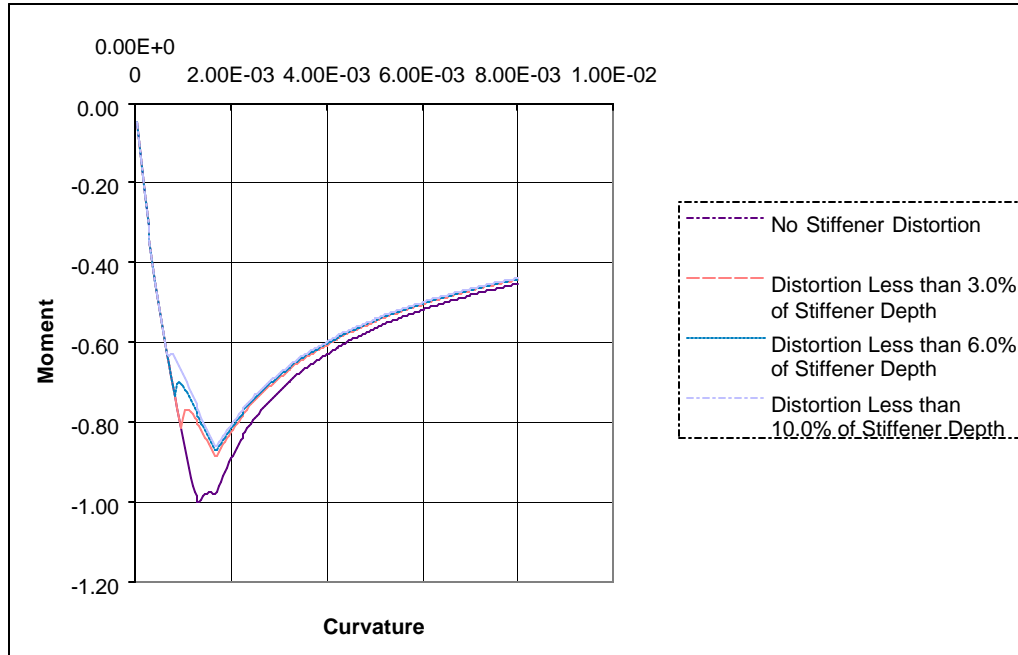


Figure 3.1 - 2: 6x4x7 HS Stiffener on 12.75# Plate

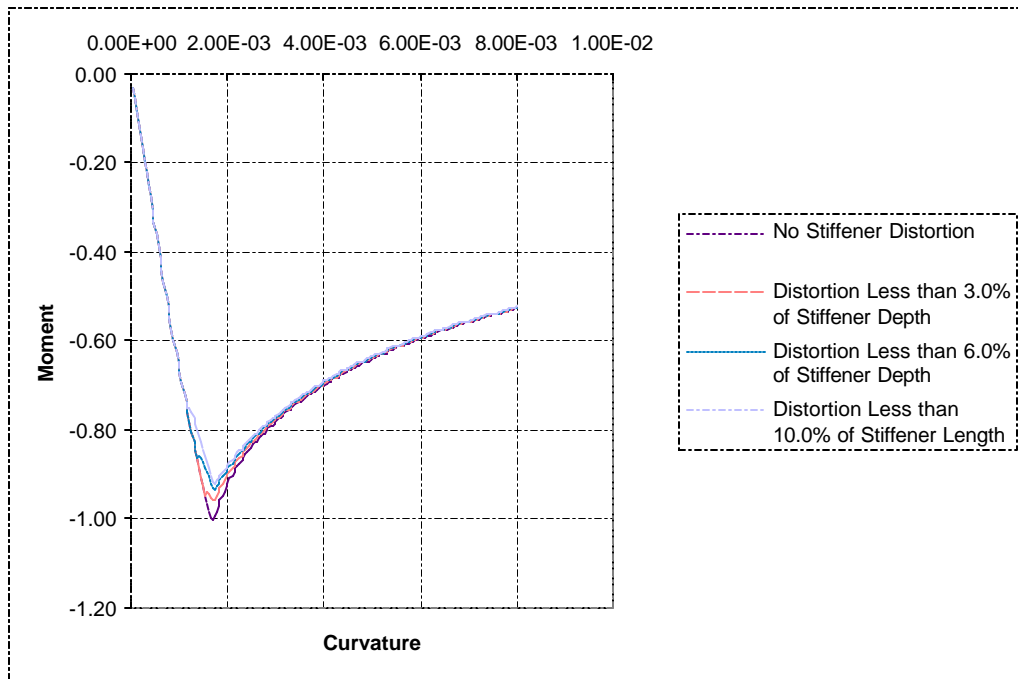


Figure 3.1 - 3: 6x4x7 HS Stiffener on 25.5# Plate

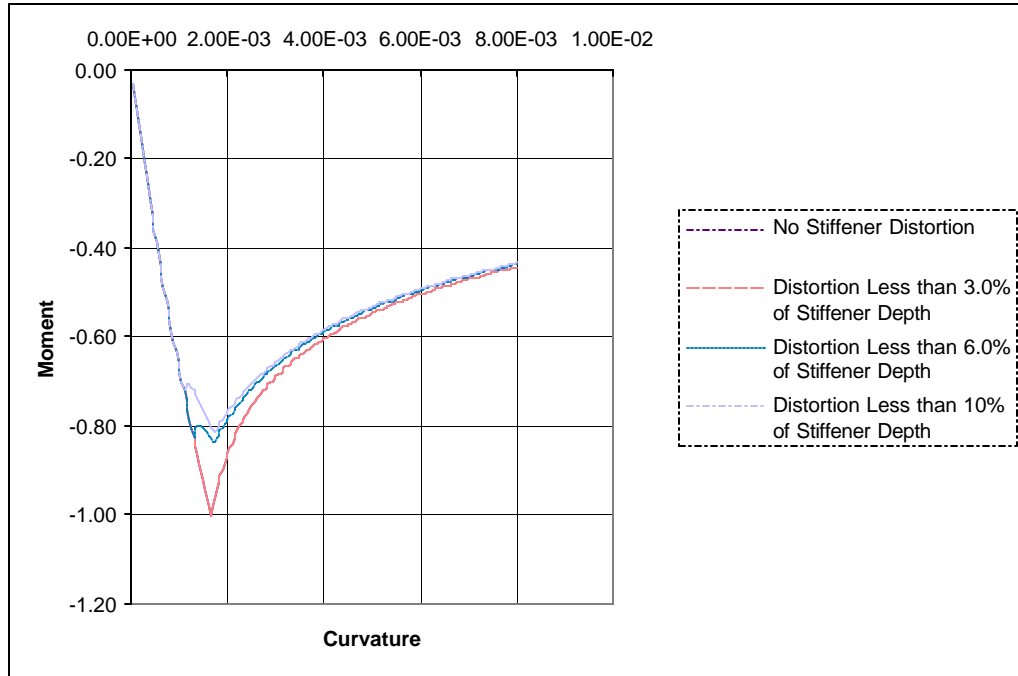


Figure 3.1 - 4: 6x4x11 HS Stiffener on 20.4# Plate

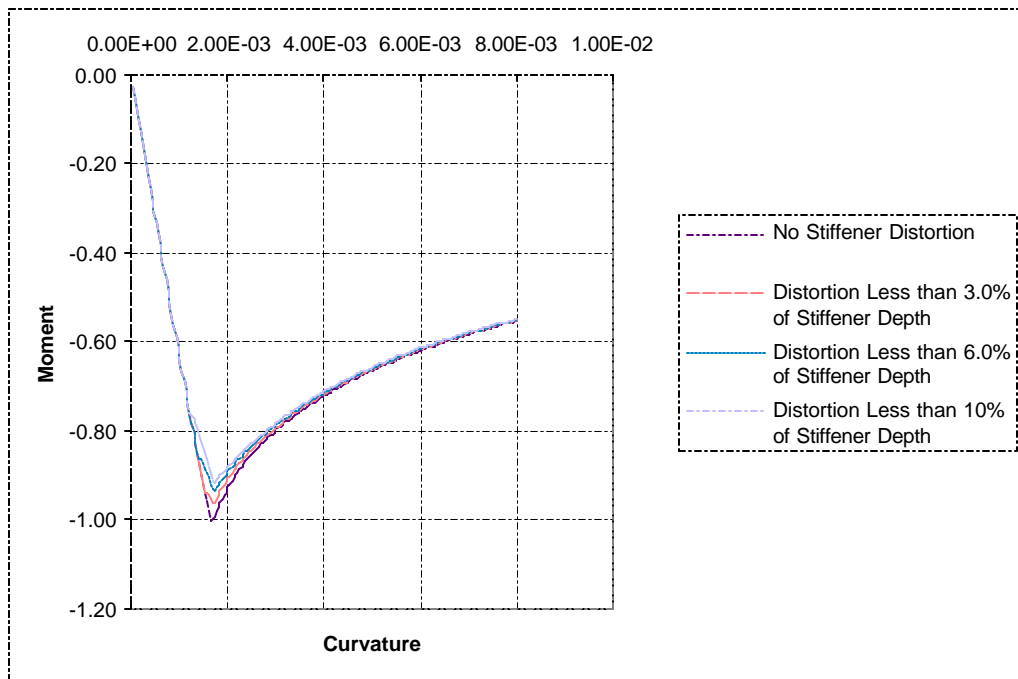


Figure 3.1 - 5: 6x4x11 HS Stiffener on 30.6# Plate

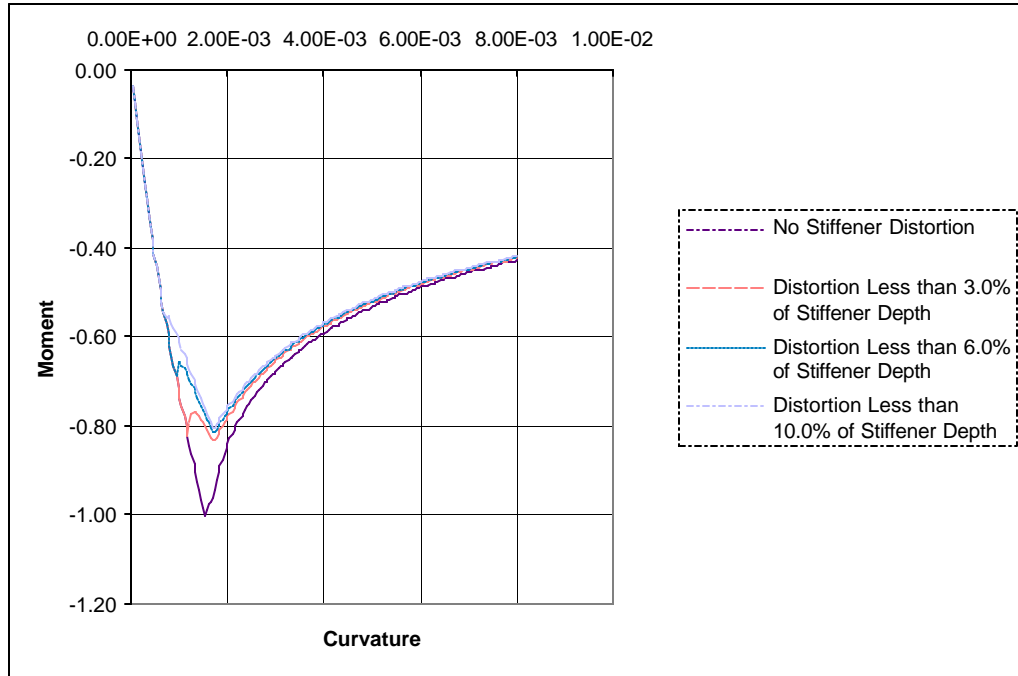


Figure 3.1 - 6: 8x4x10 HS Stiffener on 15.3# Plate

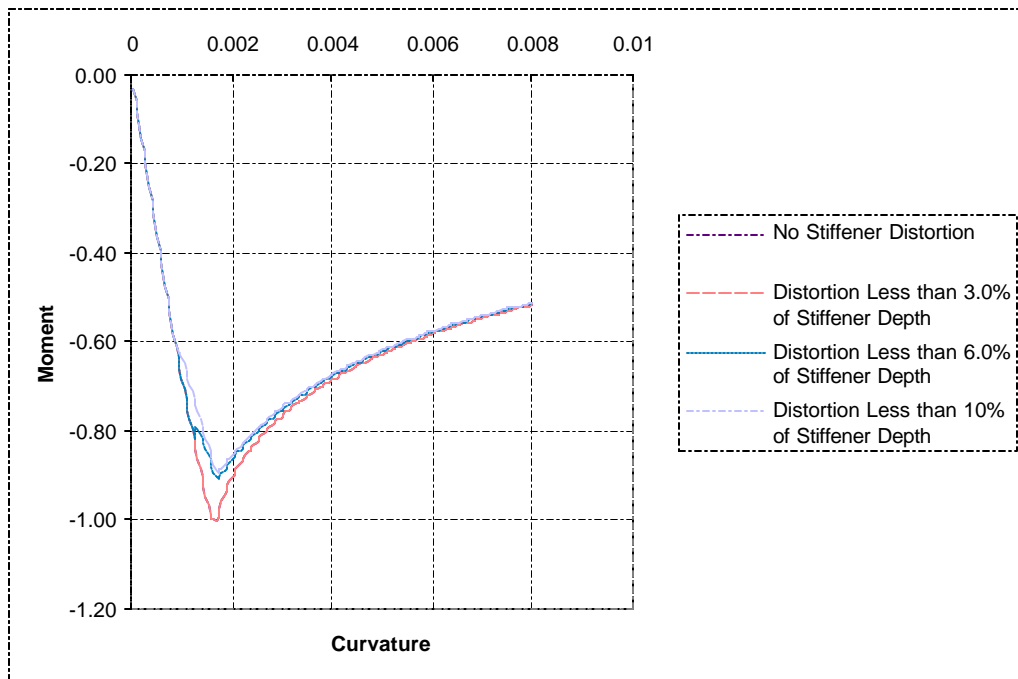


Figure 3.1 - 7: 8x4x13 HS Stiffener on 25.5# Plate

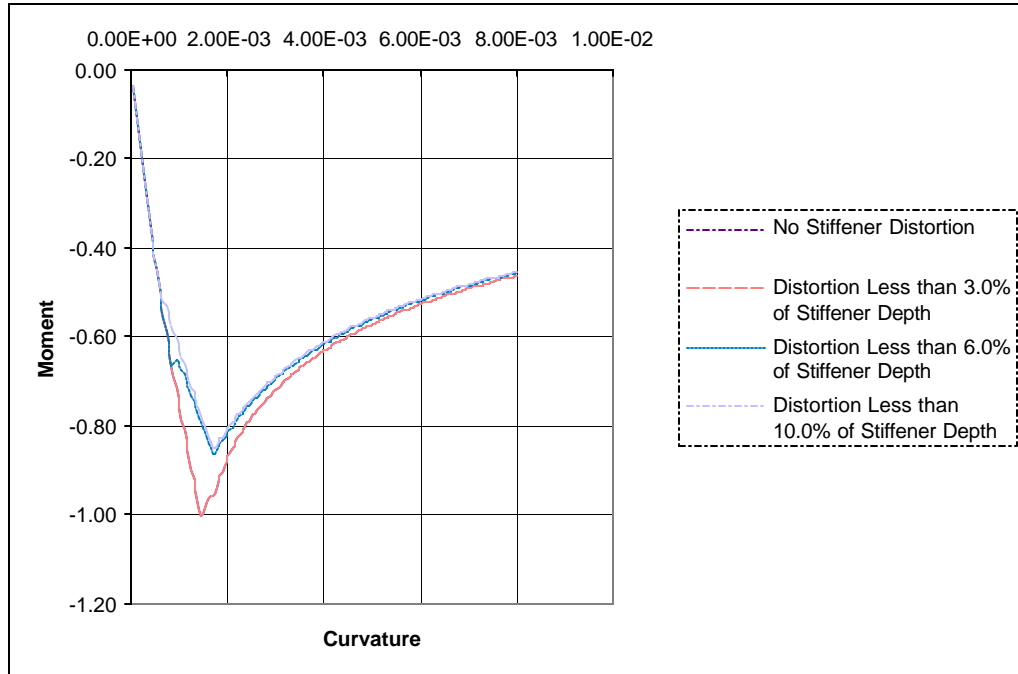


Figure 3.1 - 8: 10x4x11.5 HS Stiffener on 17.85# Plate

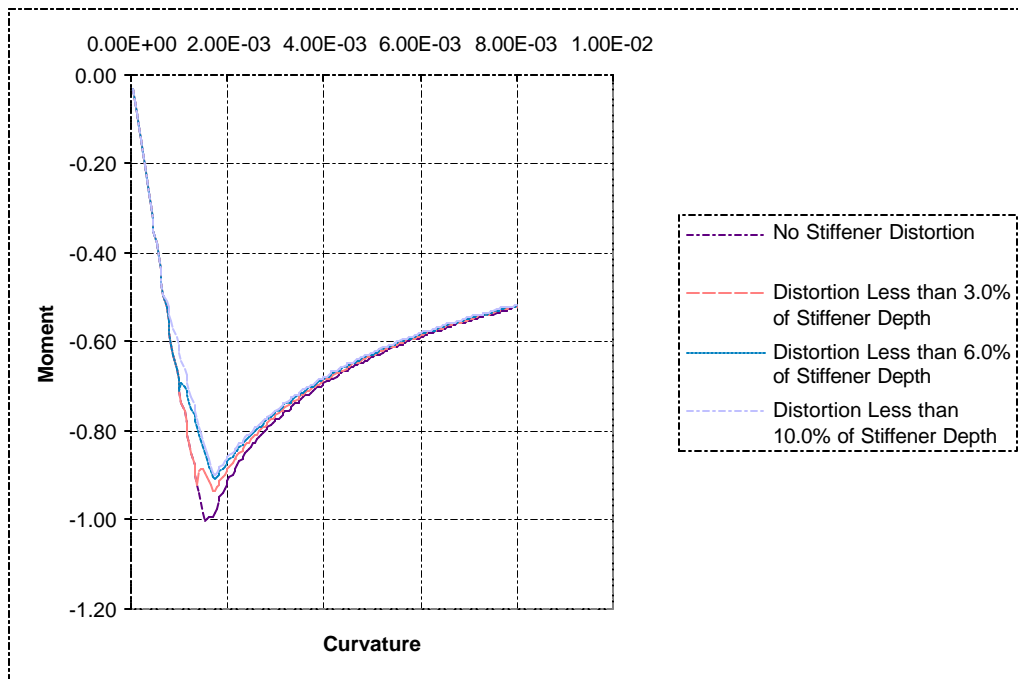


Figure 3.1 - 9: 10x4x15 HS Stiffener on 25.5# Plate

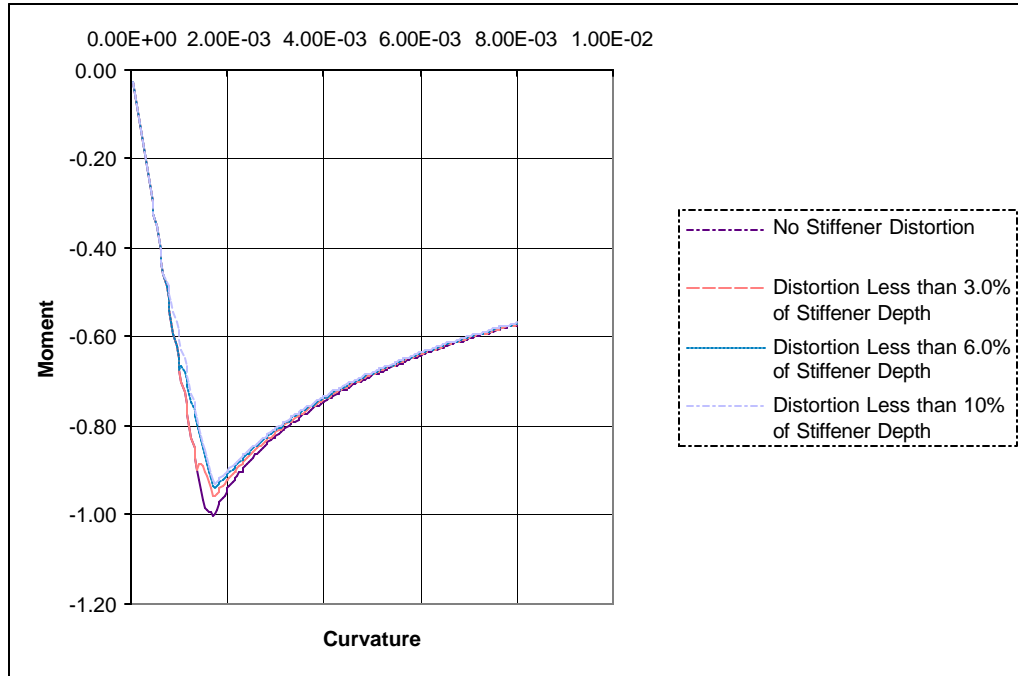


Figure 3.1 - 10: 10x4x15 HS Stiffener on 30.6# Plate

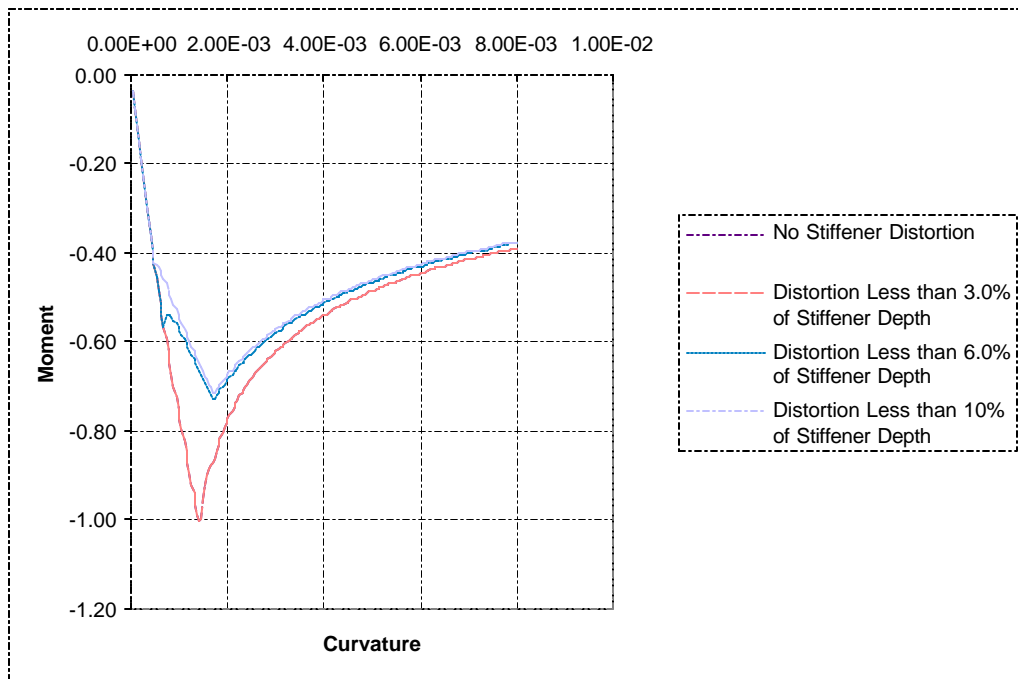


Figure 3.1 - 11: 12x4x16.5 HS Stiffener on 15.3# Plate

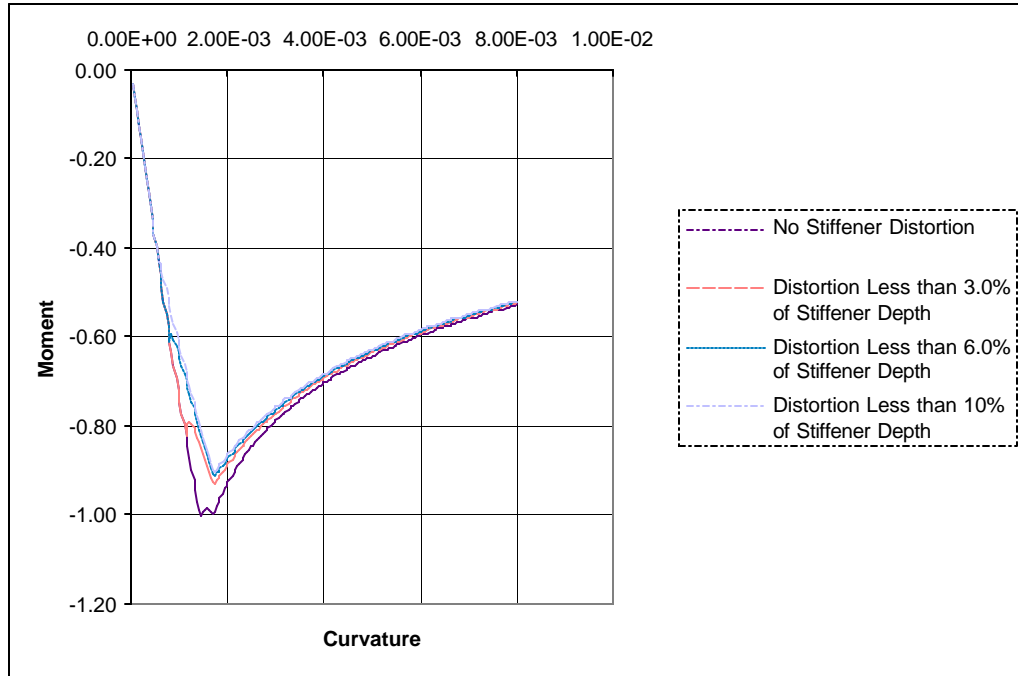


Figure 3.1 - 12: 12x4x19 HS Stiffener on 25.5# Plate

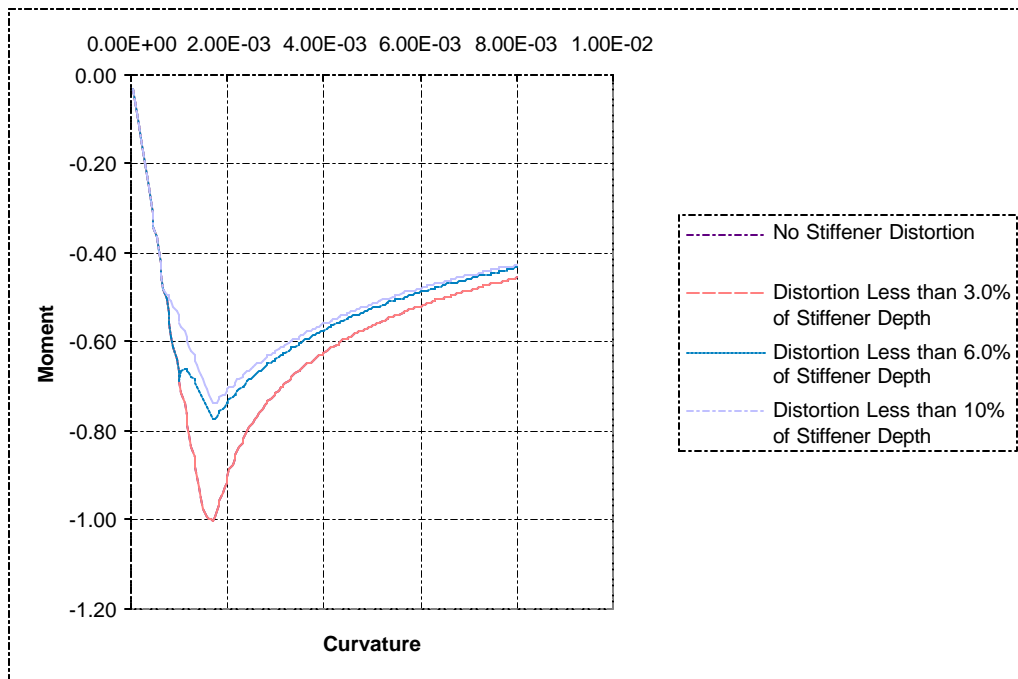


Figure 3.1 - 13: 18x7x12.75#/17.85# HS Stiffener on 25.5# Plate

This type of distortion proved to have a significant effect on the tripping behavior of the local plate-stiffener combination. Although there was variation in the response of the various stiffener types, in general, there was significant degradation in component strength as distortion magnitudes increased from 3.0% and 6.0% of the stiffener depth. This trend is shown in Table 3.1 - 1.

Table 3.1 - 1: Distortion Effects on Component Tripping Capacity

Stiffener Type	Steel type	Plating Thickness (in)	Component Tripping Capacity			
			Not Distorted	Distort = 3% of Depth	Distort = 6% of Depth	Distort = 10% of Depth
6x4x7 T	high strength	0.3125	1	.88	.87	.86
6x4x7 T	high strength	0.625	1	.96	.93	.92
6x4x11 T	high strength	0.5	1	1	.84	.81
6x4x11 T	high strength	0.75	1	.96	.93	.91
8x4x10 I-T	high strength	0.375	1	.83	.81	.80
8x4x13 I-T	high strength	0.625	1	1	.91	.89
10x4x11.5 I-T	high strength	0.4375	1	1	.86	.85
10x4x15 I-T	high strength	0.625	1	.93	.91	.90
10x4x15 I-T	high strength	0.75	1	.96	.94	.93
12x4x16 I-T	high strength	0.375	1	1	.73	.71
12x4x19 I-T	high strength	0.625	1	.93	.91	.9
18x7x12.75#/17.85# I-T	high strength	0.625	1	1	.77	.74

3.2 Buckling

Similar to the tripping failure mode, non-linear finite element models were used to determine the impact of distortions on the buckling capacity of plate-stiffener combinations. Again, the models were loaded in the axial direction along the neutral axis. The models were restrained against rotations about

the longitudinal axis at the ends. The plates at both ends were restrained from rotating about the vertical axis, as was the web at the reaction end. In addition, the node at the neutral axis of the loaded edge was restrained from vertical translation and the node at the neutral axis of the reaction end was restrained from vertical and longitudinal translation. For distributing the load of the loaded end and maintaining a straight, loaded flange, bar elements with high inertial properties were again used.

The distortion that will have the most severe adverse effect on the buckling capacity of a plate-stiffener combination and the distortion selected to demonstrate the methodology in the buckling failure mode is a first mode distortion in the plane of the stiffener web. Although the load shortening curves in past versions of ULTSTR could predict the component response of this type of distortion on buckling behavior, results of the analyses are needed to more rigorously incorporate nonlinear effects on the load shortening curves. The computer program to rapidly generate deformed panel geometries was expanded to generate this type of distortion. In future studies it will be necessary to model other distortions to determine their effect on panel capacity relative to the buckling failure mode.

The nonlinear geometry, finite element solution technique was used to perform the analysis. Results of the analysis were used to incorporate distortion effects on the load shortening curves in the buckling failure mode. This was accomplished by monitoring stress increases at stiffener midspan as distortion magnitudes increase. Then, distortion amplification factors were developed based on the results. As the eccentricity of the load increases, the magnitude of the bending moment at the midspan increases, and the stress at the outer fibers is “amplified” over the value expected for a beam under pure axial load. This effect is shown in Figure 3.2 – 1 highlighting the regions of interest and the magnitudes of stress increase exhibited in the finite element analysis.

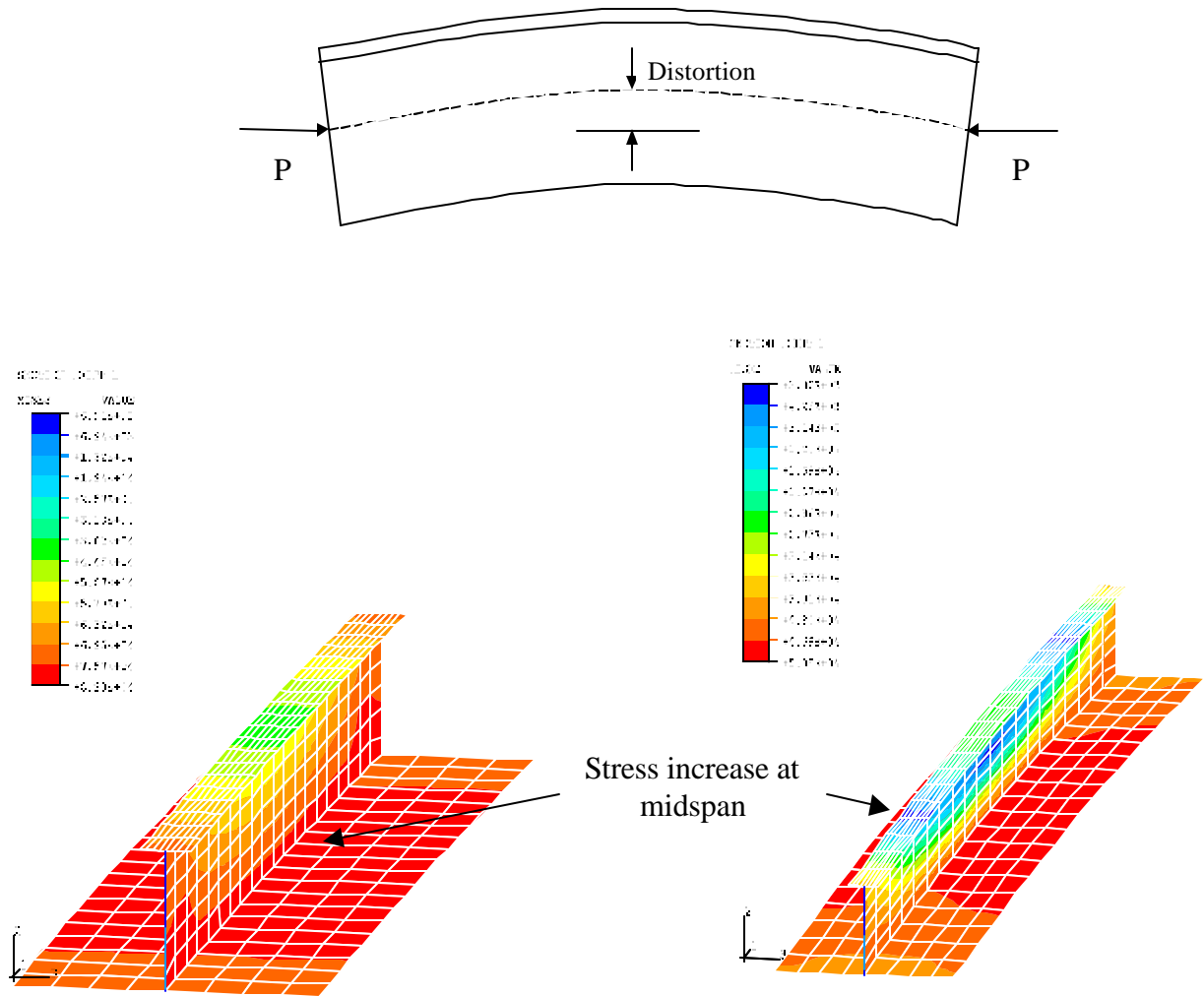


Figure 3.2 - 1: Buckling Stress Amplification

To illustrate the effect of this type of distortion on component response, several stiffeners were analyzed using ULTSTR. The stiffeners are components of cross sections and were selected to demonstrate the effect of distortions on hull girder response. To analyze the response of individual stiffeners, ULTSTR allows the user to load models axially rather than using the traditional moment-curvature approach. The midspan distortion was varied between 0.25% and 1.0% of the overall stiffener length as the stiffeners were axially loaded. The various distorted stiffener performances are shown in Figures 3.2 – 2 through 3.2 - 18.

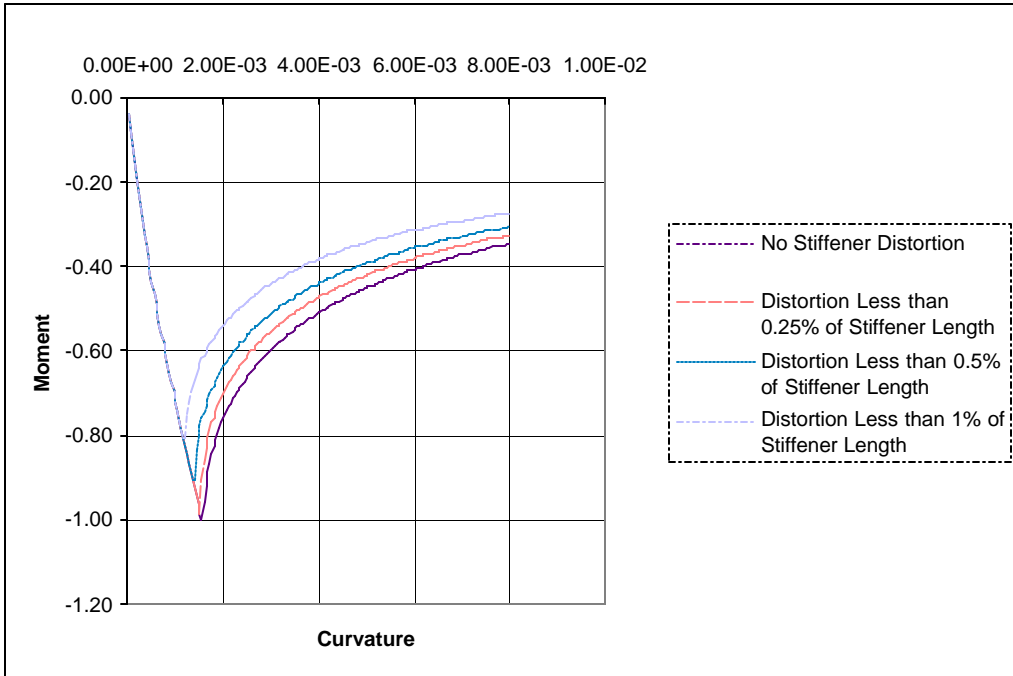


Figure 3.2 - 2: 6x4x7 HS Stiffener on 12.75# Plate

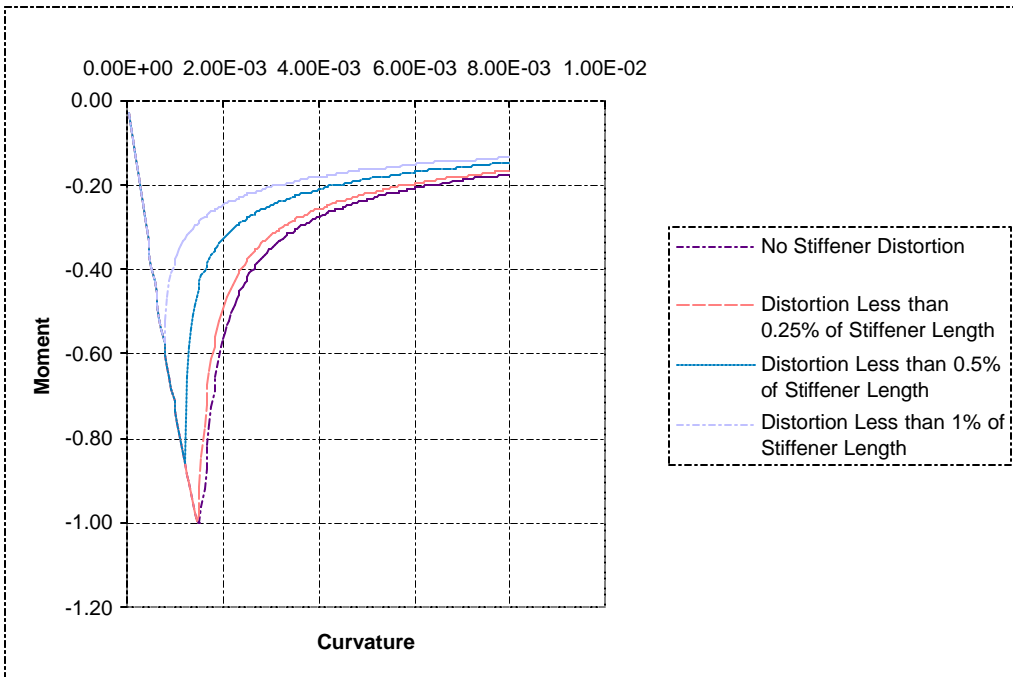


Figure 3.2 - 3: 6x4x7 HS Stiffener on 25.5# Plate

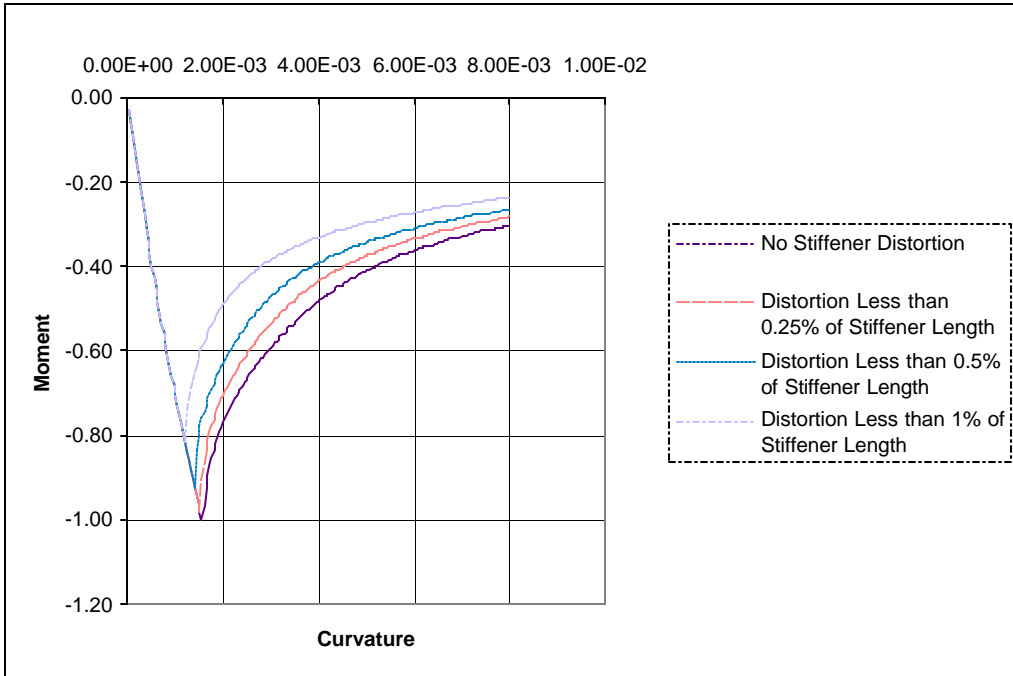


Figure 3.2 - 4: 6x4x11 HS Stiffener on 20.4# Plate

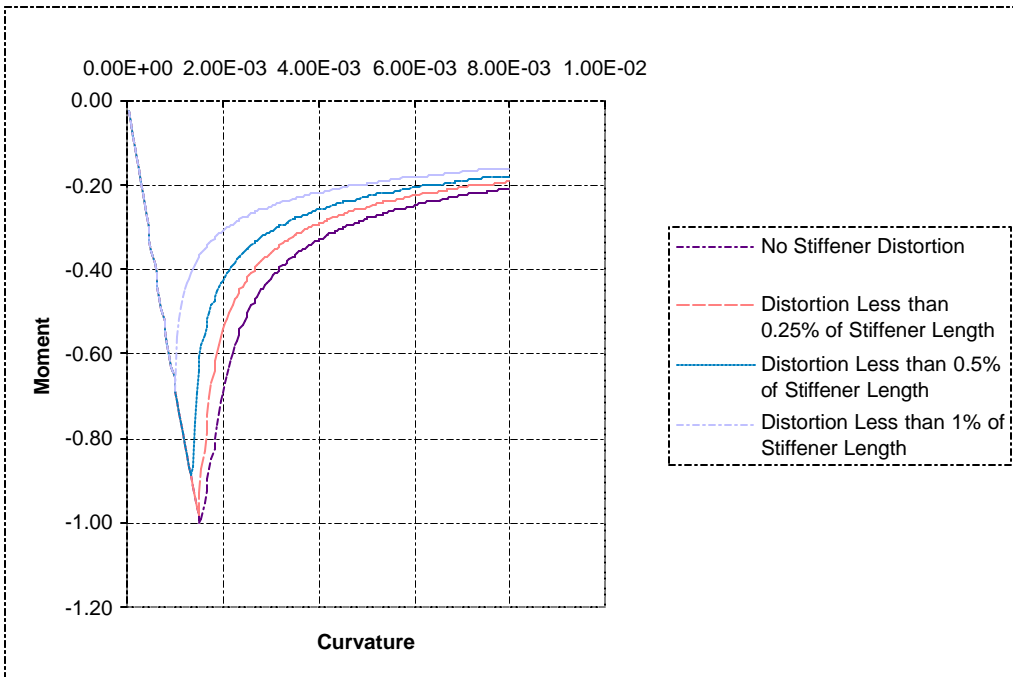


Figure 3.2 - 5: 6x4x11 HS Stiffener on 30.6# Plate

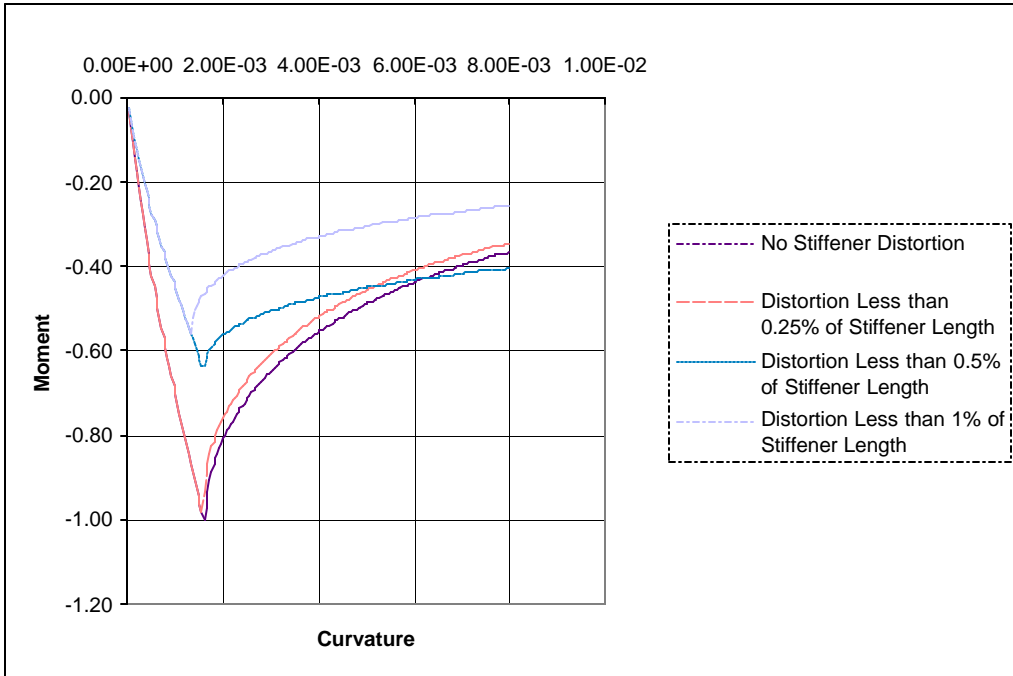


Figure 3.2 - 6: 8x4x10 HS Stiffener on 15.3# Plate

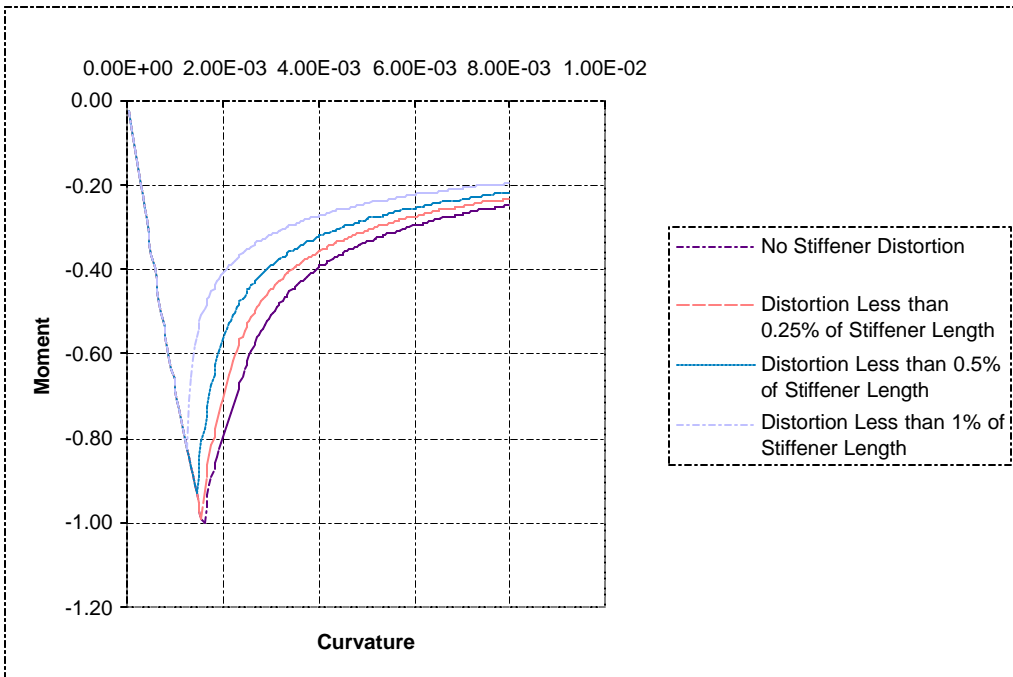


Figure 3.2 - 7: 8x4x13 HS Stiffener on 25.5# Plate

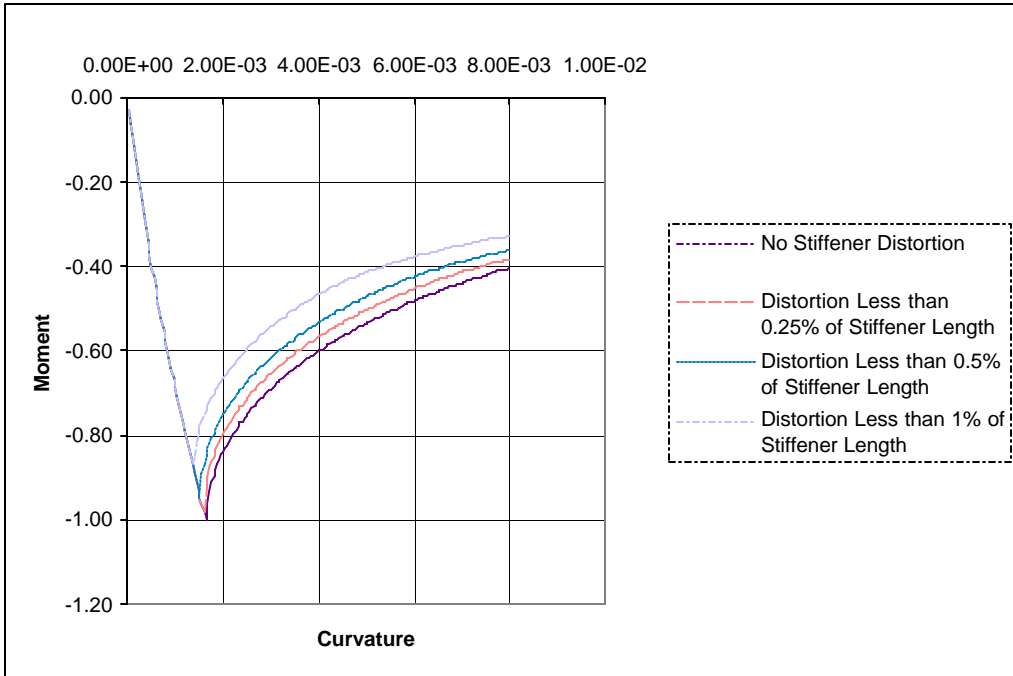


Figure 3.2 - 8: 10x4x11.5 HS Stiffener on 17.85# Plate

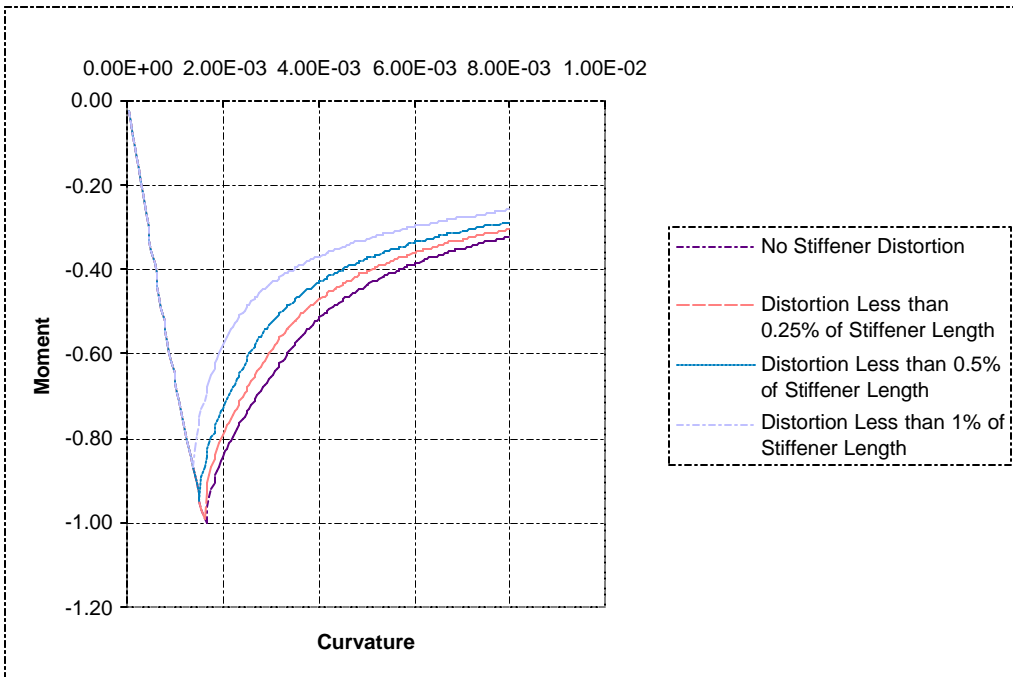


Figure 3.2 - 9: 10x4x15 HS Stiffener on 25.5# Plate

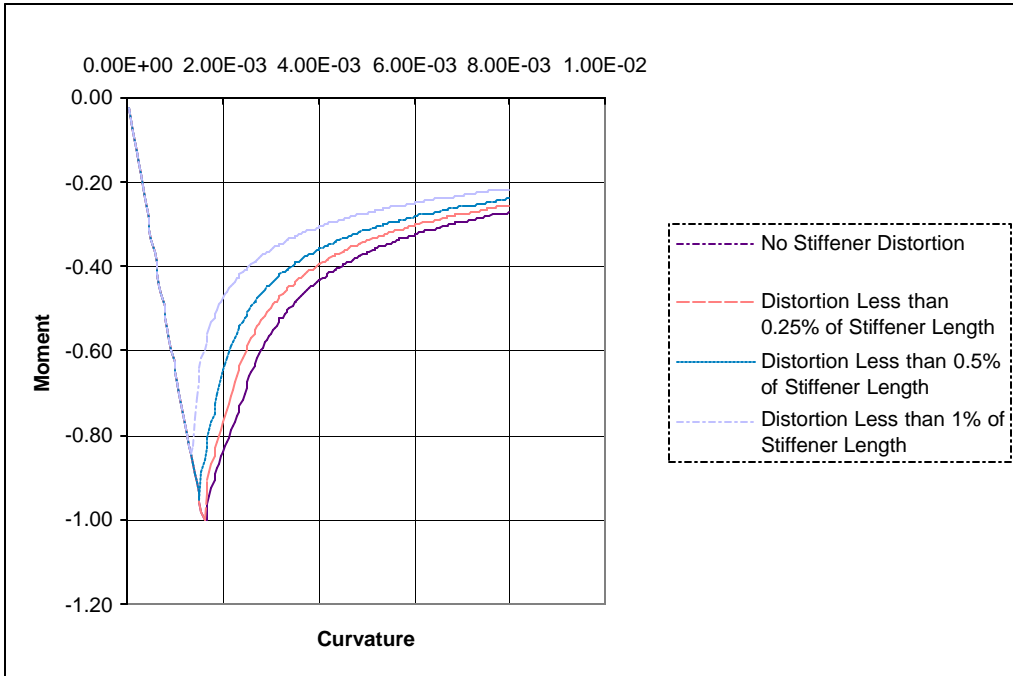


Figure 3.2 - 10: 10x4x15 HS Stiffener on 30.6# Plate

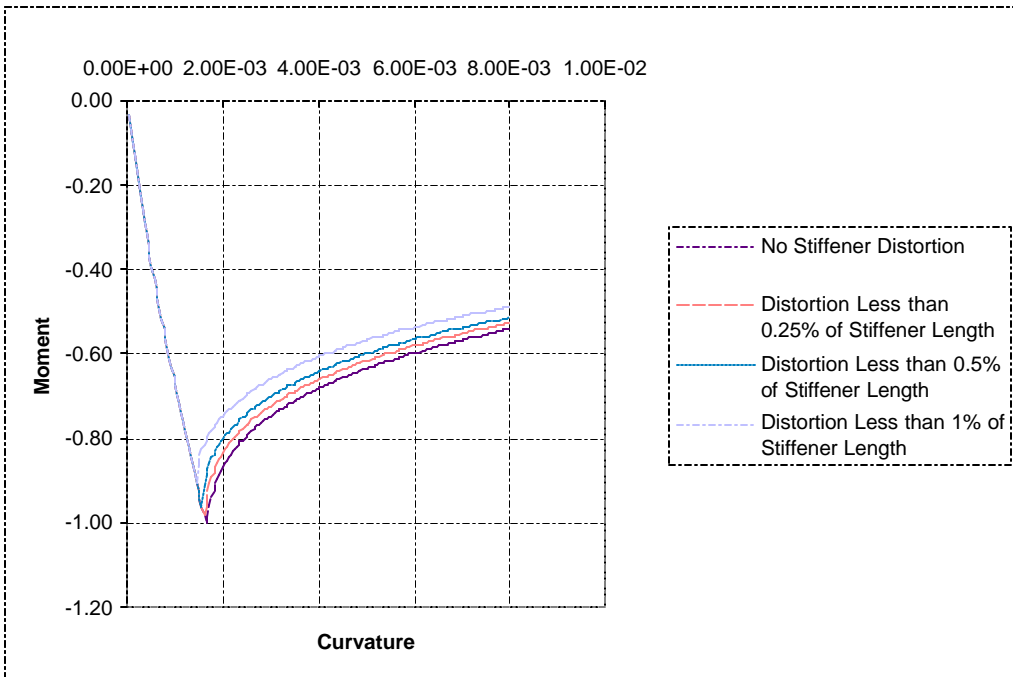


Figure 3.2 - 11: 12x4x16.5 HS Stiffener on 15.3# Plate

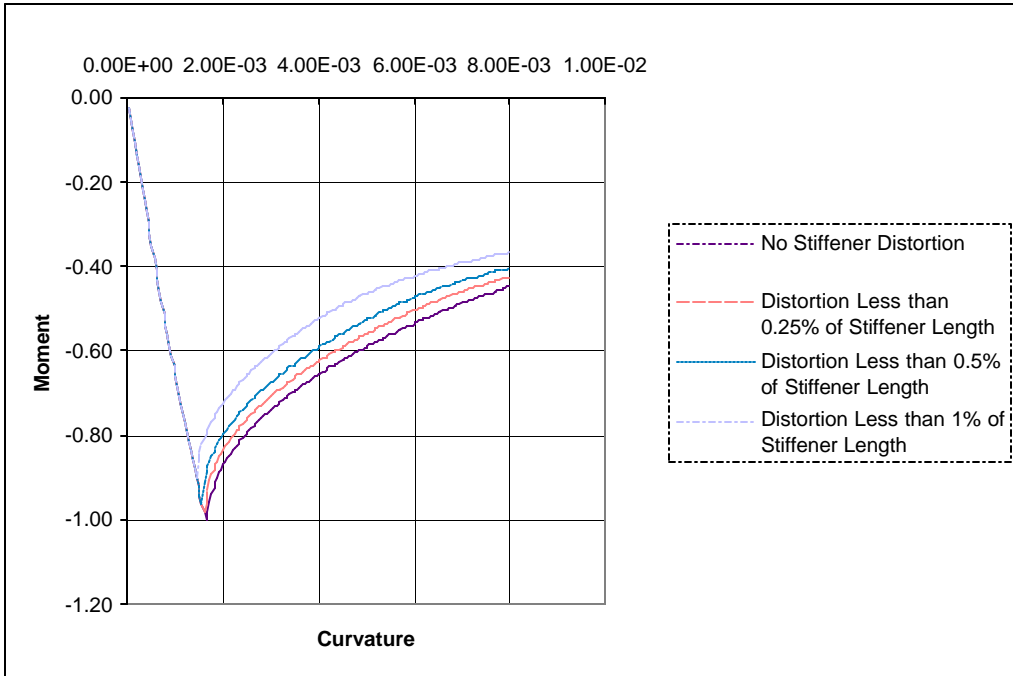


Figure 3.2 - 12: 12x4x19 HS Stiffener on 25.5# Plate

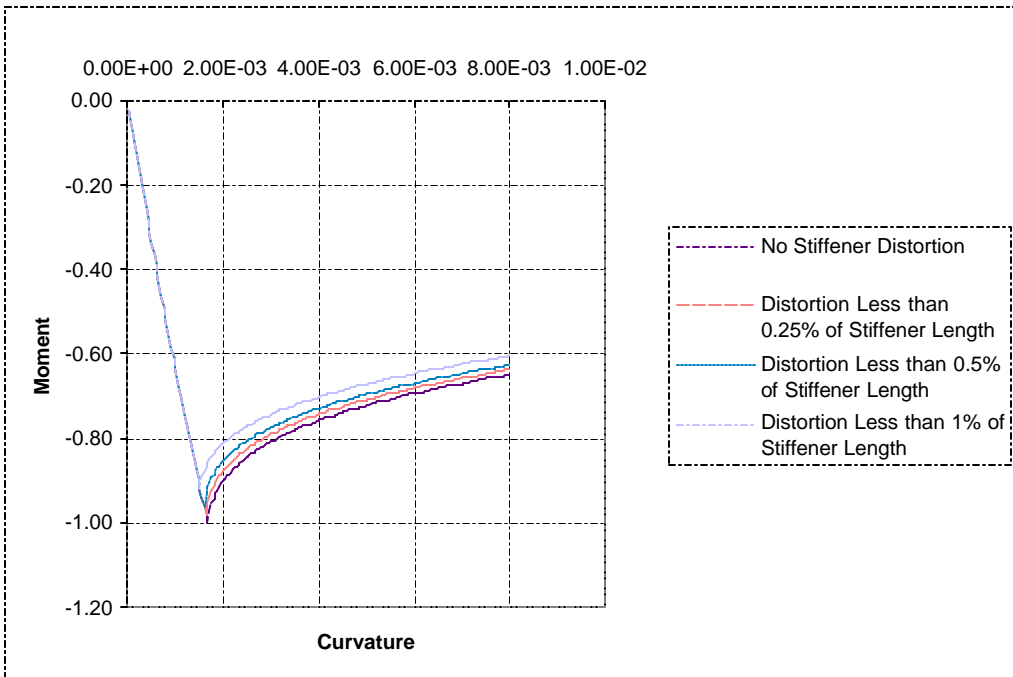


Figure 3.2 - 13: 18x7x12.75#/17.85# HS Stiffener on 25.5# Plate

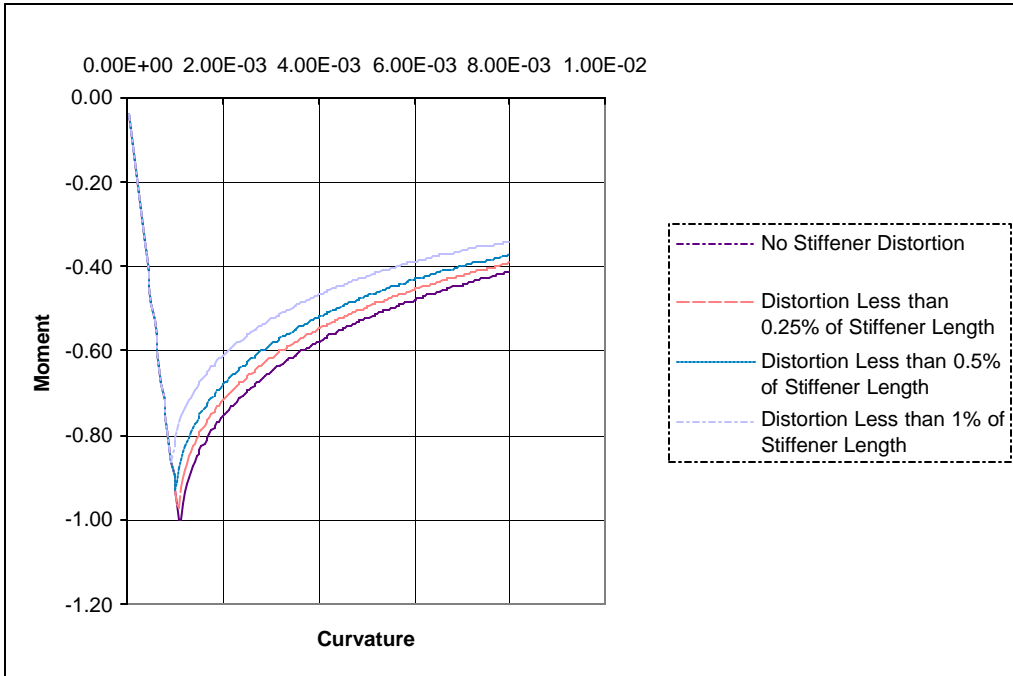


Figure 3.2 - 14: 10 x 3 1/2 MS Angle on 26.5# Plate

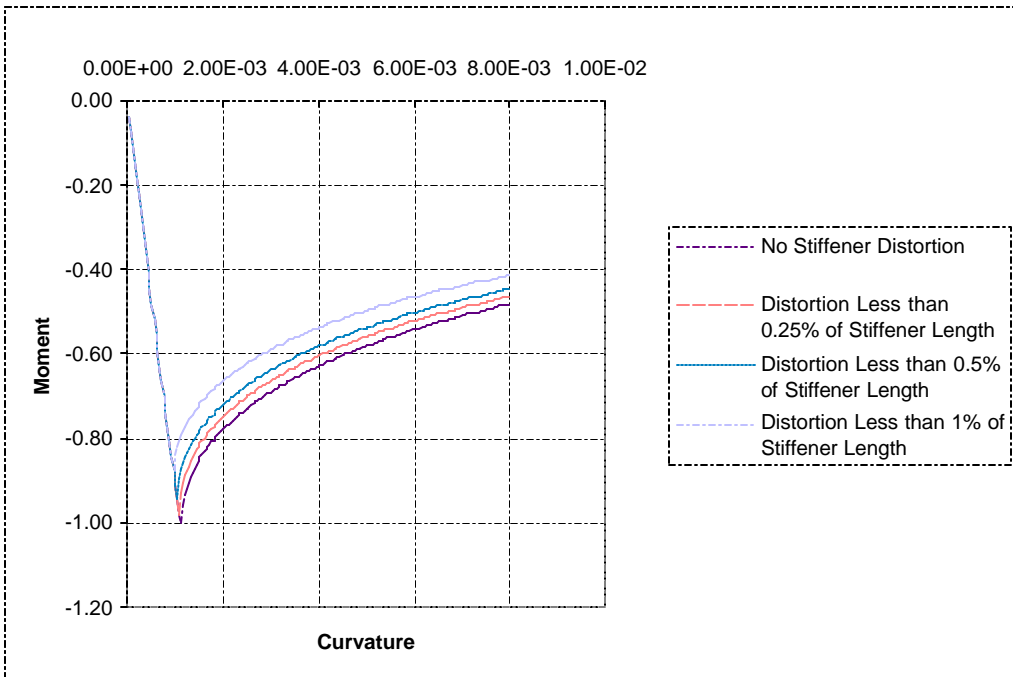


Figure 3.2 - 15: 12 x 3 1/2 MS Angle on 26.5# Plate

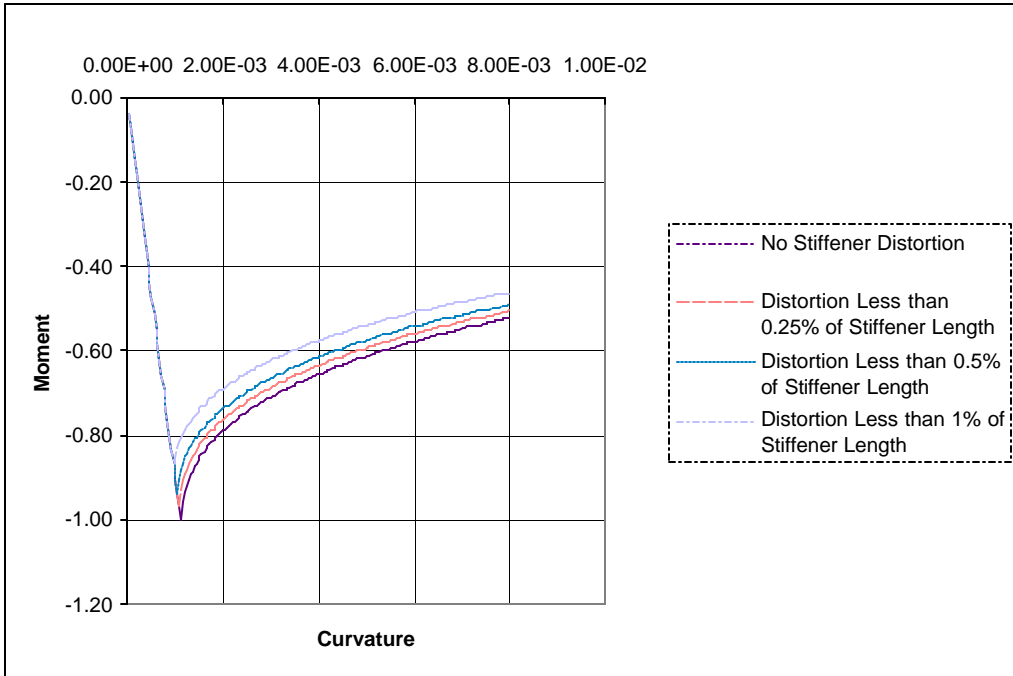


Figure 3.2 - 16: 13 x 4 MS Angle on 26.5# Plate

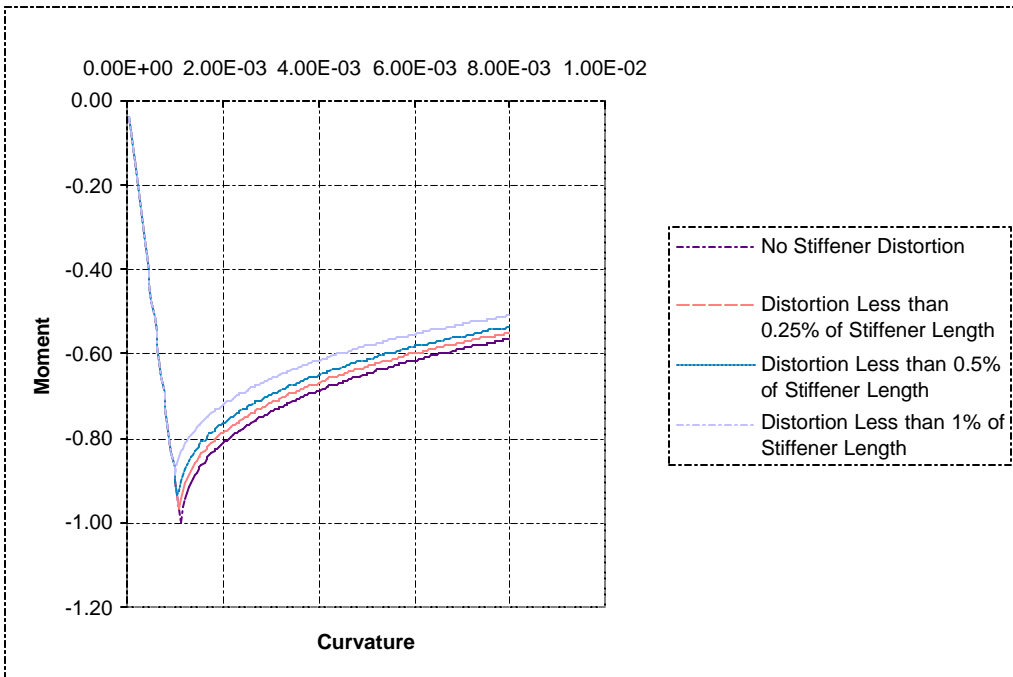


Figure 3.2 - 17: 15 x 3 3/8 MS Angle on 26.5# Plate

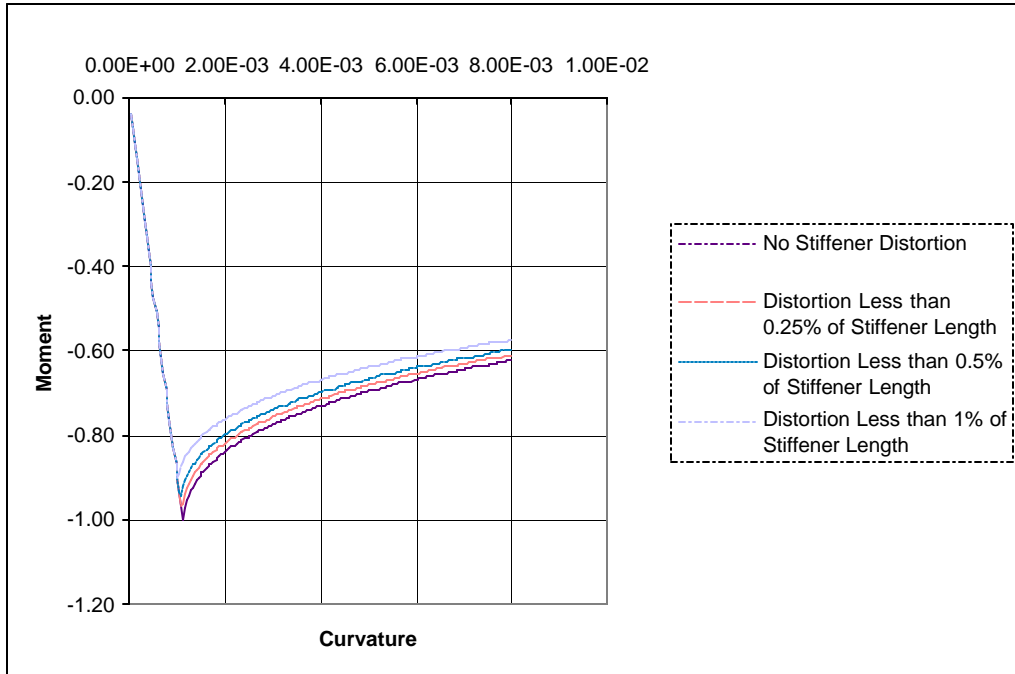


Figure 3.2 - 18: 18 x 4 MS Angle on 26.5# Plate

This type of distortion proved to have a significant effect on the buckling behavior of the local plate-stiffener combination. Although there was variation in the response of the various stiffener types, in general, there was significant degradation in component strength as distortion magnitudes increased from 0.25% and 0.5% of the stiffener span. This trend is shown in Table 3.2 - 1.

Table 3.2 - 1: Distortion Effects on Component Buckling Capacity

Stiffener Type	Steel type	Plating Thickness (in)	Component Buckling Capacity			
			Not Distorted	Distort = ¼% of Span	Distort = ½% of Span	Distort = 1% of span
6x4x7 T	high strength	0.3125	1	0.99	0.91	0.81
6x4x7 T	high strength	0.625	1	0.99	0.86	0.57
6x4x11 T	high strength	0.5	1	0.98	0.92	0.82
6x4x11 T	high strength	0.75	1	0.98	0.89	0.69
8x4x10 I-T	high strength	0.375	1	0.98	0.64	0.56
8x4x13 I-T	high strength	0.625	1	0.99	0.93	0.8
10x4x11.5 I-T	high strength	0.4375	1	0.99	0.95	0.87
10x4x15 I-T	high strength	0.625	1	0.99	0.95	0.87
10x4x15 I-T	high strength	0.75	1	1	0.95	0.85
12x4x16 I-T	high strength	0.275	1	0.98	0.96	0.9
12x4x19 I-T	high strength	0.625	1	0.98	0.96	0.9
18x7x12.75#/17.85# I-T	high strength	0.625	1	0.98	0.96	0.92
10x3½ L C/F 28.3# C	mild steel	0.65	1	0.97	0.93	0.86
12x3½ L C/F 30.9#C	mild steel	0.65	1	0.98	0.95	0.88
13x4 L C/F 35.0# C	mild steel	0.65	1	0.97	0.94	0.87
15x3 3/8 L C/F 40.0# C	mild steel	0.65	1	0.97	0.93	0.89
18x4 L C/F 58# C	mild steel	0.65	1	0.97	0.95	0.9

3.3 Summary and Conclusions

The ULTSTR approach to estimate the ultimate capacity of a hull girder under longitudinal bending conditions assumes that the collapse of the hull girder results from a sequence of failures of the local components. Therefore, before hull girder impact could be addressed, it was necessary to update the analytical expressions, or load shortening curves, describing local panel response in order to account for distorted conditions. In the current study, these expressions were updated using the finite element method. These load shortening curves should be modified further as studies are performed on different plate-stiffener combinations and the sensitivity of the various parameters on failure becomes better understood.

Local component response is not only necessary for determining the hull girder capacity but can also be used to set tolerance limits to avoid local failure. The buckling and tripping failure of distorted local components under compressive loading was investigated for several plate-stiffener combinations. There was a large reduction in buckling capacity of the limited plate-stiffener combinations before the lateral distortions approached 1% of the span length. To avoid local failures in the buckling mode it is suggested that distortions should not approach these levels. In general, at lateral distortions approaching 0.25% of the span length, plate-stiffener capacities degraded between 1% and 3%. In the tripping failure mode, as the distortion magnitude at the stiffener midspan in the plane of the flange exceeded 3% of the depth of the stiffener, there were large reductions in capacity.

4. Hull Girder Ultimate Strength Methodology Applied to Typical Sections

Thus far, we have defined a procedure for determining ultimate hull girder capacity using the computer code ULTSTR, described important failure modes and their formulations incorporated in the program, as well as recommended an approach for incorporating distortion effects into local panel response. To determine the effects of these distortions on hull girder capacity, numerous cross-sections must be evaluated. However, before ULTSTR can be used to estimate distortion effects on hull girder capacity, the accuracy of ULTSTR predictions when determining the ultimate hull girder capacity for undistorted hull girder cross-sections must be evaluated.

The ULTSTR technique has been used to determine the ultimate capacity of numerous midship cross sections. Although ULTSTR estimations are considered to be reasonably accurate, most results have not been verified experimentally. The construction of a facility in FY 93 at NSWCCD has offered us the opportunity to compare experimental results to ULTSTR predictions. This facility is capable of testing a scaled midship section to collapse under pure moment or moment-shear combinations to determine the ultimate and residual strength of these complex configurations. The results of these tests will be used as the basis for evaluating the ULTSTR approach in this study. This facility, shown in Figure 4 - 1, is capable of testing specimens up to 43" x 60" x 180" having ultimate bending capacities in excess of 12.5×10^6 ft-lbs. The specimen tested is the uni-directional double hull structure shown in Figure 4 - 2. During the test, curvature was measured using inclinometers and the moment was calculated from load levels obtained from the actuators.

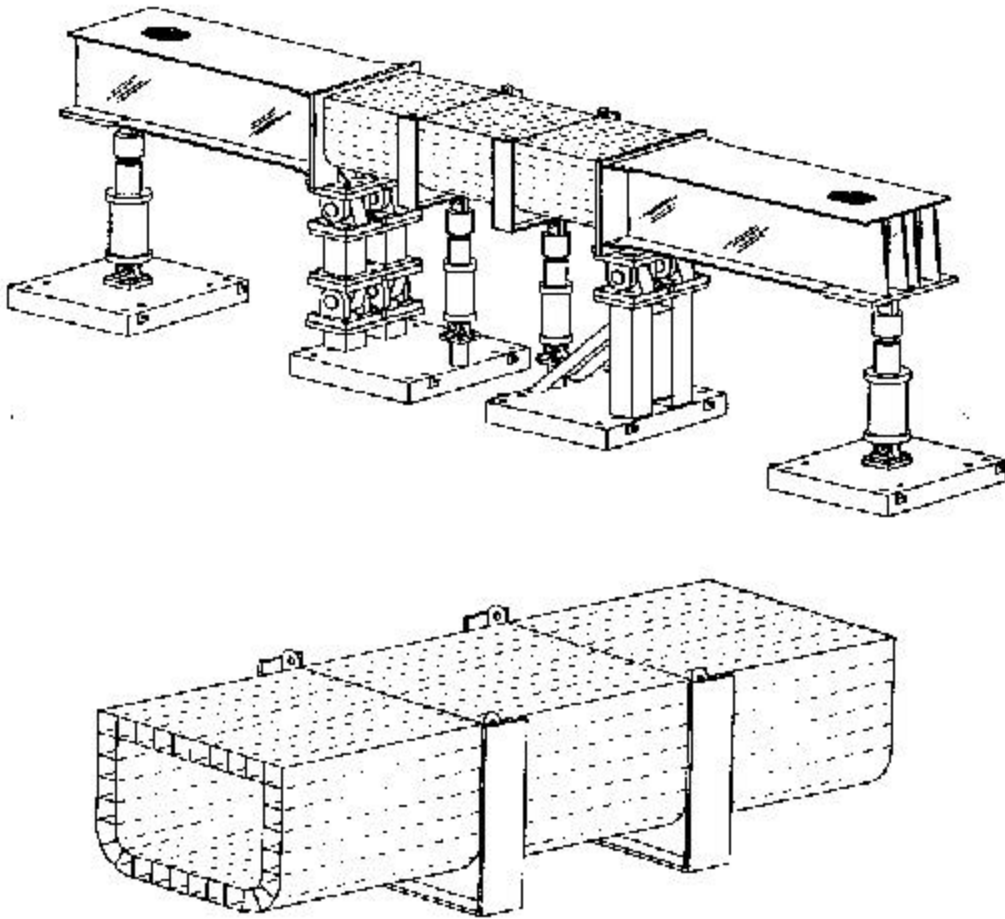


Figure 4 - 1: Six Point Bending Facility and Test Specimen

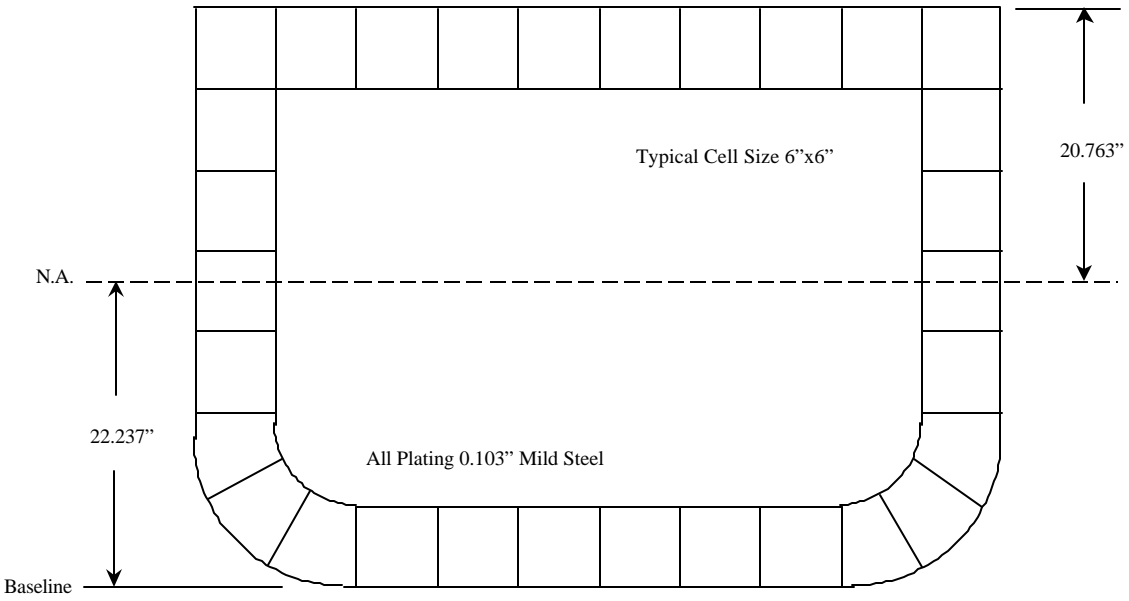


Figure 4 - 2: Uni-directional Double Hull Test Specimen

Figures 4 - 3 and 4 - 4 compare the moment-curvature relationship obtained from the hogging and sagging experiments of the uni-directional double hull specimen with the ULTSTR predictions. In both cases, the ULTSTR estimates were very close to the experimental results for predicting the linear behavior of the hull girder up to and including collapse. Post collapse predictions are not an “exact science” and need further research. These tests have and will continue to be instrumental in ULTSTR modifications.

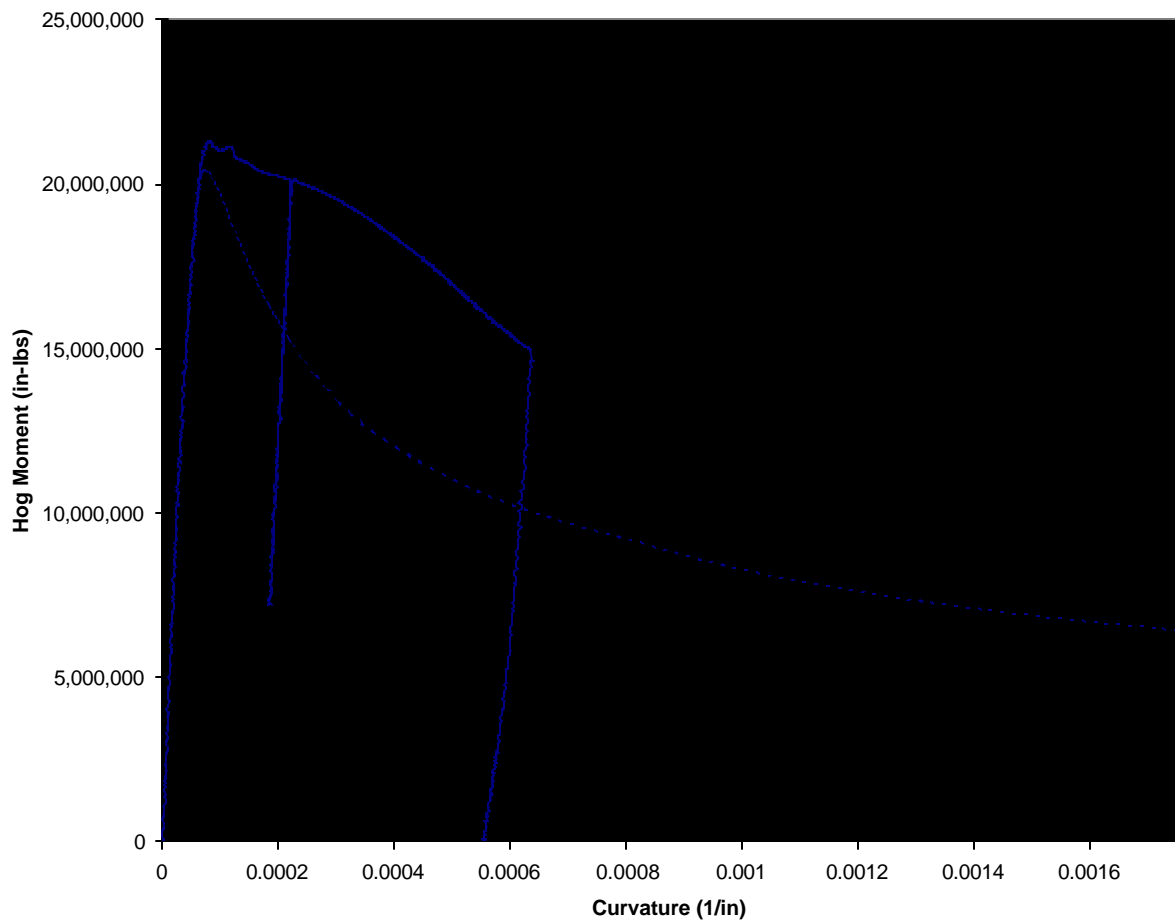


Figure 4 - 3: Hog Moment-Curvature Comparison of ULTSTR Versus Test Data for the Uni-Directional Double Hull

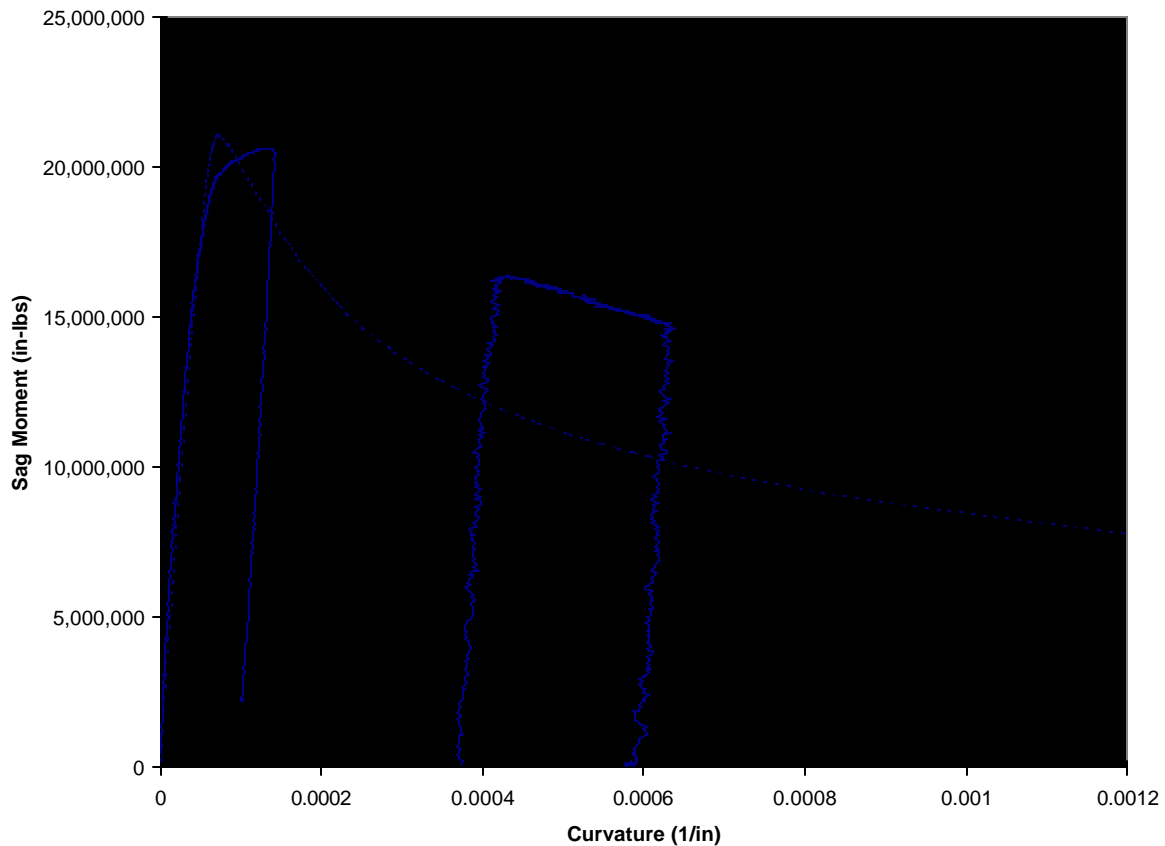


Figure 4 - 4: Sag Moment-Curvature Comparison of ULTSTR Versus Test Data for the Uni-Directional Double Hull

To some extent, this model test was also a test of plate distortion formulation on plate effectiveness relationships incorporated in ULTSTR. The ULTSTR representation of these models used moderate to severe levels of plate distortion in the mathematical model. We believed that distortions related to welding the relatively thin plating would represent moderate to severe distortions when scaled to more typical values. When comparing the results of the experiment with the ULTSTR prediction, it appears this was the appropriate condition.

4.1 Distortion Effects on Hull Girder Ultimate Strength

The ULTSTR methodology for determining hull girder ultimate strength has proven to be an effective approach to predict hull girder capacity. With the modifications for distortion effects discussed earlier, ULTSTR should prove to be an effective tool for determining distortion effects on hull girder capacity.

Ultimately, as more information becomes available to statistically describe distortion variability and as more numerical and experimental studies are performed to describe strength dependence on

distortion magnitudes, ULTSTR can be modified to run in simulation mode, randomly selecting various distortion magnitudes to determine hull girder strength variability. However, to demonstrate the methodology, a less ambitious program was necessary. Three ULTSTR models were constructed representing a frigate sized vessel, a larger destroyer type vessel and a very large vessel representing a commercial tanker. For the purpose of this study we will refer to the cross-sections as Hull F, Hull D and Hull C, respectively and they are shown in Figures 4.1 – 1 through 4.1 - 3.

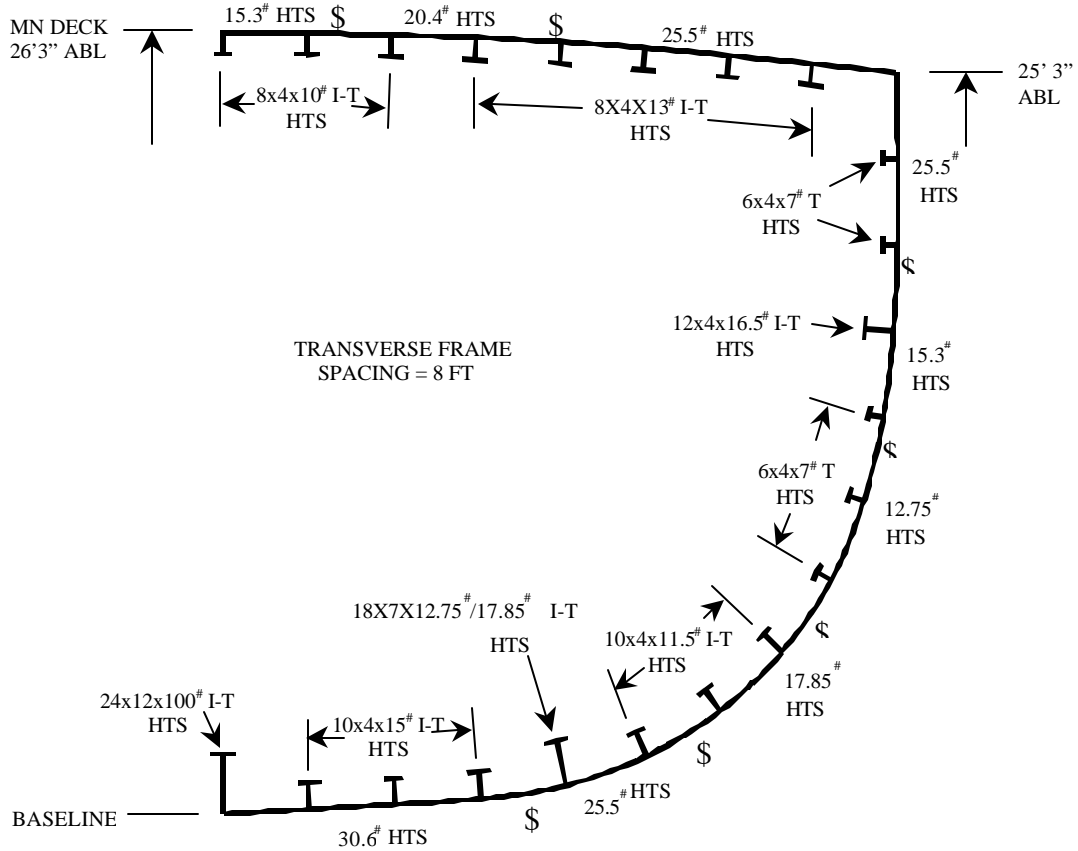


Figure 4.1 - 1: Hull F Midship Section

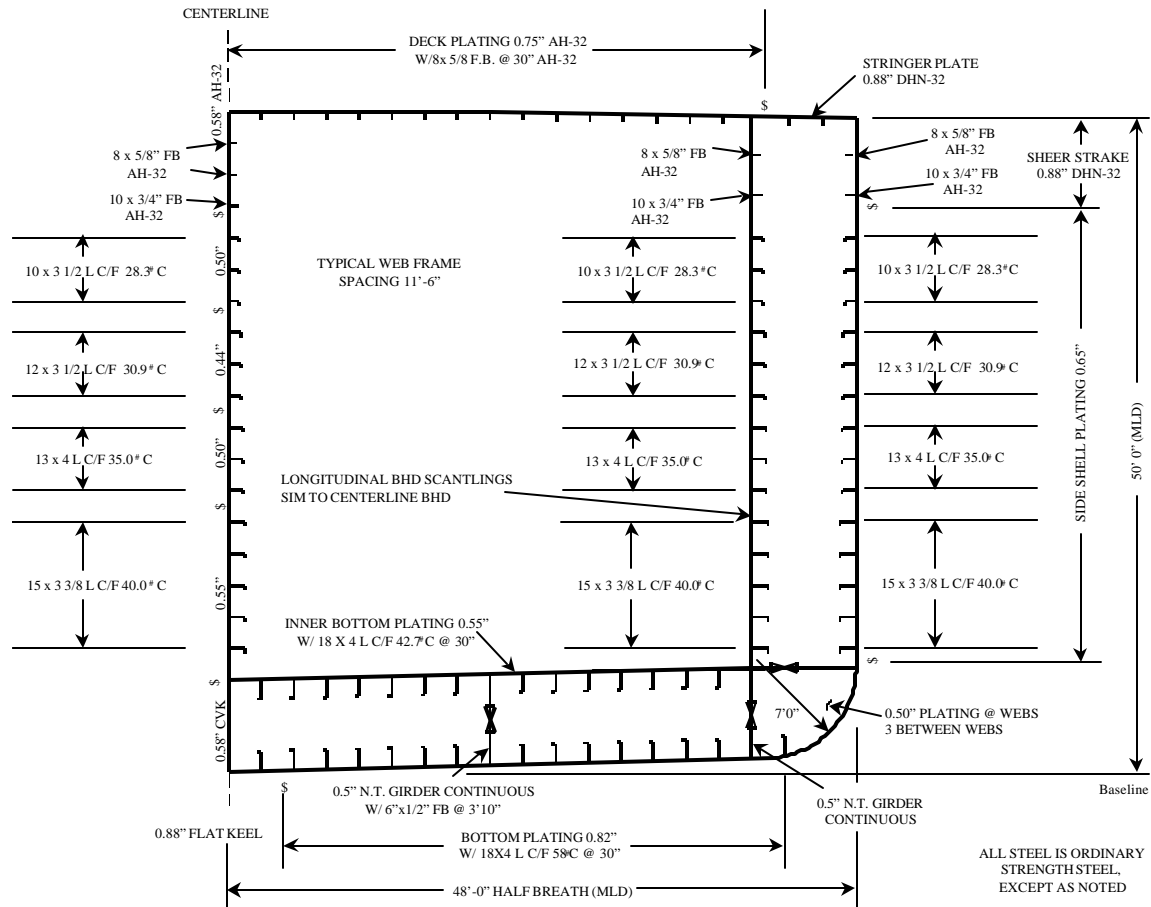


Figure 4.1 - 3: Hull C Midship Section

4.1.1 Plating Effectiveness Effects

New welding techniques are effective in reducing distortions resulting from the welding process, but significant plate distortions continue to occur. The combination of modal shape and amplitude of these distortions is very difficult to determine, but this information is necessary when attempting to evaluate structural performance. For this reason, empirical expressions developed from tests are effective, if not necessary, when describing the structural response relating to this type of distortion and the methodology ULTSTR uses. As described earlier, ULTSTR uses a set of empirical expressions developed from test data to describe plating effectiveness characteristics. Basically, a panel performed ideally in test conditions was defined to have no distortion, and the panels exhibiting the greatest strength degradation compared to ideal conditions are defined as having severe levels of distortion. Although this manner of defining plate effectiveness does not explicitly state distortion amplitudes, it does a reasonable job of defining the strength characteristic ranges you can expect from the construction process. Therefore, using ULTSTR we can effectively bound the effect of plating distortion on hull girder strength by assuming the separate conditions of a hull girder constructed of ideal panels

(undistorted panels) and a hull girder entirely constructed of poorly performing panels (severely distorted panels). Ideally, as information becomes available that statistically describes the percentage of the various distorted panels expected during fabrication, ULTSTR can be modified to run in simulation mode and yield ultimate strength expectations rather than bounds.

Figures 4.1.1 – 1 through 4.1.1 - 6 show the moment-curvature results of the ULTSTR analysis for the three hulls considered. The hull plating distortions included no plating distortion, moderate plating distortion, moderate to severe distortion, and severe distortion. As with all of the moment-curvature plots, moment values were divided by the moment capacity of the undeformed cross-section. Therefore, a moment of 1 corresponds to the ultimate strength of the undeformed cross-section.

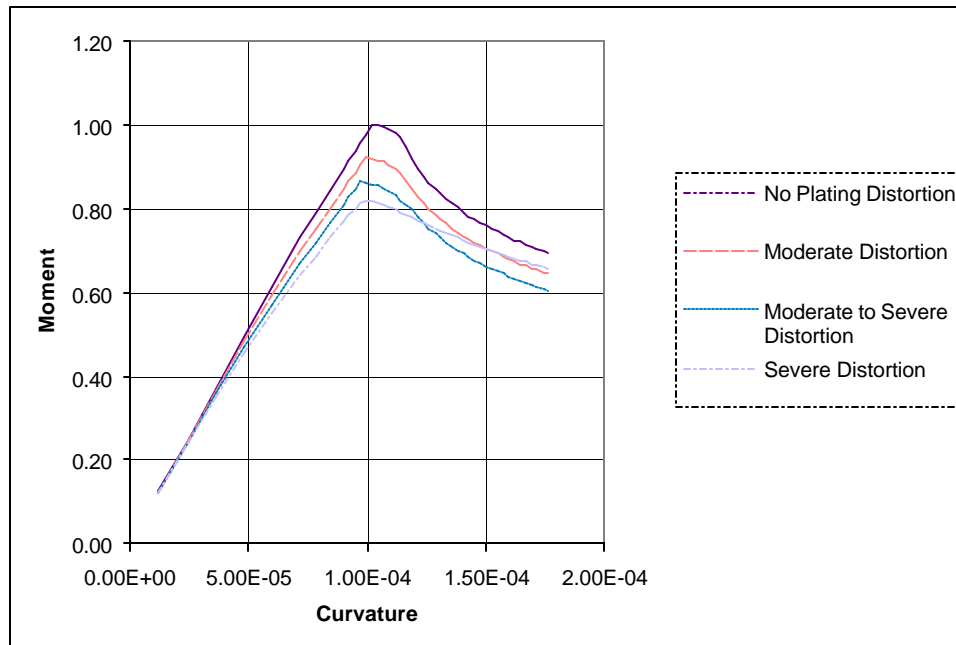


Figure 4.1.1 - 1: Hull F Ultimate Hogging Comparison Evaluating Plating Effectiveness Effects

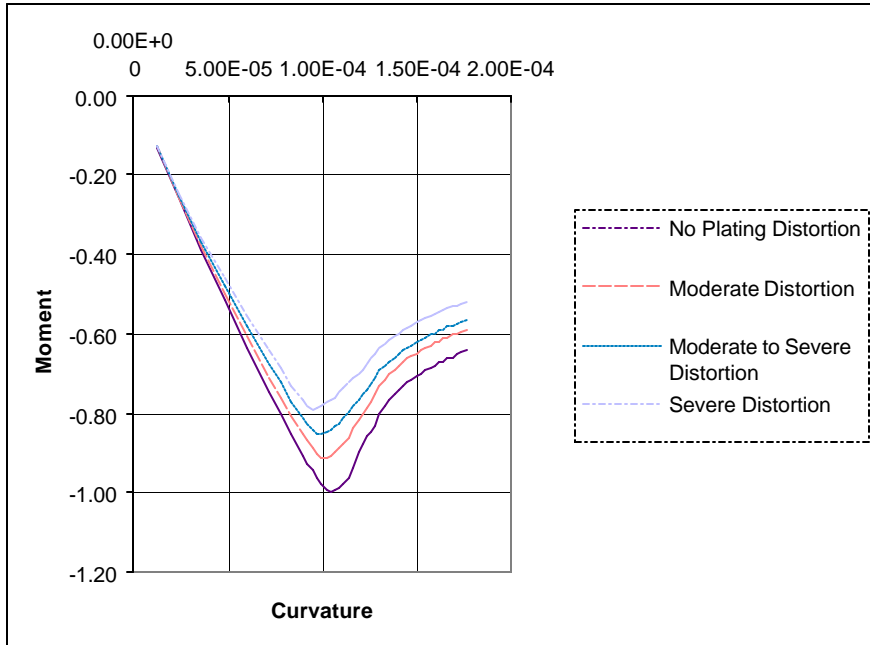


Figure 4.1.1 - 2: Hull F Ultimate Sagging Comparison Evaluating Plating Effectiveness Effects

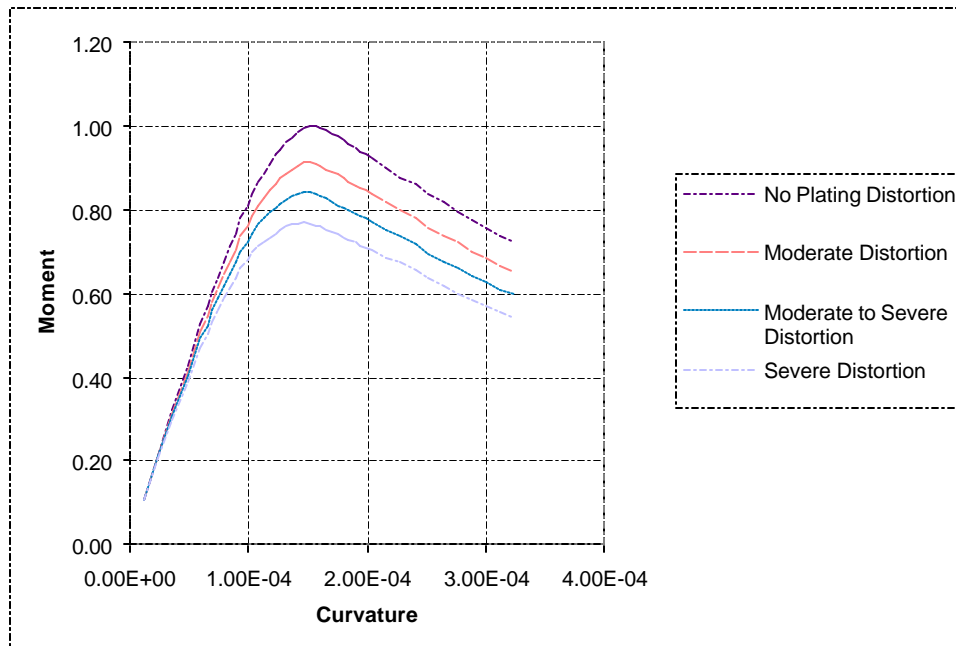


Figure 4.1.1 - 3: Hull D Ultimate Hogging Comparison Evaluating Plating Effectiveness Effects

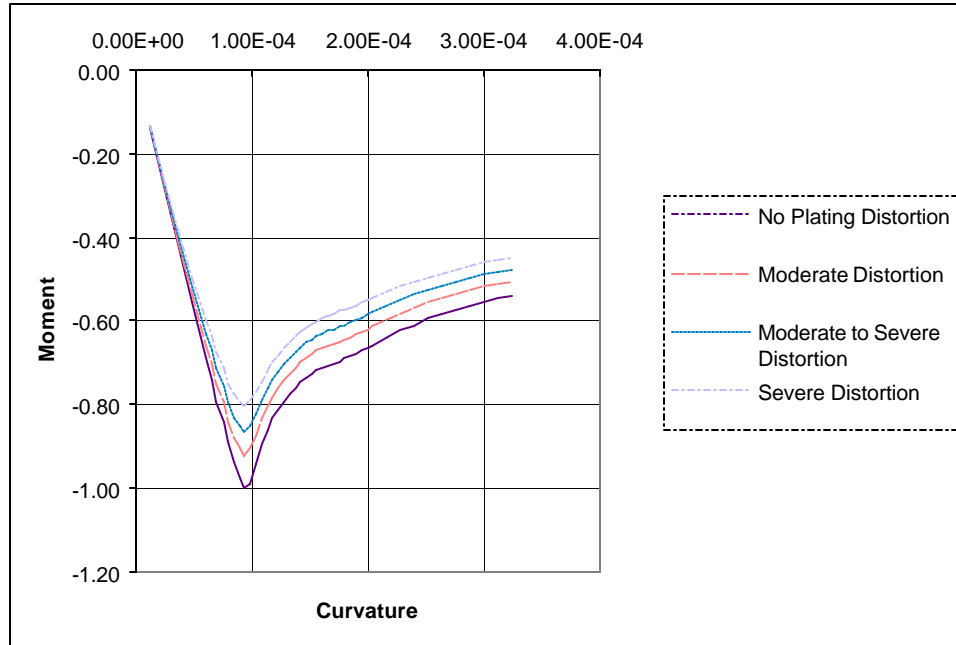


Figure 4.1.1 - 4: Hull D Ultimate Sagging Comparison Evaluating Plating Effectiveness Effects

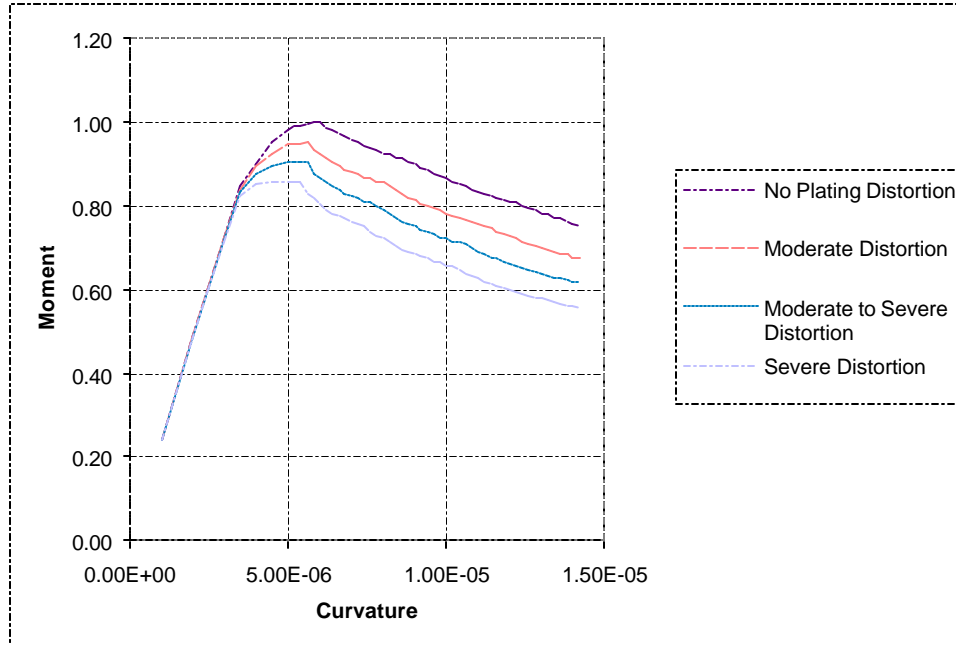


Figure 4.1.1 - 5: Hull C Ultimate Hogging Comparison Evaluating Plating Effectiveness Effects

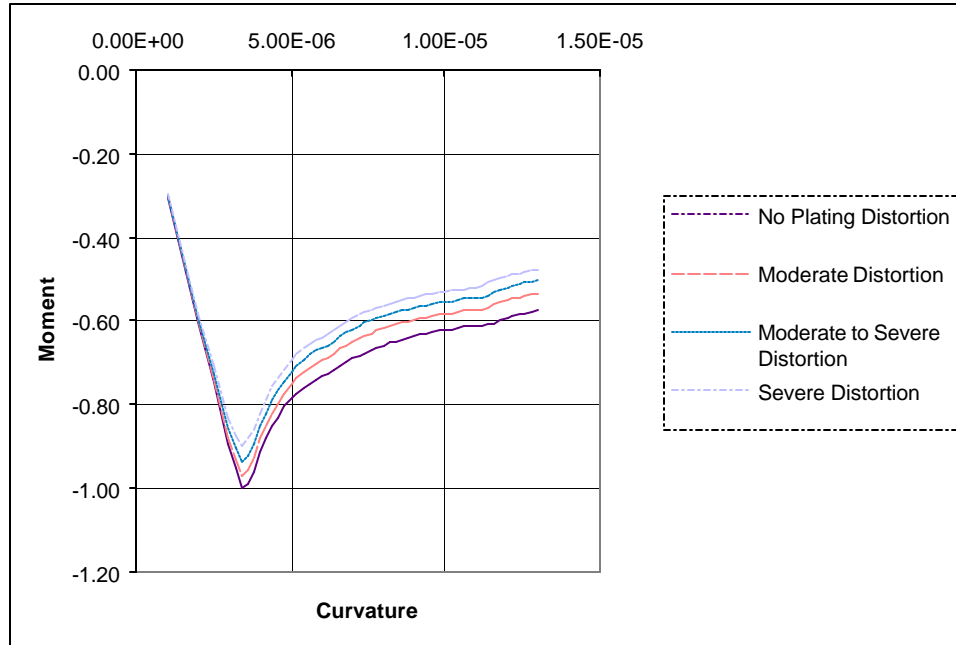


Figure 4.1.1 - 6: Hull C Ultimate Sagging Comparison Evaluating Plating Effectiveness Effects

The graphs above indicate that the midship sections respond differently to plating deformations, with the tanker configuration showing the smallest change in ultimate strength when plating distortions increased. One reason for this is the increased “hard” intersections occurring in double hull configurations.

In general, ultimate strength degradation from ideal plating conditions for the three hulls under normal fabrication conditions, i.e. moderate distortion, was between 2% and 10%. This relatively small decrease in capacity is an indication that the fabrication procedures and standards in practice ensure a high retention of ultimate strength capacity. However, the 20% loss in capacity shown in some of the figures under severely distorted conditions warn against relaxing plating distortion tolerances further.

4.1.2 Stiffener Tripping Effects

As with plate distortions, as statistical information becomes available on stiffener web, out-of-plane distortions, reliability methods could be used to assess hull girder capacity. Using the reliability methods described earlier, hull girder failure probabilities could be determined with each panel deformation randomly selected according to a given distribution. In this study, it was assumed that all the stiffeners in the cross section were distorted the same amount. This would give an ultimate capacity of the “worst case scenario”, that is, the capacity of the hull girder if all the panels were deformed the maximum amount. Figures 4.1.2 – 1 through 4.1.2 - 6 show the moment-curvature results of the ultimate strength analysis of the three midship sections as stiffener out-of-plane distortions increase.

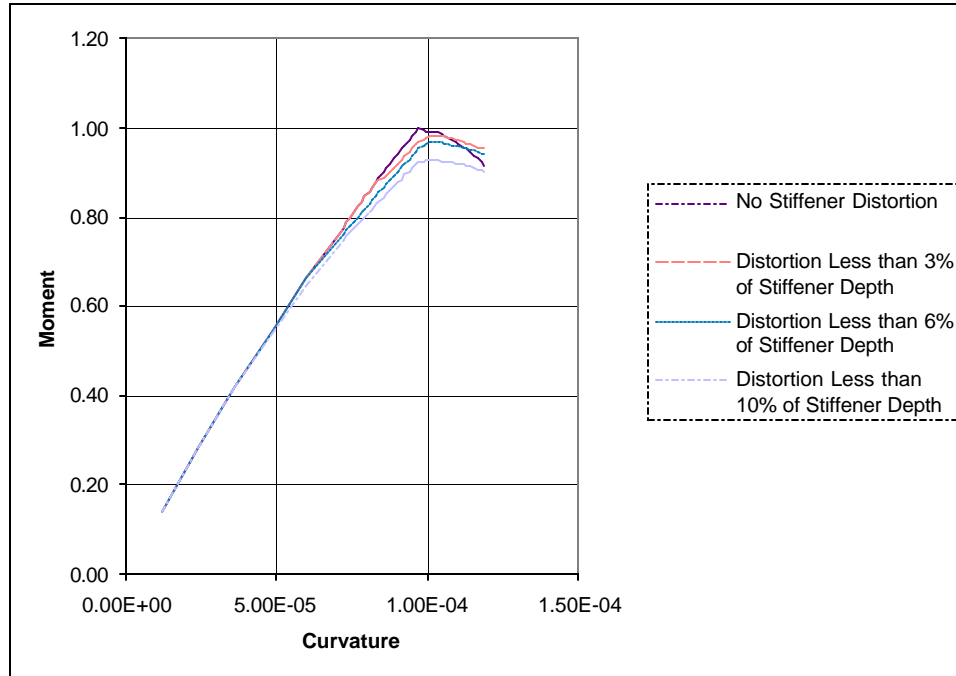


Figure 4.1.2 - 1: Hull F Ultimate Hogging Comparison Evaluating Stiffener Tripping Effects

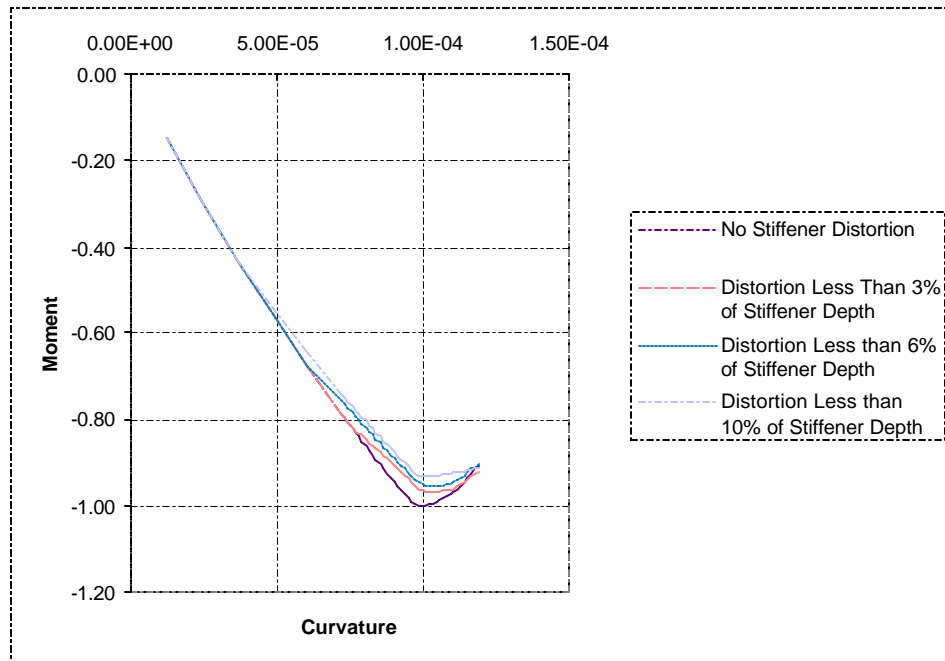


Figure 4.1.2 - 2: Hull F Ultimate Sagging Comparison Evaluating Stiffener Tripping Effects

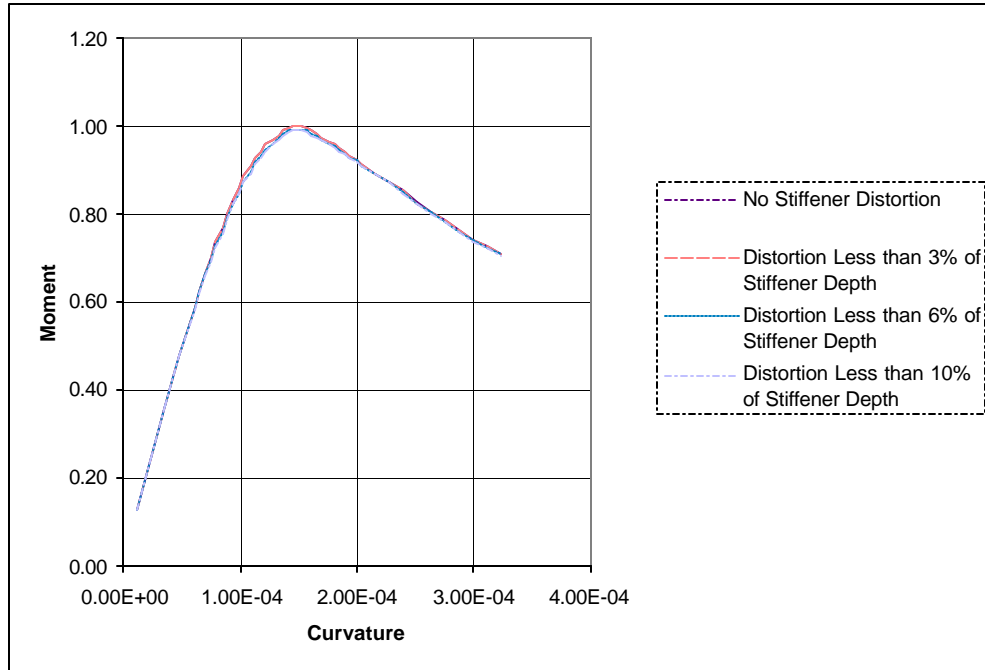


Figure 4.1.2 - 3: Hull D Ultimate Hogging Comparison Evaluating Stiffener Tripping Effects

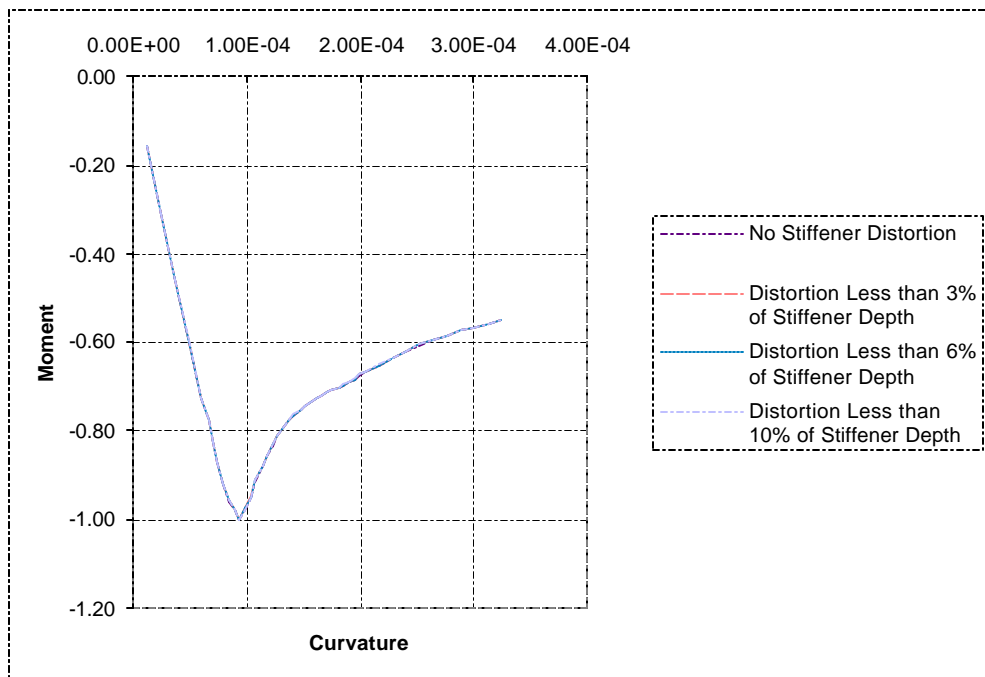


Figure 4.1.2 - 4: Hull D Ultimate Sagging Comparison Evaluating Stiffener Tripping Effects

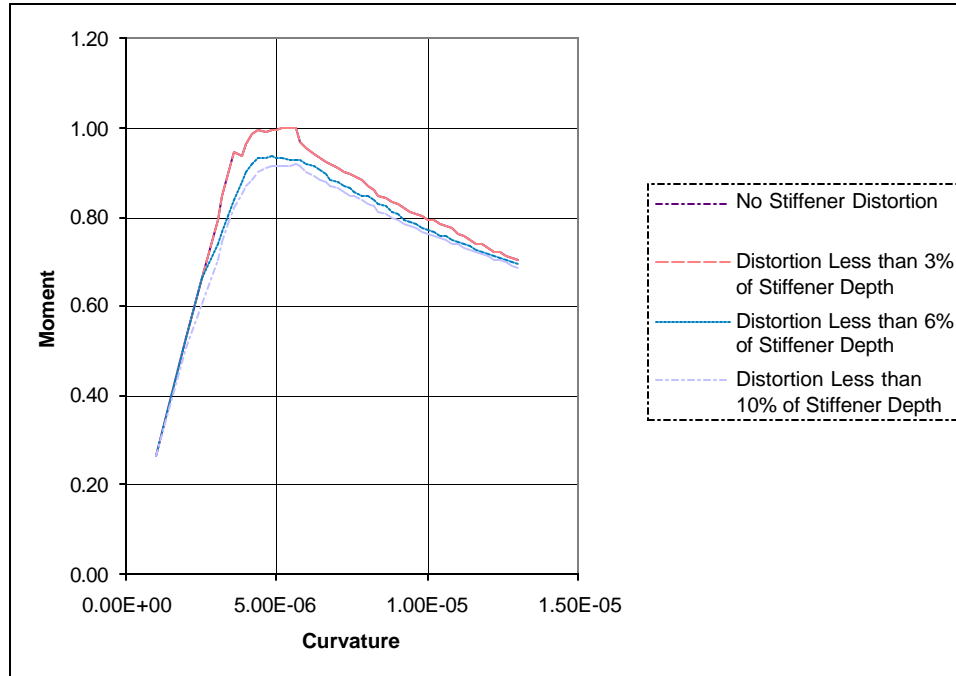


Figure 4.1.2 - 5: Hull C Ultimate Hogging Comparison Evaluating Stiffener Tripping Effects

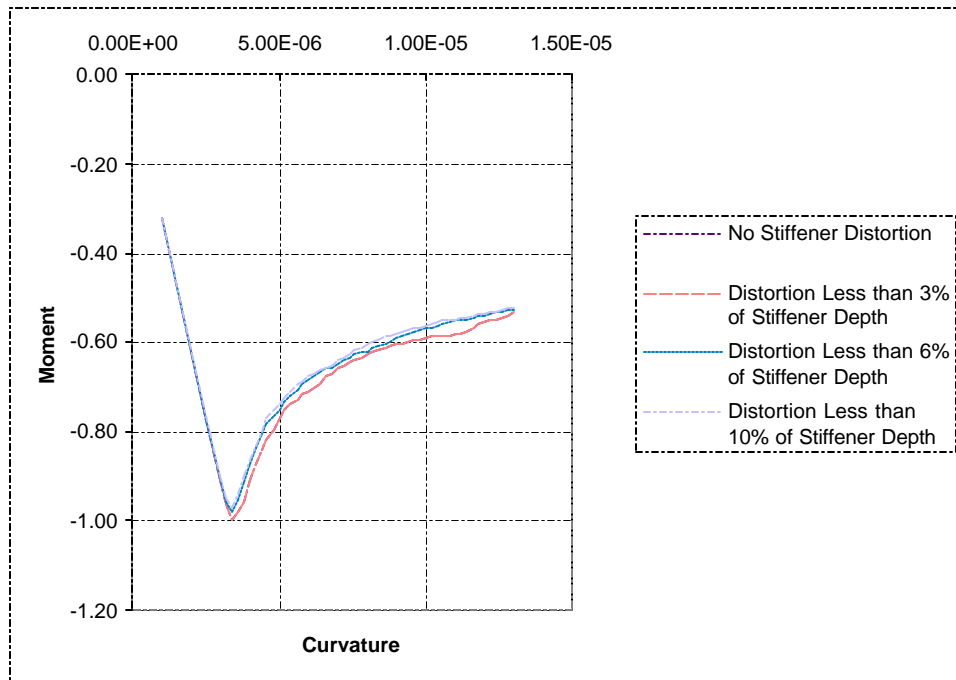


Figure 4.1.2 - 6: Hull C Ultimate Sagging Comparison Evaluating Stiffener Tripping Effects

The moment-curvature results described in the graphs above indicate that the ultimate strength of the three hulls varied greatly under this type of distortion. Ultimately, the main reason for this variation is that tripping failure is only one of the failure modes of the local components. Different cross sections will have a different percentage of the components fail in the tripping mode. For example, a cross section composed largely of “hard corners” would not be influenced as greatly by distortions critical in the instability failure modes. However, from a strength standpoint, it would appear that this type of distortion does not impact hull girder capacity as much as plating distortion in the three hull forms investigated. As the distortion amplitude was increased to large levels, hull capacity decreased by as much as 10% in certain cases.

4.1.3 Stiffener Buckling Effects

Beam-column buckling is another of the failure modes investigated in this study. Lateral distortion of the stiffener was considered the distortion having the largest impact on the buckling capacity of the plate-stiffener combination. Figures 4.1.3 – 1 through 4.1.3 - 6 show the moment-curvature results of the ultimate strength analysis of the three midship sections as the lateral distortion imposed on the stiffener increased. In the buckling analyses, distortion amplitudes were a function of stiffener length. As with the previous analyses, the entire hull cross-section was assumed to have the same distortion levels.

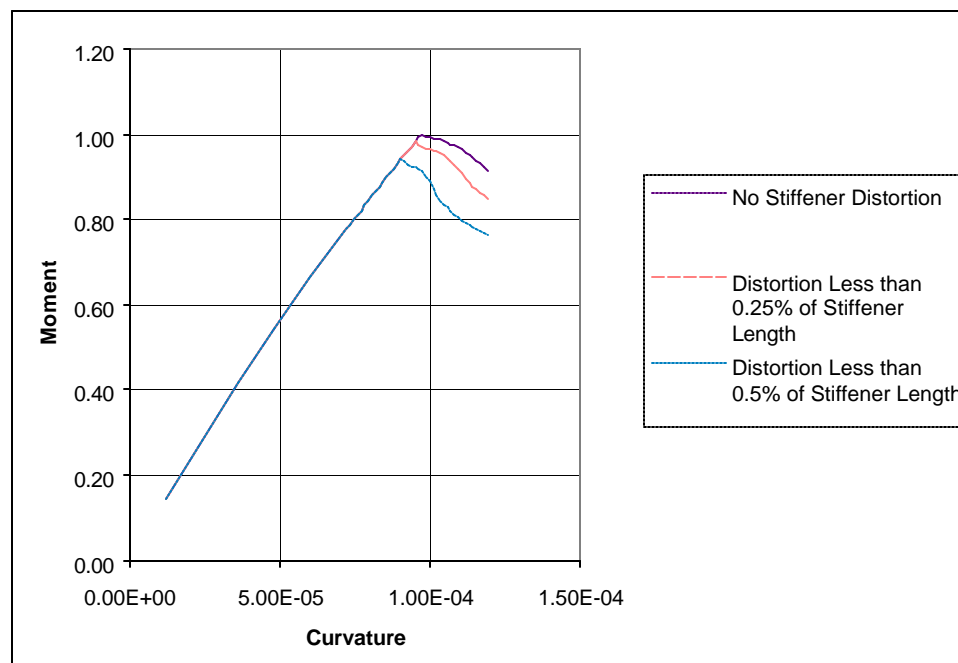


Figure 4.1.3 - 1: Hull F Ultimate Hogging Comparison Evaluating Stiffener Buckling Effects

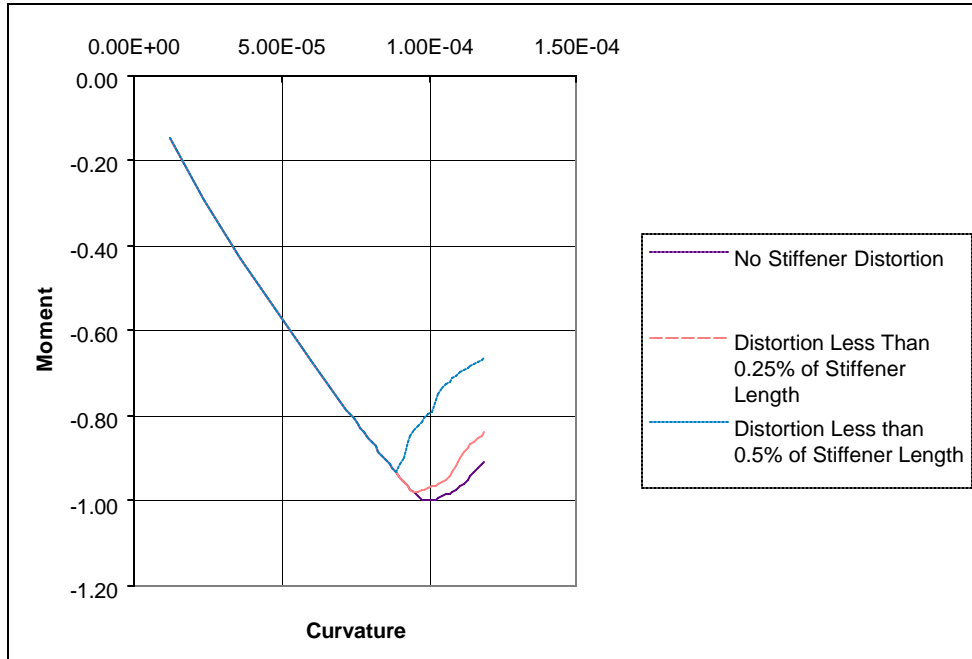


Figure 4.1.3 - 2: Hull F Ultimate Sagging Comparison Evaluating Stiffener Buckling Effects

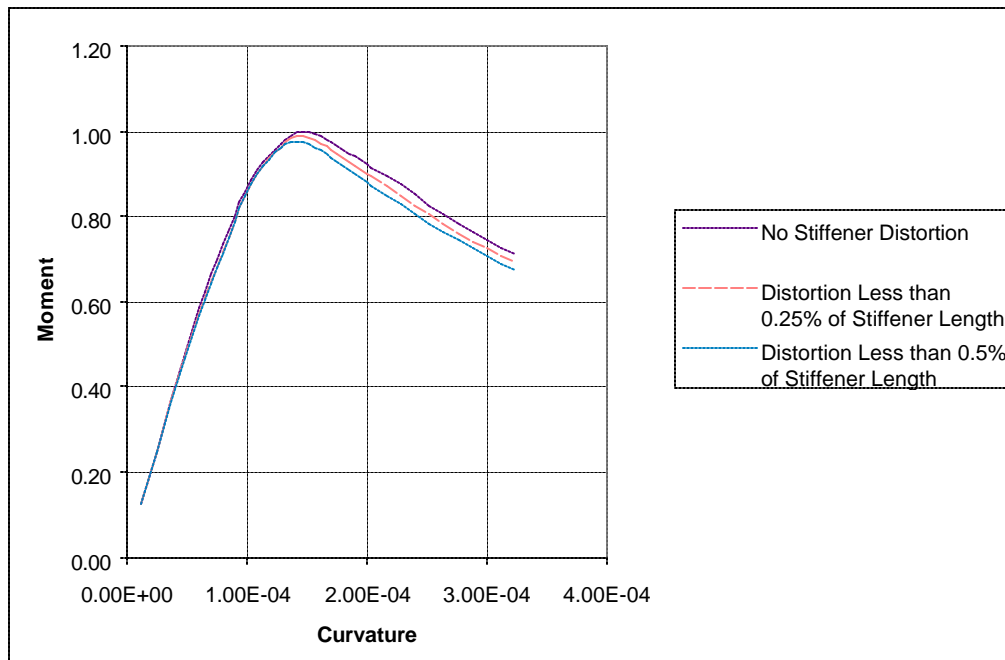


Figure 4.1.3 - 3: Hull D Ultimate Hogging Comparison Evaluating Stiffener Buckling Effects

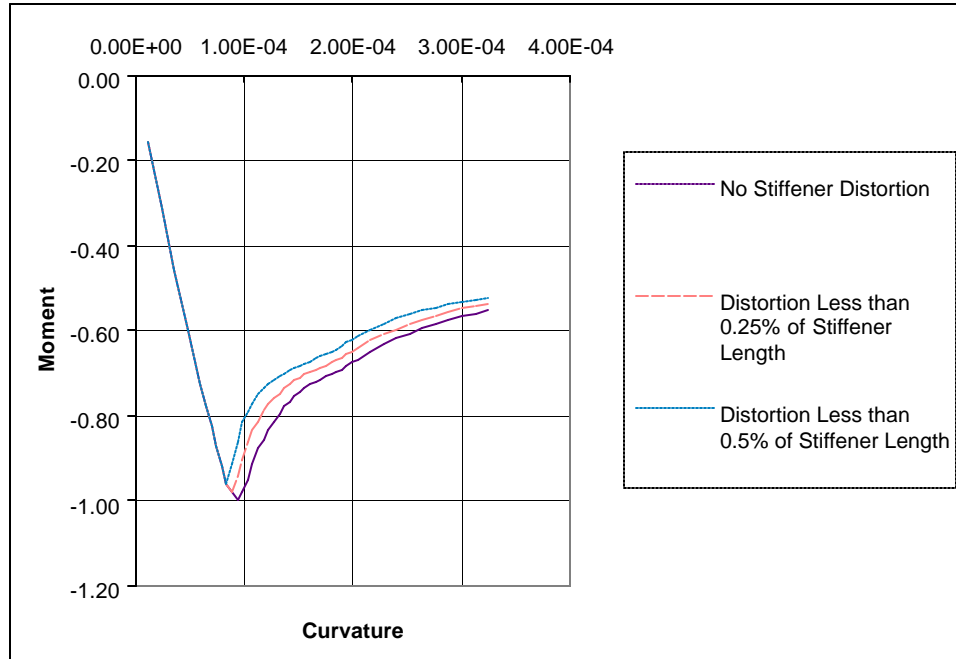


Figure 4.1.3 - 4: Hull D Ultimate Sagging Comparison Evaluating Stiffener Buckling Effects

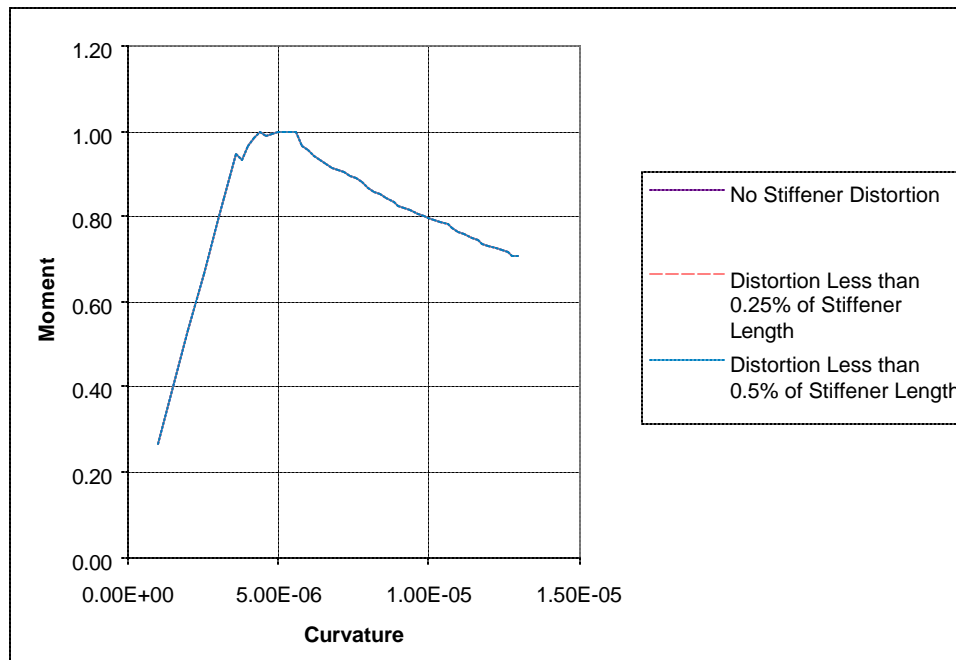


Figure 4.1.3 - 5: Hull C Ultimate Hogging Comparison Evaluating Stiffener Buckling Effects

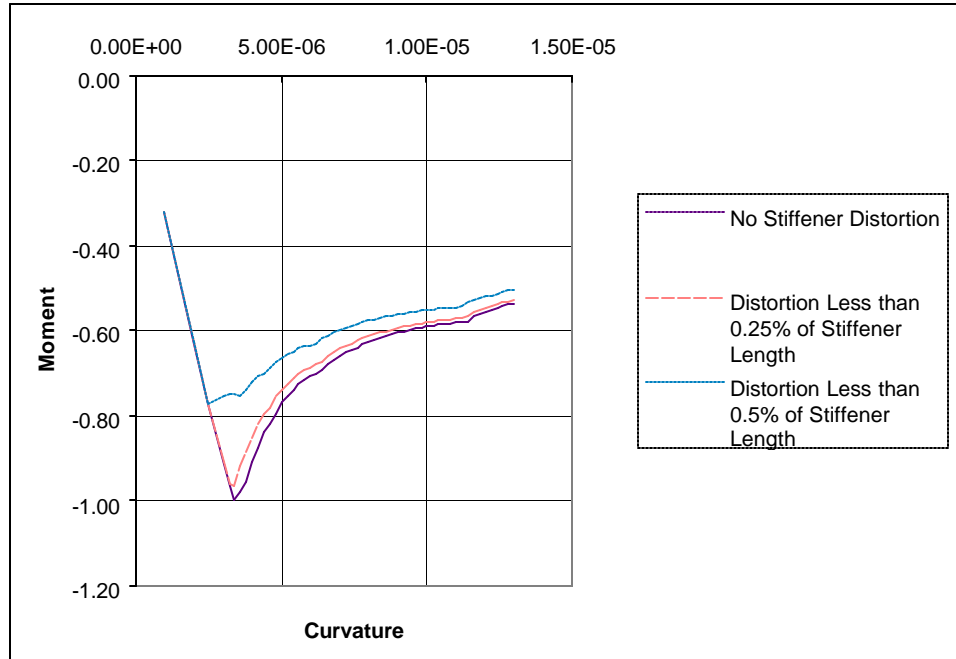


Figure 4.1.3 - 6: Hull C Ultimate Sagging Comparison Evaluating Stiffener Buckling Effects

Lateral distortion of the stiffener and its effect on the buckling capacity of the plate stiffener combination had a significant effect on ultimate hull girder capacity. At distortion levels approaching ½ % of the stiffener length, degradation of 10-15% was not uncommon. This effect was obviously minimized, however, when the plate-stiffener combination was not the critical structural component failing. For instance, in cross-sections with innerbottoms (hulls D and C), stiffener buckling would not play a predominant role in the hogging condition when the bottom structure would be in compression.

5. Fatigue

Structural assemblies that are subjected to cyclic loadings during their service life could at some time develop cracks that may self-arrest or continue to grow. If the cracks continue to grow, they might not adversely affect structure integrity or they might grow to such length that the structure is rendered inoperable or catastrophic failure occurs. If possible, the structure should be designed to an operational stress level which limits the probability of crack initiation within the service life of the ship and thus avoid the crack growth phase altogether.

The time rate at which cracks first appear in ship structures is known to depend primarily on the magnitude of the cyclic stress levels and the number of cycles that are applied to the structure at that stress level. To a lesser extent, mean level stress effects (both applied and residual), stress sequence effects, and material properties can also influence the fatigue behavior. Precisely how these effects influence the rate of fatigue damage accumulation is not fully understood, even though fatigue failures have been observed for nearly a century. This is due in part to the random nature of fatigue behavior, uncertainties associated with material properties in the welded heat affected zone, homogeneity of the material and flaw definition at the microscopic level, as well as non-uniformity of test specimens. Additional uncertainties arise not only because the actual mechanism of fatigue damage accumulation is unknown, but the fatigue loadings themselves may also occur in a random manner, which is the case for ship structures.

Since there is no way of monitoring fatigue damage accumulation, one must assume there is no damage until cyclic loading commences and that damage accumulation has reached a critical value once cracks begin to appear. Many researchers have proposed different hypotheses of how damage accumulates between these two extremes. By far the most popular method is the Palmgren-Miner (P-M) damage hypothesis (Palmgren, A. (1924) and Miner, M.A. (1945)). The continued use of this damage hypothesis no doubt stems from its simplicity and flexibility in application to any kind of cyclic loading. This damage hypothesis often produces fairly good fatigue life estimates as well. The P-M damage hypothesis assumes that fatigue damage accumulates linearly, i.e., that fatigue damage due to a given stress cycle only depends on that particular stress level, is independent of previously applied stress cycles, and is simply added on to the running total of damage due to previous stress cycles.

5.1 Operational Profile

The first part of any fatigue analysis procedure is to define the loadings to which the structure will be subjected. In the case of surface ships, this involves defining an operational profile or the piecewise assortment of conditions that make up the ship's anticipated service environment. The conditions are defined in terms of speed, heading and significant wave height. Time spent in each of the individual operating environments is then determined from the product of total time at sea and probabilities of wave height occurrence, spectral formulation for a given significant wave height, and speed and heading combination for a given range of wave height. A representative operational profile can typically be defined by three speeds, four headings, and sixteen sea conditions defined by significant wave heights up to 16 meters (in one meter increments). If one chooses to use the Ochi 6-parameter family of wave spectra, each sea condition will be defined by 11 different spectral formulations and probabilities of occurrence. An assemblage of 2112 different structural responses can therefore make up a single typical operational profile.

By setting up this aggregate profile of individual operating conditions, structural responses can be quantified statistically and dealt with more appropriately on a rational basis. Fatigue damage assessments can then be made either on an ordered recompilation of all the individual responses, i.e. constructing an exceedance curve, or by assessing each individual response separately and accumulating the fatigue damage from each response.

5.2 Seaway Induced Loads

Seaway induced loads imposed on a ship are nearly impossible to predict as a function of time. However, after the loading occurs, seaway induced loads can easily be measured. The ship loading at any instant of time cannot be predicted with certainty since the ocean surface is a random time varying elevation. However, the statistics of wave height and ship responses tend to remain constant, or stationary over extended periods of time. Methods have been developed to describe these responses, ever changing in the time domain, to essentially a constant form in the frequency domain.

In the frequency domain, a complicated time history is decomposed into its basic frequency components. The amplitudes of these components at a given frequency are essentially squared, averaged and plotted as a function of frequency to produce power spectral density (PSD) curves. These curves identify the concentration of response energy as a function of frequency.

If the system is linear, both the (structural) response and input loading (wave height) spectral densities can be used to calculate response amplitude operators (RAOs) by dividing the response by the input at each frequency increment. “Root” RAOs are then obtained by taking the square root of the quotient. The resulting plot of structural response per unit wave height is characteristic of that particular ship operating at that particular heading and speed, and is independent of the input excitation (wave height). The ship response (for a given speed and heading) to different sea conditions can then be obtained by multiplying the RAO by the desired wave height spectra. RAOs effectively separate the ship response characteristics from the loading (wave) environment. For a given heading and speed, RAOs are either obtained experimentally from full-scale sea trials and scaled model tests, empirically from algorithms based on these types of measurements, or even analytically. RAOs are typically determined experimentally. It is assumed here that the ship responses have a symmetric distribution about a zero mean level which corresponds to a narrowband Gaussian process, i.e. are Rayleigh distributed.

The properties of the power spectral density curve obtained by calculating area moments of the power spectral density curve about the ordinate axis, are particularly important in order to characterize the entire stochastic response process. Specifically, the zero and first area moments are used to determine the variance and average cyclic frequency for each response. Assuming the responses follow a Rayleigh probability distribution, the variance defines the distribution and the product of the average encounter frequency and the time spent in a given condition provide the expected number of cycles. These two pieces of information provide the basis for constructing the response exceedance curve.

The primary fatigue loads imposed on a ship are longitudinal vertical bending moments due to changes in wave height, and hull girder whipping as a result of wave impact. These types of loads have been characterized from several full-scale trials and model tests as a function of principal ship dimensions and the anticipated operational profile of the ship. The operational profile is a function of the ship’s service life spent at sea, broken down into time spent operating at specific speeds, headings, and

sea states. A method of combining the above parameters to obtain an estimate of lifetime longitudinal bending moments is also provided in Sikora (1983) and Sikora (1998).

These estimates of lifetime bending moments can conveniently be expressed in the form of an exceedance curve that is simply a cumulative histogram of cyclic loading excursions, offset by the still water bending moment. The exceedance curve is constructed by analyzing each individual Rayleigh distributed response. The area under the Rayleigh probability density function beyond a given response value is directly proportional to the number of cycles exceeding that value. The number of cycles exceeding a given response can therefore be obtained by integrating the Rayleigh probability density function from that response to infinity and multiplying that area by the total number of cycles in that response. The total number of cycles exceeding a given response value is the running total of similar calculations performed on all the other responses. Repeating this process for several other response values results in a series of discrete points of this response exceedance curve.

To perform the fatigue analysis, the bending moment load history must be converted to a stress history, or stress exceedance curve. Keeping in mind that the bending moment exceedance curve coefficients define the bending moments at a particular location along the ship's length, then the stress exceedances anywhere on that cross section can be obtained provided the section modulus is known, as defined by 5.2 - 1. Stress exceedances at any location along the hull girder can be obtained if the longitudinal bending moment distribution and the section properties along the length of the ship are known. For this report, discussion is limited to a single point somewhere on the midship cross section.

$$s = \frac{Mc}{I} = \frac{M}{S} \quad (5.2 - 1)$$

In order to determine the fatigue strength of the structure, the actual distribution of stress must be known throughout the structure, the point being that actual stresses should be used for fatigue analyses and not design stresses. All material which will be stressed and consequently contributes to the section modulus must be included, whether it was included in the traditional design process or not, e.g. ballistic protection systems, aircraft carrier sponson structure, deckhouses, etc. For example, if the ship has a deckhouse long enough to contribute to its longitudinal strength, the actual hull girder stress associated with the design bending moment will be lower than the design stress, and should be used in the fatigue damage calculations. The actual stress level can be determined from either full-scale measurements, finite element or rigid vinyl modeling, or a detailed stress analysis procedure for hull deckhouse interaction, such as Kammerer's method (Kammerer, J.T. (1966)). Once the actual stress acting at the point of interest is determined from the known bending moment for that section, the stress exceedance curve is obtained by dividing all the bending moment exceedance coefficients by the effective section modulus.

Obviously, the fatigue analysis can be performed for different design stress levels by simply scaling the stress exceedance curve such that the design stress can be parametrically varied to determine the most fatigue efficient primary design stress for a given application.

For applications involving fatigue analysis of a given detail for an entire ship (e.g. butt welds) the stress level at stiffener butt welds located throughout the ship are of interest. For this case a stress factor table would be constructed from a detailed stress analysis of the entire ship. The stresses throughout the ship would then be normalized to a single reference point, the keel amidships. The stress exceedance curve for any point on the ship could then be obtained by scaling the reference point stress

exceedance curve by the appropriate stress factor from the stress factor table. However, this approach only includes stresses resulting from primary bending and does not include the contribution of pressure loads. If secondary loading conditions significantly influence stresses in the region of interest, they should be accounted for in the analysis.

5.3 Fatigue Strength Curves

The second item needed to implement the cumulative damage theory is the ship's structural behavior characteristics to applied cyclic loads, or the joint detail's fatigue resistance to applied stress. There are many factors that influence fatigue strength of a ship structure, component, or specimen. These factors include but are not limited to, material type, material strength, size of the structural element, residual state of stress, welding material and strength, geometrical stress concentrations, type of loading (axial, bending, torsion), environment (air, seawater, temperature), surface treatment (shot peening, surface hardening), surface finish (pitting, rust polished, flush ground welds, as-welded), and welding and fabrication defects.

The fatigue strength is generally characterized by cycling the structural element at a constant load (or stress) level until failure occurs or a practical limit in the number of cycles is reached and the test is suspended. This procedure is repeated at several different stress levels to determine the relationship between applied stress and the number of cycles to failure.

Due to the nature of fatigue, and the many factors which affect it, seemingly identical structural elements will fail after a different number of cycles, even though they were tested under the same conditions. It has become customary to develop S/N diagrams to graphically illustrate the fatigue strength of a structural element. The S/N diagrams are generated by plotting the applied stress (S) on the ordinate versus the number of cycles to failure (N) on the abscissa, and fitting the data to a power function of the form shown in Equation (5.3 - 1).

$$Life = A(Stress)^B \quad (5.3 - 1)$$

Fatigue data generally plot as a straight line on a log log graph (or log(stress) versus log (life) on a regular graph). The inherent scatter can therefore be quantified by performing a least squares fit of the fatigue data to a linearized form of Equation 5.3 - 1, shown as Equation 5.3 - 2.

$$Log(Life) = Log(A) + B(Log(Stress)) \quad (5.3 - 2)$$

The resulting best fit straight line is referred to as the average or mean line (assuming the log(Life) data to be normally distributed), and can be used to estimate the mean life for a given stress level, as shown in Figure 5.3 – 1. At low stress levels, some data appear to approach a stress corresponding to infinite life (for all practical purposes); this stress is referred to as the endurance limit.

Although an endurance limit exists under constant amplitude loads, test results produced under random loads indicate better agreement with P-M predictions when the constant amplitude endurance limit is known and the S/N curve extended linearly at the same slope.

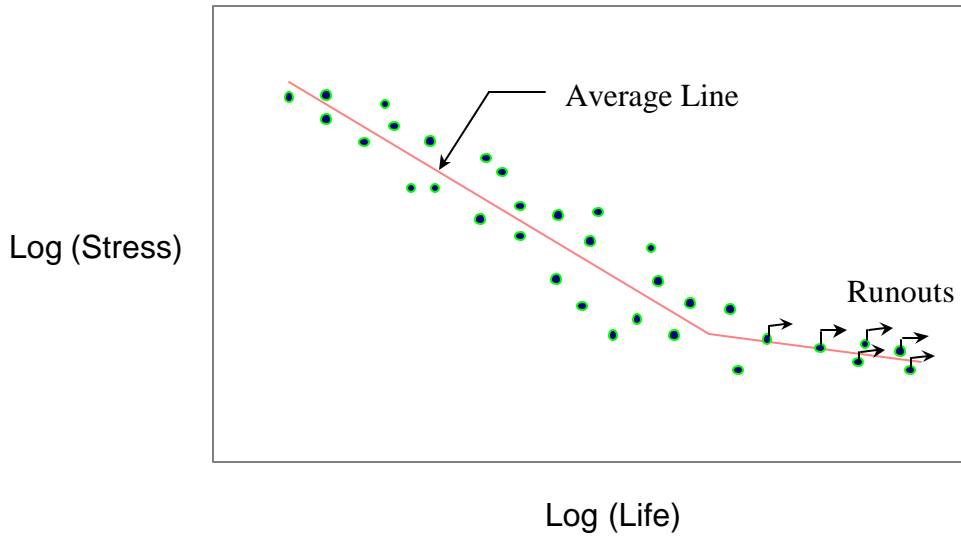


Figure 5.3 - 1: Conventional S/N Fatigue Diagram

If S/N data for other than the mean line are required, e.g. 10% probability of failure, a family of S/N curves can be plotted, each corresponding to a particular probability of failure. This family of curves is referred to as P/S/N curves (Probability, Stress, Number of cycles). There are two ways of defining the P/S/N curves, depending on the number of points available for the analysis. The first method is for the case when a limited number of data points exist at several different stress levels. The data are fit to Equation 5.3 - 1, and the scatter is quantified by the standard estimate of error, or the standard deviation of the differences between the actual data and the data as calculated by the best fit straight line. The data can then be treated as though the scatter in the log(Life) direction follows a normal (Gaussian) probability distribution. The family of curves therefore run parallel to one another, with the mean life line representing 50% probability of failure; a line one standard deviation below the mean would represent a 15.87% probability of failure; two standard deviations below the mean line would represent 2.28% probability of failure, etc. This type of plot is illustrated in Figure 5.3 - 2.

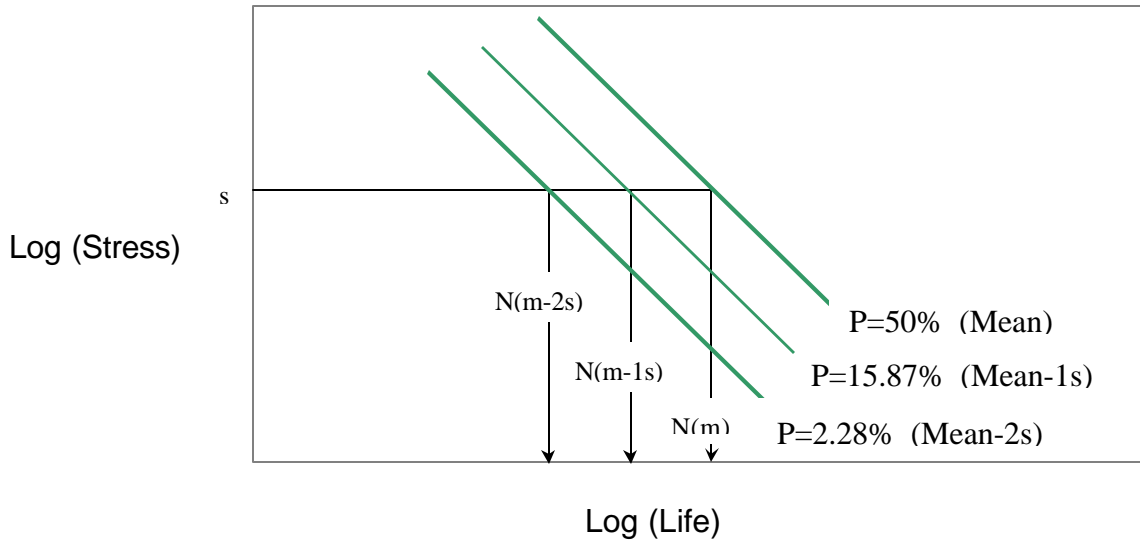


Figure 5.3 - 2: S/N/P Diagram (Constant Scatter in Life at a Given Stress)

Fatigue data, however, can also show an increase in scatter with decreasing stress level. If sufficient data are available at several different stress levels, then the data at each stress level can be fit to a specific probability distribution for that stress level. Having defined the probability distribution at each of the different stress levels, lives corresponding to a particular probability of failure are calculated at each of the stress levels and then fit to Equation 5.3 - 2. This process is then repeated for many different probabilities of failure to generate a family of P/S/N curves. An example of such a plot is shown in Figure 5.3 - 3.

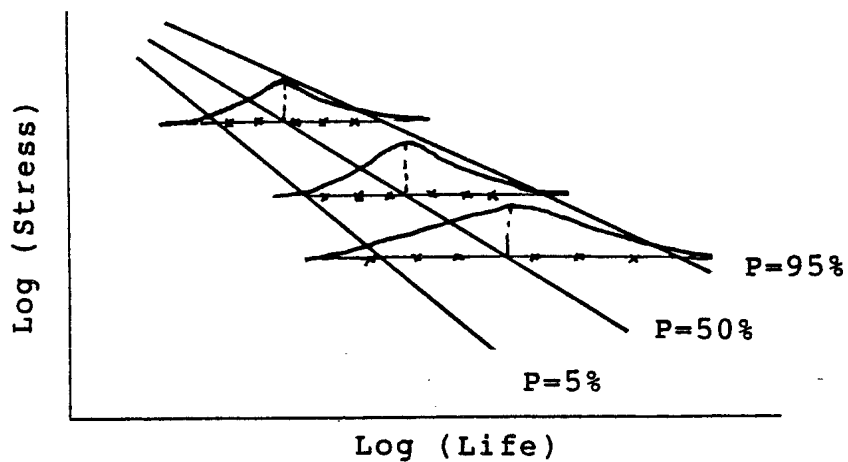


Figure 5.3 - 3: S/N/P Diagram (Increasing Scatter in Life with Decreasing Stress)

Constant amplitude S/N curves for most materials or structural elements generally follow a different slope at the low-stress, high-cycle region of the S/N curve and therefore exhibit a knuckle or bend in the region of transition. This condition can be handled by considering a bi-linear S/N curve,

where the fatigue characteristics are defined by two straight lines, the first portion of the curve defined by $\log(A1)$ and $B1$, and the second portion by $\log(A2)$ and $B2$. Although of little interest for surface ship application, a third linear portion of the S/N can exist at the high stress, low cycle region of the S/N curve near the yield and ultimate strengths of the material or structural element, producing a tri-linear curve which define the fatigue characteristics. Random amplitude tests have shown, however, that a single line S/N curve produces better agreement between prediction and experimental fatigue lives than a bi-linear S/N curve; in essence ignoring endurance limit effects.

The definition of applied stress may vary when dealing with fatigue data from different sources. Constant amplitude fatigue tests are run at specific “R” ratios. An “R” ratio is defined as the ratio of the minimum stress to the maximum stress of a constant amplitude test. An “R” of zero would indicate cycling from a minimum stress of zero to a maximum tensile stress; an “R” ratio of -1 would indicate fully reversed stresses where the minimum stress is the same value in compression as the maximum stress in tension. In addition, data are sometimes reported in terms of “equivalent $R = -1$ stress” or are reported in terms of stress range. Data in terms of different “R” ratios or equivalent stresses may follow any one of several mean stress correction relationships. One such relationship is known as the Modified Goodman Relationship, which is expressed below.

$$\frac{S_{amp}}{S(R = -1)} + \frac{S_{mean}}{S_{ult}} = 1 \quad (5.3 - 3)$$

This equation relates the maximum and minimum stresses to the ultimate tensile stress and accounts for mean level effects. This equation can be more conveniently written in the form of Equation 5.3 – 4, having solved for the equivalent $R = -1$ stress in terms of the other parameters.

$$S(R = -1) = \frac{\frac{1}{2}(S_{max} - S_{min})}{1 - \frac{\frac{1}{2}(S_{max} + S_{min})}{S_{ult}}} \quad (5.3 - 4)$$

Data in terms of stress range do not account for mean stress effects and are only defined by the excursion in stress between the minimum and maximum stress levels. This relationship is given by Equation 5.3 – 5.

$$S_{range} = S_{max} - S_{min} \quad (5.3 - 5)$$

It appears that large welded structural components made of thick members exhibit less mean stress effect than small, thin welded specimens. This may be due to the presence of high residual stress levels, on the order of the yield strength, in the large welded components that are not present in the smaller specimens.

Either of these two conventions can be used in the cumulative damage calculations. However, both the applied stresses and cycles defined by the exceedance curve and the cycles to cause failure at a certain stress level defined by the fatigue S/N curve have to be consistent, both in terms of equivalent $R = -1$ stress or stress range.

5.4 Linear Cumulative Damage Theory

Linear cumulative damage theory was originally proposed by Palmgren (Palmgren, 1924) and later developed from a consideration of the work done during each loading cycle by Miner (Miner, 1945). “Miner’s Rule” as it is commonly referred to, assumes that fatigue damage accumulates linearly and is independent of any neighboring stress cycles. Fatigue damage at a given stress level is defined as the ratio of the number of applied cycles to the number of cycles at which failure occurs. In equation form, Miner’s Rule is expressed as;

$$\sum_{i=1}^B \frac{n_i}{N_i} = K \quad (5.4 - 1)$$

Where n_i is the applied number of cycles at the i^{th} stress level, N_i is the number of cycles to failure at the i^{th} stress level, B is the number of stress levels and K is the summation constant usually taken as unity. Miner’s Rule is applied by first dividing up or discretizing the stress exceedance curve into “ B ” discrete blocks along the abscissa or “cycles” axis. The maximum and minimum stresses, corresponding to number of cycles exceeded, are then calculated at both the left hand side and the right hand side of each block. The average maximum stress acting within the block is obtained by averaging the maximum stress calculated at the left hand side and the maximum stress calculated at the right hand side of the block. The average minimum stress acting within the block is calculated similarly. The number of cycles applied within the block is the difference between the number of cycles exceeded at the right hand side and the number of cycles exceeded at the left hand side of the block. These calculations are repeated for each block, resulting in a maximum stress, a minimum stress, and a number of applied cycles having been defined for each block.

Having determined a maximum and minimum stress for each block, the appropriate stress level is calculated from either Equation 5.3 - 4 or Equation 5.3 - 5, depending on whether equivalent $R = -1$ stress or stress range is being considered. The number of cycles to cause failure at that stress level is then calculated from Equation 5.3 - 2 using the appropriate values for $\log(A)$ and B for the material being used. The values of $\log(A)$ and B must be consistent with the way the applied stresses are defined, i.e., equivalent $R=-1$ stress or stress range.

Whether using equivalent $R=-1$ stress or stress range approach, the damage incurred at the i^{th} stress level within the i^{th} block is the ratio of the number of applied cycles within the block to the number of cycles to cause failure at the i^{th} block stress level. Repeating these calculations for all the blocks and summing the damages for each block results in the total fatigue damage the structure will accumulate within the number of years represented by the exceedance curve.

If the summation of damage is less than the summation constant, K , (usually taken to be unity) the structure will, according to the theory, successfully complete its service life and still have some reserve life before experiencing fatigue failure. If the summation of damage is greater than K , fatigue failure is expected before the service life is reached. The fatigue life is therefore defined by Equation 5.4 - 2, relating the service life, summation constant, and accumulated damage.

$$\text{Fatigue Life} = \frac{\text{Service Life} \cdot K}{\sum_{i=1}^B \frac{n_i}{N_i}} \quad \text{Equation (5.4 - 2)}$$

The summation constant K can either be determined experimentally to accurately predict fatigue life for analysis of a particular application or be used to apply a factor of safety to the calculated fatigue

life in the design process, most analyses use a summation constant of unity. Experiments have shown that using a summation constant of unity will usually result in fairly accurate estimates of fatigue life.

5.5 The Impact of Misalignments on Fatigue Life

Misalignment of a joint detail introduces loading eccentricities that can substantially increase the local stress magnitude. Finite element methods can be used to determine the stress concentration factor resulting from a given misalignment of a detail. As the local stress magnitude increases, the fatigue characteristics of the detail degrade. To determine the correlation between the stress concentration factor associated with the misalignment of the detail and the fatigue life of the misaligned detail, the fatigue strength curves of specimens deliberately misaligned a determined amount must be developed. The stress concentration factors determined by the numerical models can then be compared to the experimentally determined S/N curves to determine the relationship between the stress increase caused by the misalignment and the fatigue strength reduction. Although sizeable databases of fatigue strength curves exist for various aligned details, this database will need to be constructed for misaligned details as well.

A series of fatigue tests were performed on aligned cruciforms and cruciforms deliberately misaligned half of the base plate thickness to determine the impact of the misalignment on fatigue performance. The cruciform is shown in Figure 5.5 - 1.

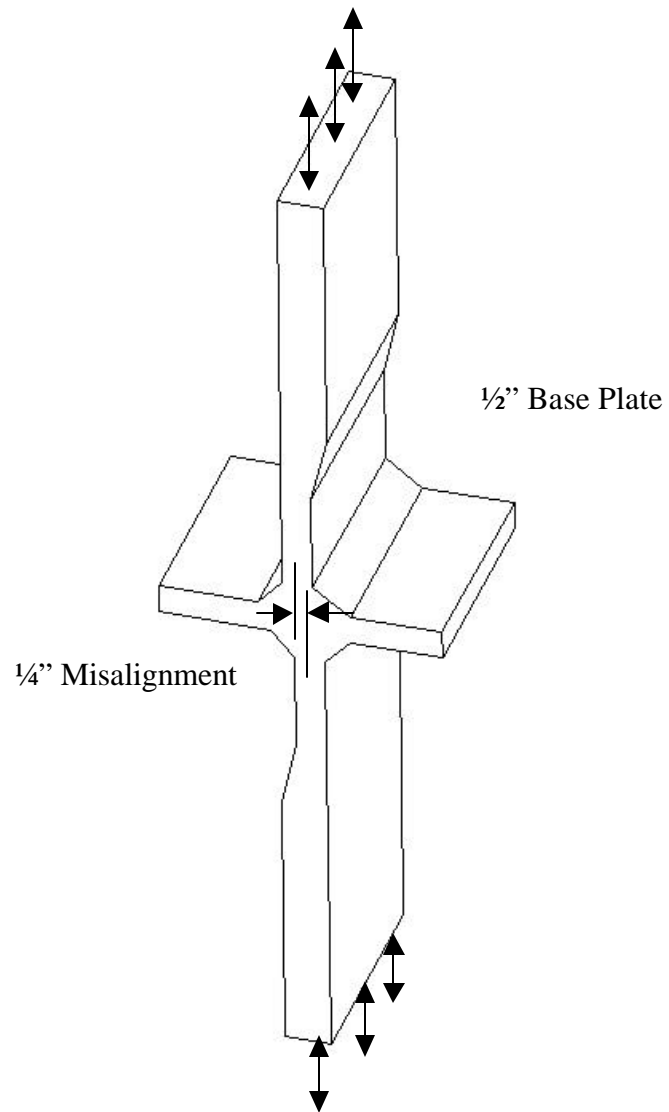


Figure 5.5 - 1: Misaligned Cruciform

The cruciforms were made out of various steels and were cycled at constant amplitude values varying between 7.5 ksi and 30 ksi. Results of the fatigue tests for the mild steel specimens are shown graphically in Figure 5.5 - 2.

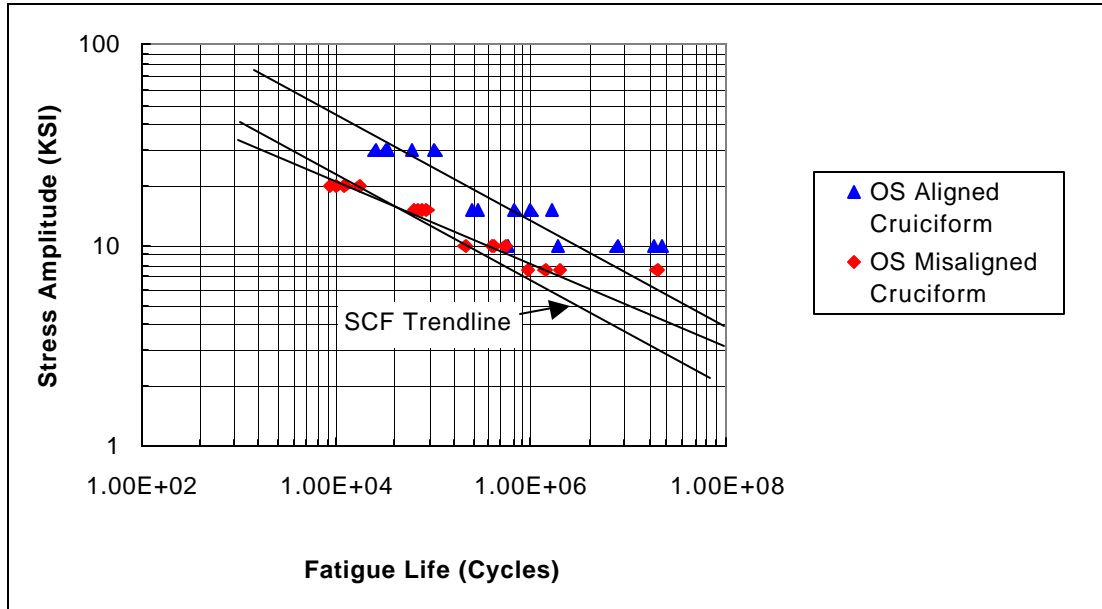


Figure 5.5 - 2: Fatigue of Aligned and Misaligned Detail

In the figure “stress amplitude” refers to the nominal far field stress magnitude. The peak stress occurring in the misaligned cruciform will actually be significantly higher than the far field stress amplitude shown in the figure. To determine the peak stress value for the misaligned detail, finite element analysis (FEA) was used. The FEA indicated a stress concentration factor associated with this misalignment to be approximately 2 times that of an aligned cruciform. If fatigue life were only a function of peak stress, the aligned and misaligned cruciforms’ trendlines would have the same slope, and the fatigue life of a misaligned specimen at a given far field stress amplitude would be the same as the fatigue life of the aligned cruciform at double the far field stress. Assuming this linear inverse correlation between peak stress magnitude and fatigue life of the detail, a “Stress Concentration Trendline” can be developed and is also shown in Figure 5.5 – 2. As shown in the figure, this “Stress Concentration Factor (SCF) trendline” can be used to estimate the fatigue performance of this misaligned detail, however, it does not exactly predict the fatigue performance of the misaligned cruciform as compared to the aligned cruciform. Therefore, in this case, the relationship between the stress concentration factor and fatigue life is not a linear inverse relationship and to define a more accurate trendline further fatigue tests with other misalignment magnitudes are recommended.

The stress concentration factor for a steel detail remaining in the linear, elastic range is not material dependant, and, for the most part, the S/N curves for the various steels are very similar. For these reasons, the type of steel selected for a particular detail does not have a significant impact on fatigue life. This behavior has become apparent as the use of higher strength materials has become more prevalent in ship construction and fatigue problems have arisen. Although the use of higher strength steels in the strength deck and keel fibers of the hull girder can significantly increase ultimate capacity, it does not improve fatigue performance. In fact, as higher strength material is used to reduce weight, the hull girder section modulus is reduced and the primary stresses increase. This causes a reduction in the

fatigue life of the hull girder. The stress concentrations associated with misalignments will further degrade fatigue performance and should be carefully analyzed before reducing the design primary stresses for higher strength steels.

The means exist to estimate the fatigue lives of aligned and misaligned details throughout the hull girder cross-section. If the fatigue strength curves are known for the details in a ship cross section, one can begin to design the ship for a given service life and determine tolerance criteria for individual details. When considering fatigue due to vertical bending loads, misalignment tolerances for a detail near the neutral axis of the hull girder cross section could be relaxed as compared to the same detail near the outer fibers and still exhibit the same fatigue life. Therefore, misalignment tolerances should be used as a guide, but should be flexible and allow for relaxation if evidence is produced that the fatigue life of the misaligned is not degraded to a level below the operational life it is intended. A fatigue assessment as described in this report could be used as a means of evaluating the fatigue performance of a detail for this purpose. Of course, vertical bending is not always the only significant loading condition for a given detail and other significant loadings such as lateral bending, pressure heads and combined bending and pressure loads should be addressed when needed.

6. Conclusions and Recommendations for Future Work

This report describes an approach for determining appropriate tolerance limits on distortions resulting from the ship construction process. The approach focuses on the structural impact of the distortions and, therefore, provides a rational structural basis for determining tolerance limits. It addresses both strength and fatigue issues relevant to deformed and misaligned structure. Hull girder performance is characterized by the loss of load carrying capacity of the cross section, based on predictions made by the computer program ULTSTR. ULTSTR estimates the ductile collapse of the hull girder assuming the collapse results from a sequence of failures of local components. Closed form solutions describing the structural response of these local components have been updated in ULTSTR based on finite element methods to account for fabrication-induced imperfections. An approach to determine appropriate maximum misalignment amplitudes based on fatigue considerations is also described. This approach also uses finite element methods to determine stress concentration factors associated with misaligned details.

The methodology developed in this effort to determine distorted structural response was used to evaluate the impact of several distortions on the buckling and tripping capacity of numerous plate-stiffener combinations. The distortions believed to have the largest effect on tripping and buckling capacity were considered. Future efforts should evaluate the effect of other types of distortions on buckling and tripping capacity. Eventually, other plate-stiffener combinations should also be investigated to complete a database on the most commonly used plate-stiffener combinations.

The impact of the distortions on the tripping and buckling capacity of the stiffeners selected to demonstrate the methodology was varied. In general, as imperfections were introduced, there was an immediate drop in tripping and buckling capacity as compared to the undistorted shape. As the distortions approached the tolerance limits, the tripping capacity of the selected stiffeners degraded significantly, dropping on the average 10%-15%. Similarly, the buckling performance degraded as the distortions approached the tolerance limits, where reduced buckling capacity's exceeding 15%-20% were not uncommon. Based on these results, performance of the stiffeners at current tolerance levels is marginal and caution should be exercised before further relaxing of the tolerances is considered, particularly near the outer fibers of the hull girder.

The impact of the distortions on hull girder capacity was addressed by assuming that all the structural members were deformed an identical amount. Hull girder capacity was reduced between 5% and 10% as distortion magnitudes approached their tolerance limits. In the future simulation techniques should be used to determine the hull girder capacities. The techniques should use realistic, randomly generated distorted components with varying degrees of distortions.

Recent efforts developing databases describing the fatigue characteristics of various welded details and advancements in the ability to predict cyclic structural loadings resulting from a given operational profile make it possible to design a hull girder for a given operational life. These databases should be used when defining appropriate primary stress allowables for the higher strength steels whose details have very similar S/N curves as similar mild steel details but are currently allowed to significantly higher primary stress levels. These efforts are also critical in identifying optimum inspection schedules and probable fatigue crack initiation sites for inspections.

Although numerical methods can be used to estimate the fatigue life of a misaligned detail as compared to the aligned detail by relating stress concentration factors to fatigue performance, further fatigue tests are needed to expand the database and provide more accurate fatigue strength curves for misaligned details. Eventually, the degree of misalignment allowed for a particular detail should be highly dependent on the location of the detail on the hull girder cross-section and the operational life needed. Economic decisions can then be made trading off costs associated with tighter tolerances and longer operational lives versus less stringent tolerances and shorter operational lives.

Acknowledgement

The advice of the Project Technical Committee (PTC) is greatly appreciated. Members of the committee provided valuable advice and direction during technical discussions throughout the project. The authors would also like to single out Phil Rynn (ABS) for his efforts, serving as the PTC chairman and Mr. Jerome Sikora (NSWCCD), Mr. Robert Michaelson (NSWCC) and Mr. Jeff Beach (NSWCCD) for their technical assistance.

The committee members included:

Bill Siekierka	COTR, SSC
Bob Sielski	National Acad. Sci.
Steve Sharpe	USCG, ABS
Phil Rynn (chair)	ABS
David Rypien	ABS
Neil Pegg	DREA
Marty Hecker	USCG
Alan Brown	MIT
Justus Benckhuysen	CCG
Chao Lin	MARAD
Thomas Ingram	ABS
Jerry Snyder	NAVSEA
Jerry Sikora	NSWCCD

References

Adamchak, J.C. (1975), "A Rapid Technique for Predicting the General Instability of Ship Grillages with Elastically Constrained Edges", NSRDC Report 4604.

Adamchak, J.C. (1979), "Design Equations for Tripping of Stiffeners Under Inplane and Lateral Loads", DTNSRDC Report 79/064.

American Society of Testing and Materials (ASTM Designation: F 1053- 87).

Ayyub, B.M., Muhanna, R. and Daniel Bruchman (1997), "Uncertainty in Marine Structural Strength Due to Variability in Geometry and Material Properties", Technical Report NSWCCD-TR-65-96/05, Naval Surface Warfare Center, Carderock, Md.

Ayyub, B.M., Chao, Ru-Jen, Bruchman, D.D. and John Adamchak (1995), "Reliability Assessment for Hull-Girder Bending of Naval Vessels", Technical Report CARDEROCKDIV-U-SSM-65-95/38, Naval Surface Warfare Center, Carderock, Md.

Clarkson, J. (1965), The Elastic Analysis of Flat Grillages with Particular Reference to Ship Structure, Cambridge University Press.

Dow, R.S., R.C. Hugill, J.D. Clark and C.S. Smith (October, 1981), "Evaluation of Ultimate Ship Hull Strength", Joint Society of Naval Architects and Marine Engineers/Ship Structures Committee Extreme Loads Response Symposium, Arlington, Virginia.

Evans, J.H. (1975), Ship Structural Design Concepts, Cornell Maritime Press.

Faulkner, C., J. Adamchak, G. Snyder and M. Vetter (1973), "Synthesis of Welded Grillages to Withstand Compression and Normal Loads", Computers and Structures, Vol. 3, pp 221-246.

Frost, N.E., et al (1974), "Metal Fatigue", Oxford University Press.

Kammerer, J.T. (March 1966), "A Design Procedure for Determining the Contribution of Deckhouses to Longitudinal Strength", Third Annual Symposium, Association of Senior Engineers, Bureau of Ships.

Lipson, C. and N.J. Sheth (1973), "Statistical Design and Analysis of Engineering Experiments", McGraw-Hill Book Co., Inc., New York.

Miner, M.A. (1945), "Cumulative Damage in Fatigue", Journal of Applied Mechanics, Volume 12.

Minnick, P. V., and St. John, J.W., "Material Properties of Steel Plate Used in the Construction of Navy Ships." NKF Engineering, Inc., (1987).

Ostapenko, Alexis (October, 1981), "Strength of Ship Hull Girders Under Moment, Shear and Torque", Joint Society of Naval Architects and Marine Engineers/Ship Structures Committee Extreme Loads Response Symposium, Arlington, Virginia.

Palmgren, A. (1924), "Die Lebanstaver von Kugellagern", ZVDI, Volume 68.

Sikora J.P., et al (May 1983), "A Method for Estimating Lifetime Loads and Fatigue Lives for SWATH and Conventional Monohull Ships", Naval Engineers Journal, Val. 95, No.3.

Sikora J., (November 1998), "Cumulative Lifetime Loadings for Naval Ships", 1998 International Mechanical Engineering Congress & Exposition, Anaheim, CA, USA

PROJECT TECHNICAL COMMITTEE MEMBERS

The following persons were members of the Project Technical Committee that represented the Ship Structure Committee to the Contractor as the resident subject matter experts. As such they performed technical review of the initial project proposals to select the contractor, advised the contractor in cognizant matters pertaining to the contract of which the agencies were aware, performed technical review of the work in progress, and edited the final report.

Project Technical Committee Chairperson

Mr. Philip Rynn American Bureau of Shipping

Project Technical Committee Members

Mr. Marty Hecker United States Coast Guard

Cdr. Steve Sharpe United States Coast Guard

Mr. Justus Benckhuysen Canadian Coast Guard

Mr. Rong Huang Chevron

Mr. Bruce Jackson Bath Iron Works Corp - GD Marine Div.

Mr. Jerry Snyder Naval Sea Systems Command

Mr. Robert Sielski CMS

Mr. Alan Brown Massachusetts Institute of Technology

Mr. David Rypien American Bureau of Shipping

Dr. Neil Pegg Defence Research Establishment Atlantic

Mr. Chao Lin Maritime Administration

Mr. John Baxter American Bureau of Shipping

Contracting Officer

Mr. Siekierka Naval Sea Systems Command

Executive Director

Lieutenant David J. Martyn United States Coast Guard

Administrative Assistant

Ms. Jeannette Delaney Q Systems, INC

RECENT SHIP STRUCTURE COMMITTEE PUBLICATIONS

Ship Structure Committee Publications on the Web .All reports from SSC 392 and forward are available to be downloaded from the Ship Structure Committee Web Site at URL:

<http://www.shipstructure.org>

SSC 391 and below are available on the SSC CD-ROM Library. Visit the National Technical Information Service (NTIS) Web Site for ordering information at URL:

<http://www.ntis.gov/fepc/cpn7833.html>

SSC Report Number Report Bibliography

- SSC 410 **Fatigue of Aluminum Structural Weldments** R. Kramer, P. Fontneau 2000
- SSC 409 **Guide to Damage Tolerance Analysis of Marine Structures** I. F. Glen, A. Dinovitzer, L. Malik, R. I. Basu, R. Yee 2000
- SSC 408 **Detection Probability Assessment of Visual Inspection of Ships**, L .A. Demsetz, J. Cabrera 1999
- SSC 407 **Optimal Strategies for Inspection of Ships for Fatigue and Corrosion Damage**, K. Ma, I. R. Orisamolu, R. G. Bea, 1999
- SSC 406 **Sea Operational Profile for Structural Reliability Assessments**, I. F. Glenn, R. B. Paterson, L. Luznik, 1999
- SSC 405 **Fatigue Resistant Detail Design Guide for Ship Structures**, I. F. Glenn, A. Dinovitzer, R. B. Paterson, L. Luznik, C. Bayley, 1999
- SSC 404 **Ship Structural Integrity Information System (SSIS) Phase III: Ship Quality Information System**, H. P. Reeve, R. G. Bea, 1998
- SSC 403 **Design Guide for Marine Applications of Composites**, E. Greene, 1997
- SSC 402 **Guide to Damage Tolerance Analysis of Marine Structures**, R. D. Yee, L. Malik, R. Basu, K. Kirkhope, 1997
- SSC 401 **State of the Art in Hull Reponse Monitoring Systems**, S. B. Slaughter, Dr. M. C. Cheung, D. Sucharski, B. Cowper, 1997
- SSC 400 **Weld Detail Fatigue Life Improvement Techniques**, K. J. Kirkhope, R. Bell, L. Caron, R. I. Basu, 1997